SYNTHESIS, CHARACTERIZATION OF MICROPOROUS AND ORGANO FUNCTIONALIZED MESOPOROUS SOLID CATALYSTS AND THEIR APPLICATIONS IN FINE CHEMICALS SYNTHESIS

A THESIS

SUBMITTED TO THE

UNIVERSITY OF PUNE

FOR THE DEGREE OF

DOCTOR OF PHILOSOPHY

(IN CHEMISTRY)

BY

C.VENKATESAN

CATALYSIS DIVISION

NATIONAL CHEMICAL LABORATORY

PUNE- 411008

INDIA

APRIL 2004

…To the feet of my beloved Master

CERTIFICATE

Certified that the work incorporated in the thesis, **"Synthesis, Characterization of Microporous and Organo Functionalized Mesoporous Solid Catalysts and their Applications in Fine Chemicals Synthesis"** submitted by **Mr. C.Venkatesan,** for the Degree of **Doctor of Philosophy,** was carried out by the candidate under my supervision in the Catalysis Division, National Chemical Laboratory, Pune 411 008, India. Material that has been obtained from other sources is duly acknowledged in the thesis.

Dr. A.P. Singh

(Research Supervisor)

ACKNOWLEDGEMENTS

I take this opportunity to sincerely thank my research supervisor **Dr. A.P. Singh** who allowed me think independently and crystallized out with a right shape and properties through his inspiring guidance and constant motivation. He has taught me scientific and non-scientific lessons better and to remain optimistic. I am grateful to him for giving me liberty in the work undertaken and for continuous encouragement during the course of the present study. I preserve an everlasting gratitude for him.

I am thankful to Dr. S. Sivasanker, Head of Catalysis Division, Dr. A. V. Ramaswamy, former Head of Catalysis Division, NCL, for providing divisional facilities.

I am grateful to all scientific and non-scientific staff members of the Catalysis Division, Centre for Materials Characterization, Micro Analysis, and CMET for all their help in characterizing catalysts, discussions and useful suggestions.

I always had a learning inspiration from my labmates: Shahida, Sushama, Jaimol, Vandana, Chidambaram, Sudhir, Muthukumar, Sachin, Surendran, Shainaz, Shylesh, Shrikant, Sanskriti, Neelu, and Jino. Their co-operation, splendid suggestions and encouragement made this thesis a possible one.

I am also thankful to my numerous friends: Amit, Anand, Anandaraj, Anirban, Bala, Bennur, Biju, Chandrakumar, Devaraj, Dheendhayal, Dhanashree, Jayanthi, Kala, Grish, Laha, Mahesh, Marimuthu, Mangalesh, Murugan, Muthurajan, Selvakannan, Senthil Kumar, Patra, Pai, Pasupathy, Peter, Pranjal, Pratheep, Pratap, Raja, Ramesh, Ramalingam, Reddy, Sekarmithran, Selvaraj, Shailaja, Shiju, Shylesh, Sankar, Sharda, Shetty, Sonu, Smitha, Surekha, Thomas, Tressa, Vaithyanathan, Venkatathri, Vijay, for their charming company, help and everlasting prayer.

I am obliged to my parents, brother, brother-in-law, sisters, my friends and other family members for their love, unfailing support, tremendous patience, sacrifice and encouragement they have shown in their own way during my long period of studies. They have been a constant source of strength and inspiration for me.

I am grateful to Mr. R.K. Pandit and Dr. Meenakshi for their parental care and constant encouragement throughout my studies.

Finally, my thanks are due to Council of Scientific and Industrial Research, New Delhi, India for granting Senior Research Fellowship and Dr. P. Ratnasamy, former Director and Dr. S. Sivaram, Director, NCL, Pune for allowing me to carry out my research and extending all possible infrastructural facilities at NCL, and permitting me to submit the present work in the form of thesis.

(C.Venkatesan)

CONTENTS

Chapter 1. Introduction

Chapter 2. Synthesis and Characterization

Chapter 5. Self-Condensation of acetophenone

Chapter 6. Palladacycle-MCM-41catalysts for C-C Coupling reactions

1.1. Catalysis

Catalysis is a process in which the chemical reactions are facilitated by mere presence of catalysts and plays a vital role in nature and society since almost every reaction requires a catalytic material [1]. Catalysts are substances that facilitate a chemical reaction by lowering the energy barrier of the reaction pathway and thus increasing the reaction rate [2]. Three groups of materials can be recognized as catalysts on the basis of nature of the substances: homogeneous catalysts, bio-catalysts (e.g. enzyme), and heterogeneous catalysts. The description of a catalyst as homogeneous or heterogeneous, generally taken to refer to its phase relative to that of substrate, is equally applicable to the structural anisotropy of the active site. Homogeneous catalysts, mainly soluble transition metal complexes do offer a potentially well-defined metal environment, which translates into greater selectivity in the transformations effected at the metal center [3]. Rapid developments in homogeneous catalysts can accrue because soluble catalyst systems are much more amenable to study than bulk metals: the ability to monitor molecular changes in organo-metallic complexes enables a level of mechanistic understanding which remains without parallel in the long established field of heterogeneous catalysis [4]. Bio-catalytic methods based on enzyme catalysis, originally limited to the production of natural microbial metabolites, have expanded greatly in the last decade, to encompass synthesis not only of natural and unnatural products of opposite configuration, but of chiral synthons for use in building up novel chemical entities [5]. Porous solids (zeolites, charcoal, etc.), layered silicate sheets (clays), layered metal oxides (sulfated zirconia, tungstated zirconia, etc.), and bulk metal oxides (spinels, MgO, etc.), heteropoly acids are some of the well-known heterogeneous catalysts [6-10]. Table 1 gives general classification of heterogeneous catalysts and their corresponding applications.

Table 1.1 General classification and application of heterogeneous catalysts.

Class of catalysts	Examples	Applications
Metals (supported-mono, bi-, multi-metallic), alloys, etc.,	Pt, Pd, Rh, Ni, Fe, Co, Cu, Ag, etc., on SiO_2, Al_2O_3, activated carbon, and others.	Hydrogenation-dehydrogenation, aromatization, oxidation.
Metal oxides (amorphous and crystalline) and mixed metal oxides (acidic or basic or redox)	MgO, CuO, SiO_2-Al_2O_3, zeolites, mesoporous metal oxides, AlPOs, SAPOs, oxides of Bi-Mo, Fe-Mo, perovskites, spinels, fluorites	Alkylation, acylation, cracking, isomerization, oxidation, disproportionation, dehydration-hydration, ammoxidation, amination.
Metal sulfides (supported)	Co-Mo, Ni-Mo, Ni-W on Al_2O_3, SiO_2 or other supports.	Hydrodesulfurisation, hydrotreating, hydrogenation
Metal salts	$Zr_3(PO_4)_4$, ZnS, $LaPO_4$, sulfates, carbonates.	Etherification, amination
Ion-exchange resins	Nafion-H, amberlyst resins	Etherification, dehydration-hydration, esterification
Heteropolyacids (supported)	$H_3PW_{12}O_{40}$, $H_3Pmo_{12}O_{40}$, $H4SiW_{12}O_{40}$	Acid catalyzed reactions, oxidation condensation
Clays and pillared clays, hydrotalcites.	Kaolinite, K-10 Montmorillonite, Al-pillared montmorillonite	Acid-catalyzed reactions, cracking, alkylation, nitration
Immobilized enzymes	Aspartase, nitrilase, amilase	Hydration, amination
Metal complexes (supported or encapsulated)	Metal porphyrins, salens and pthalocyanins)	Selective oxidation

They are either highly crystalline or amorphous in nature. According to the inherent size of the pores or voids the substances possess, the materials are further divided into three types: Microporous (pore size ca. 0.3-2 nm), mesoporous (pore size ca. 2 –20 nm) and macro porous (pore size >20 nm). Microporous materials include zeolites, clays, and sulfated metal oxides and mesoporous materials (M41S family, SBA family) are both academically and industrially interested and as the pores are small enough to sieve the molecules of certain molecular diameter these materials are called as molecular sieves. Table 2 typically lists some zeolites

and molecular sieves with variable pore sizes, mostly in the microporous range prior to the discovery of MCM-41 [11].

Table.1.2 Pore size definition of zeolites and molecular sieves

Pore size (Å)	Definition	Typical material	Ring size	Pore diameter (Å)	References
>500	macroporous				
20-500	mesoporous	MCM-41		15-100	73, 74
<20	microporous				
	Ultralarge pore	cloverite	20	6.0 x 13.2	11a
		JDF-20	20	6.2 x 14.5	11b
		VPI-5	18	12.1	11c
		$AlPO_4$-8	14	7.9 x 8.7	18
	Large pore	faujasite	12	7.4	15
		beta	12	7.6 x 6.4	30
		mordenite	12	6.7 x 7.0	17
		$AlPO_4$-5	12	7.3	18
		ZSM-12	12	5.5 x 5.9	16
	Medium pore	ZSM-48	10	5.3 x 5.6	16
		ZSM-5	10	5.3 x 5.6; 5.1 x 5.5	16
	Small pore	CaA	8	4.2	15
		SAPO-34	8	4.3	19

It is estimated that molecular sieves are responsible for the production of more than 85% of all bulk chemicals as well as intermediates and fine chemicals, and for the destruction of pollutants, such as NO_x and chlorinated hydrocarbons [12]. Fine chemicals are synthesis products aimed at chemical uses as intermediates in the manufacturing of various chemical substances such as pharmaceuticals, flavors, essences, agro-chemicals and detergents etc.

Among the solid acid-base catalyst that are employed in various industrial processes for the production of fine chemicals zeolite catalysts represent 45% in different processes such as for alkylation, acylation, amination, cracking, etherification, esterification, condensation reactions etc.

1.2. Zeolites: General introduction and historical development

Zeolite [in Greek "zeos" and "lithos", meaning "boiling stones"] group of minerals was discovered in 1756 and named by the Swedish mineralogist Baron Cronstedt [13]. Zeolites are ordered porous crystalline aluminosilicates having a definite crystalline structure within which there are a large number of small cavities, which may be inter connected by a number of still small channels or pores [14]. These cavities and pores are uniform in size within a specific zeolite material. Zeolites are having regular, well-defined channel structures and micro pores (4-14Å) with high surface area (~700 m^2/g) and adsorption capacity with controllable adsorption properties. Since the dimensions of these pores are such as to accept for adsorption molecules of certain dimensions while rejecting those of large dimensions, these materials are known as "microporous molecular sieves" and are utilized in a variety of ways to take advantage of these properties. Synthetic zeolites are used commercially more often than mined natural zeolites, due to the purity of the crystalline products, the uniformity of particle sizes, which usually can be accomplished in manufacturing facilities, and the relative ease with which syntheses can be carried out using rather inexpensive starting materials. They are widely used as ion exchangers and sorbents in hydrocarbon conversion catalysis and separations. Zeolites are highly thermal and mechanical stable for better industrial application. The diversity of interest in zeolite chemistry has been fueled by the economic rewards of industrial applications of zeolites, by ongoing development in synthesis

procedures, and by the application of new techniques to zeolite characterization especially by X-ray diffraction. Many of these zeolites have come to be designated by letter or other convenient symbols, as illustrated by zeolite A, X, and Y [15], zeolite ZSM-5, ZSM-12, ZSM-48 [16], zeolite mordenite [17], merely to name a few. Crystalline structures of the zeolite type but containing tetrahedrally coordinated Si, Al, P as well as transition metals and many group elements with the valence ranging from I to V such as, B, Ga, Fe, Cr, Ti, V, Mn, Co, Zn, Cu, etc., have also been synthesized with the generic name of zeotype, including $AlPO_4$, SAPO, MeAPO, and MeAPSO type molecular sieves [18-20]

1.3. Zeolites: Structural and compositional aspects

Molecular sieve zeolites are crystalline aluminosilicates constructed from $(SiO_4)^{4-}$ and $(AlO_4)^{5-}$ tetrahedra that share vertices. Consequently, the crystalline framework has net negative charge due to the presence of alumina tetrahedral, which must be compensated by associated cations, e.g., Na^+, K^+, Ca^{2+}, H^+, NH_4^+, etc. The individual tetrahedra are always close to regular, but because the shared oxygen linkage can accommodate T-O-T angles [T, tetrahedral species (silicon or aluminum)] from 130° to 180°, they can be combined into a variety of framework structures. These tetrahedra are coordinated such that the zeolites have regular, open framework structures resulting in a high surface area. Access to the interior of zeolite crystals is controlled by windows of peripheral oxygen atoms. In practical zeolite catalysis, these windows involve eight, 10 or 12 oxygens. Window dimensions depend on the structure of the zeolite. For example, the elliptical 12-rings of mordenite differ from the more symmetrical rings of zeolite X. Both the size and shape of windows can influence access to the interior of zeolite crystals, as can counter-ions (cations). The active sites of zeolites are predominantly inside the pores and cavities of the zeolite and can be either *intra* or *extra*-

framework species. The strength and concentration of these sites can also be tailored to a specific application [21].

1.4. Acid properties of zeolites

1.4.1. Brønsted acid sites

Pure siliceous zeolites are electrically neutral. By replacing silicon (tetrahedrally coordinated with oxygen atoms) having a formal charge of 4^+ in the zeolite lattice with aluminum (formal charge 3^+) a negatively charged tetrahedron is created. The negative charge is balanced by a cation either NH_4^+, alkali cations like Na^+, K^+ or H^+ ions. The protons are formally assigned as bonded to the bridging oxygen of a Si-O-Al bond to form hydroxyl groups that act as strong Brønsted acids at the solid/gas interface. The overwhelming evidence is that hydroxyls within the zeolite channels provide the active Bronsted sites [22]. These are usually prepared via ammonium ion exchange:

$$NaZ + NH_4^+(aq) \rightleftharpoons NH_4Z + Na^+(aq)$$

$$NH_4Z \rightleftharpoons NH_3(g) + HZ$$

They are also prepared via hydrolytic process involving water coordinated to polyvalent cations: $M(H_2O)^{n+} \rightleftharpoons MOH^{(n-1)+} + H^+$

This generates protonic sites within the zeolite. In silica rich zeolites, where acids do not destroy the structure, the hydrogen forms (HZ) can be prepared by direct exchange of Na^+ by H^+ using mineral acids. Brønsted acid sites will have acid strength, which depends on their environment, i.e. depending on chemical composition and the structure of the zeolite [23]. The local environment of the acid site in a molecular sieve is determined by the structure, i.e. the coordination of the TO_4 tetrahedra in the framework (topology). This leads to different amounts of topologically different T sites, i.e. sites in tetrahedral position. In this way, LTL zeolites would have two, MOR four and MFI twelve different T sites [24], while FAU

structures have no inequivalent T sites. These different tetrahedral positions differ in T-O-T bond angles and T-O bond lengths [25,26].

Bronste sites

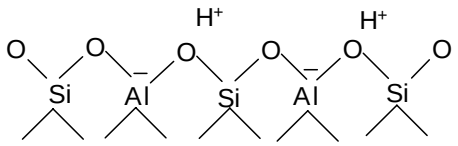

(A)

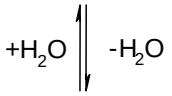

Lewis sites

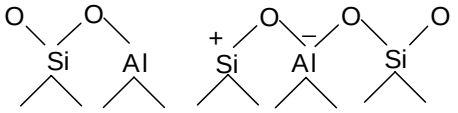

(B)

1.4.2. Lewis acid sites

Lewis acid sites (electron pair acceptor sites) are related to the formation of positively charged oxide clusters or ions within the porous structures of the zeolites. These species are typically alumina or silica/alumina, formed by extraction of aluminum from the lattice, or metal ions exchanged for the protons of acid sites. The former type of Lewis acidity, i.e. aluminum oxide clusters containing alumina in octahedral and tetrahedral coordination will usually be a stronger Lewis acid than exchangeable metal cations ("true" Lewis acids) [27].

'True Lewis site'

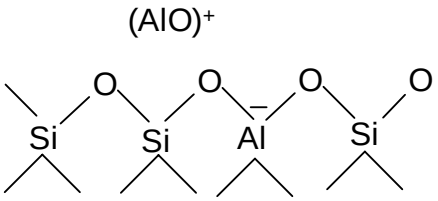

(C)

Lewis acid sites are acting also as hydride (or anion) receptors in a variety of reactions.

1.4.3. Zeolite beta

Zeolite beta, a high silica, large pore crystalline aluminosilicate material first synthesized by Wadlinger et al in 1967 [28], possesses an intergrowth of two or three polymorphs having a three-dimensional system of inter connected 12 membered ring channels

with pore diameters of 0.55 x 0.55 nm and 0.76 x 0.64 nm [29, 30]. Owing to its high acidity and peculiar pore system, zeolite beta receives much attention as a potential catalyst in fluid catalytic cracking [31], hydro treating [32], isobutene alkylation with 1-butene or 2-butene [33, 34], alkylation of C-8 aromatics [35], acylation of aromatics [36,37] etc.

1.5. Basic zeolites

Solid base catalysts exhibit high activities and selectivities for many kinds of reactions, including condensations, alkylations, cyclisations, and isomerization; however, many of these processes are carried out industrially using liquid bases as catalyst [38-40]. These applications can require nearly stoichiometric amounts of the liquid base for conversion to the desired product. Replacement of liquid base catalysts with solid base catalysts allows easier separation from the product as well as possible regeneration and use. Basic solids also have the added advantages of being noncorrosive and environmentally friendly, which allows easier disposal. The Basicity of ion-exchanged zeolites arises from the framework negative charge [41]. Occlusion of alkali metal oxide clusters in zeolite cages via decomposition of impregnated alkali metal salts results in a further increase in the Basicity of these materials [42-47]. The supported species are typically introduced through wet impregnation of a solution containing the solvated precursor into the zeolite pores. Calcination decomposes the occluded compounds and creates the supported alkali metal oxides. Zeolite K-L is mostly used base catalysts for varieties of organic reactions [48,49].

1.6. Zeolites: Synthesis and mechanism

Since the earliest reports of zeolite synthesis by Barrer in the 1950s this field has resembled a scavenger hunt for new materials [50,51]. The synthesis of most molecular sieve zeolites is carried out in batch systems, in which a caustic aluminate solution and a caustic

silicate solution either formed *in situ* or addition as such, are mixed together, and the temperature held at some level above ambient (60-180°C) at autogenous pressures for some period of time (hours-days). A wide range of zeolites could be synthesized quite readily in the laboratory from aluminosilicates gels [52]. An amorphous viscous alumino-silicate gel phase normally becomes less viscous as the temperature is raised, but this is not universally true for all the cases. As the synthesis proceeds at elevated temperatures, zeolite crystals are formed by nucleation step, and these zeolite nuclei then grow larger by assimilation of alumino-silicate material from the solution phase. Simultaneously, the amorphous gel phase dissolves to replenish the solution with alumino-silicate species. In short, the two phases have different solubilities, with the solubility of amorphous gel being higher than that of the crystalline zeolite phase. The first step in the transformation of gel usually involves the formation of the smallest entity having the identity of new crystalline phase, the crystal nucleus that is followed by the subsequent assimilation of mass from the solution and its reorientation into ordered crystalline material via crystal growth. The many different silicate zeolite structure types are summarized in a general formula as solid solution series:

$$A^{x+}_{(4-w)/y/x}[Si_{1-y}T_y{}^{w+}O_2]*zH_2O*nM,$$

Where A=mono- or divalent cations

T=tetra-, tri-, di-, or mono valent cations tetrahedrally coordinated by oxygen; M= neutral atomic or molecular guest species; x, y, z and n denotes integer.

Different structure types, the void space in zeolites is generated by structure directing agents (SDA), also called template molecules, which determine by their size, geometry, and charge distribution in advance the size and geometry of the pores [53,54]. The incorporation of a template during the synthesis of a solid contributes, by the bonds, which are set up, to the stability of the solid and allows its formation. By a templating effect, it controls the formation of a potentially microporous framework structures. The removal of the template after

synthesis by thermal treatment provides the microporous voids (channels and cavities) of dimensions corresponding to the size of template molecule. According to the nature of the T elements the charge density of the framework and the shape of microporous spaces, different stabilizing interactions can be produced by template-template bonds and/or template framework bonds (cation-anion, dipole-ion, hydrogen and/or van der Walls bonds). Thus the type of inorganic or organic template species, viz. framework-charge compensating cations (Na^+, Ca^{2+}, R_4N^+, etc.), molecules (H_2O, amines, alcohols, etc.) or ion-pairs (NaCl, Pr_4NF, etc.).

Zeolites are meta-stable phase that are produced via kinetic path. A thermodynamic analysis of a complete zeolites synthesis shows that there is both an enthalpic and entropic driving force. The structure directing agents (SDA) become hydrophobically hydrated entities in water provide these two forces that drive zeolites crystallization. The enthalpic force is because the SDA would rather be enclathrated in he hydrophobic silicate than in water and the entropic force is because release of hydration sphere reduces overall order. As the zeolites crystallization is a kinetically controlled process, and in high silica synthesis it is usually the structure that nucleates first that is ultimately produced [55-56]. In the more aluminum rich synthesis, zeolites with large cavities (connected by small pore networks), are the likely products if he guest organo-cation (template) is incorporated into the crystallizing host lattice. In the high silica synthesis, large pore zeolites can be obtained but they tend to be one-dimensional, parallel pore systems. The cavity-type materials, which are more likely to form with the smaller organo-cations. Zeolite crystallization proceeds through two primary steps: nucleation of discrete particles of new phase, and subsequent growth of those entities. Fig.1.1 illustrates the proposed structure for the inorganic-organic entities, and their role in synthesis process [57].

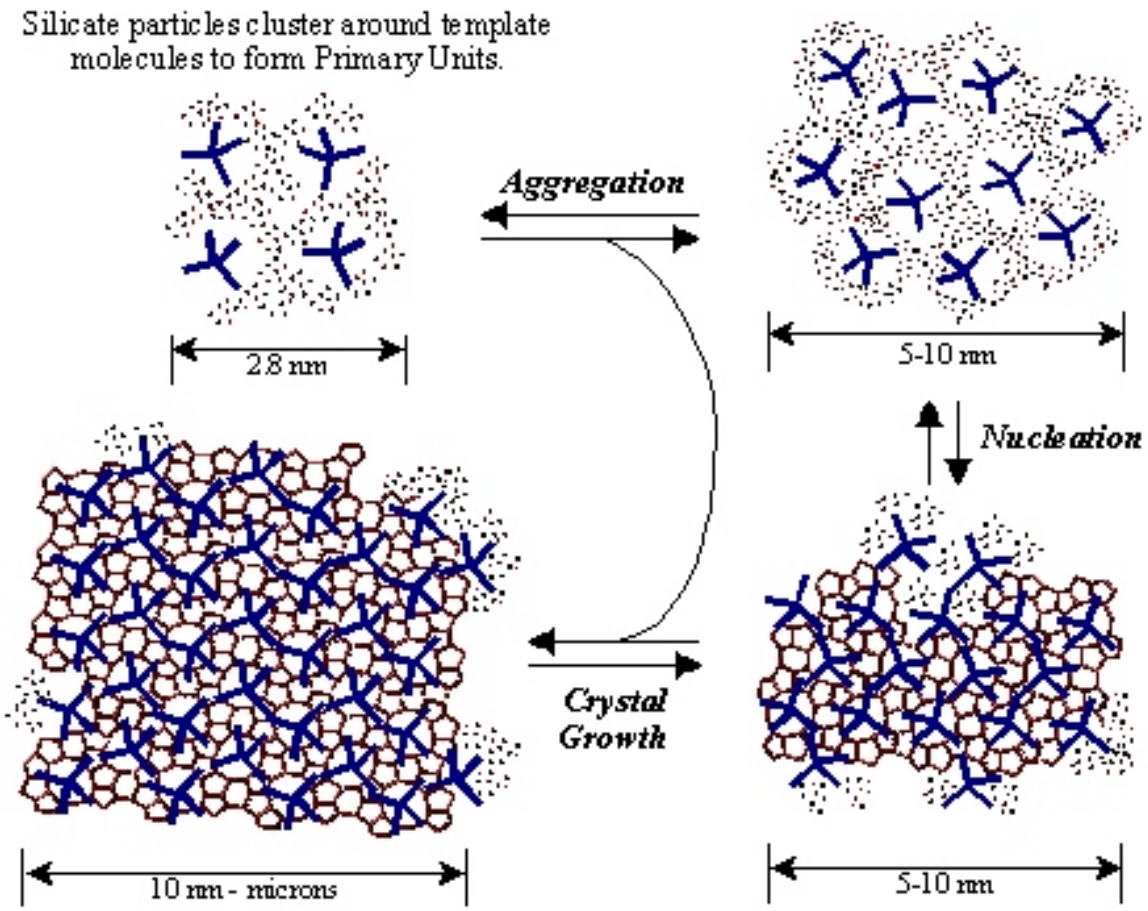

Fig. 1.1 Schematic illustration of the proposed conceptual model for the template facilitated nucleation and crystal growth of all-silica ZSM-5.

1.7. Shape selective catalysis in zeolites

Zeolites are crystalline aluminosilicate porous architecture materials with very regular pore dimensions in the order as the dimension of most simple organic molecules (e.g. from ca. 0.3 nm to ca 0.7 nm). Hence they possess molecular sieving property. The combination of both properties viz. pores of molecular dimensions and catalytically active sites inside the pores is exploited to control the selectivity of catalytically conducted organic reactions. Shape selectivity also depends on the molecular dimensions of reacting and diffusing species, i.e. reactant molecules, transition states, intermediates and/or products.

The diffusivity in zeolites is relatively slow. Since diffusion of molecules within zeolites is thought to proceed by thermally activated jumps from one site to an adjacent site, it is clear that the geometry of the zeolite pores will also play an important role [58]. One should take into account that differences in diffusivities with respect to the pore dimensions can be used to increase selectivity to a given product by adequate selection of pore size of the zeolites catalyst. Diffusivities can be sharply reduced by small amounts of debris in the ores generated during zeolites synthesis or activation and also by small amounts of strongly adsorbed molecule. This effect may increase selectivity to a given product in case of unidirectional pore zeolites.

Counter diffusional effect in case of bi directional or tri directional pore system may also affect the selectivity to a given molecule. For instance, the strong interaction of phenol with the zeolites surface strongly affects the counter diffusion rates even in the case of tri directional zeolites Faujasite Y or beta. The tortuosity of the channels also has an important effect on the diffusion of molecules close in size to the diameter of the pores; the diffusivity is faster in case of tortuous free uni directional pores than bi- or tri directional pores. This brings the concept of molecular traffic control that assumes that in zeolites with channels of different pore diameter, reactant and products of different sizes can preferentially diffuse through one or the other channel [59].

1.8. Sulfated metal oxides

About two decades before, it was shown that by a sulfate treatment of oxides such as ZrO_2, TiO_2, SnO_2, Fe_2O_3, HfO_2, etc., a remarkable increase in the surface acidity and in the catalytic activity for carbenium ion reaction of the starting metal oxides was achieved [60-61]. The presence of sulfur in oxide species plays a good role in the generation of super acid sites ($H_0 < -16.04$). e.g. solid super acids such as sulfated zirconia, sulfated titania etc. have

been reported to exhibit extremely high catalytic activities for acylation and alkylation of aromatics [62,63], isomerization of paraffins [64], Beckmann rearrangement of oximes [65] etc. Sulfated zirconia is the most studied super acid catalyst.

1.8.1. Nature of acid sites

It was said that much better catalysts are obtained with sulfated samples obtained from zirconium hydroxide rather zirconium oxide. After the dried hydroxide is impregnated with a solution of H_2SO_4 or $(NH_4)_2SO_4$, the resulting solid is dried and calcined to temperatures of 500-650°C. A variable to be considered during the preparation is the normality of the H_2SO_4 solution. After H_2SO_4 impregnation, the calcinations temperature of the resulting material also plays an important role on the subsequent textural, acidity, and catalytic activity [66]. It can be assumed that the formation of acid sites involves a two-step chemical reaction between superficial hydroxyl groups of zirconium hydroxide and adsorbed H_2SO_4:

First step: impregnation-drying step

$$Zr_n(OH)_{4n} + xH_2SO_4 \longleftrightarrow Zr_n(OH)_{4n-2x}(SO_4)_x + 2x\,H_2O$$

Second step: calcinations above 400°C

$$Zr_n(OH)_{4n-2x}(SO_4)_x \longrightarrow Zr_nO_{2n-x}(SO_4)_x + (2n-x)\,H_2O$$

Several observations support this reaction scheme [66]. In this way, the presence of SO_4^{2-} anions in the zirconia framework may explain the sintering resistance and the stabilization of the tetragonal phase. The existence of an optimum for the catalytic and ionizing properties as a function of the sulfur content may be due to the maximum covering of the hydroxyl surface. Several authors have proposed that the very strong acidity is due to an increase in number and strength of Lewis acid sites [67]. Arata and Hino [68] have proposed a different structure for active site, where in the sulfate bridges across two zirconium atoms:

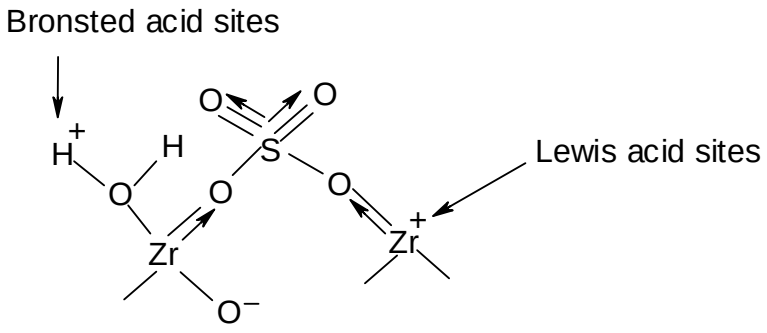

In these catalysts, the S=O group have a high double bond nature. The strength of super acid depends on the extent of losing the double bond character by an electron shift from an adsorbed basic molecule to the sulfur complex. The larger the shift, the higher the acid strength. This model implies the formation of Bronsted acid sites, formed by conversion of Lewis acid sites by sorption of water molecules. The presence of those Bronsted acid sites would allow catalytic reactions to occur at much lower temperature.

1.9. Introduction to mesoporous materials

An ever growing interest in expanding the pore sizes of zeolite type materials from micropore region to mesopores (pore size >20 Å) region in response to the increasing demands in both industrial and fundamental studies. Examples are treating heavy feeds, separating and selective synthesizing large molecules and intra zeolite fabricating technology [69-70]. Zeo-type materials, typically have a surface area of ca. >700 $m^2 g^{-1}$, which are not truly crystalline like microporous zeolites but because of rapid growth of the research on those materials make them to be classified as meso pore zeolites, with the majority of this surface inside the pores and accessible only through apertures of well-defined dimensions [71]. In 1992, researchers at Mobil Corporation discovered the M41S family of silicate/aluminosilicates mesoporous molecular sieves with exceptionally large uniform pore structures, which has resulted in a worldwide resurgence in this area [72-73]. Three different mesophases in this family have been identified, i.e. lamellar [74], hexagonal [73], and cubic

phases [75], in which the hexagonal mesophase, MCM-41, possesses highly regular arrays of uniform-sized channels whose diameters are in the range of 15-100 Å depending on the templates used, the addition of auxiliary organic compounds (co-template) and the reaction parameters. The pores of this novel material are nearly as regular, yet considerably larger than those present in crystalline materials such as zeolites, thus offering new opportunities for applications in catalysis [76] and advanced composite materials [77]. Accordingly, MCM-41 has been investigated extensively because the other members in this family are either thermally unstable or difficult to obtain

The purpose and advantages of synthesizing mesoporous materials is as follows:

1. To overcome the diffusional constraints with zeolites.
2. Very High surface area (>1000 m^2/g) and pore size distribution (20-100 A°).
3. Good host materials for guest species (i.e. heterogenization of homogeneous species or metal complexes on the walls).
4. Easier to monitor the changes made with active species via surface area measurement and pore size distribution experiment.

1.10. Synthesis and mechanism of formation of mesoporous materials

The concepts concerning M41S formation have been formulated based on the studies involving silica (or alumino-silicate)-cationic surfactant systems. Rod-like micelles have been known to form in the presence of electrolytes. The M41S materials appear to be inorganic oxide congeners of lyotropic liquid crystals (LLC) formed by the surfactants in aqueous systems. The original proposed mechanistic pathways are illustrated in Fig. 2. [73]. Under this general term, two possibilities were envisioned. The first one invoked pre-existence of surfactant aggregates or liquid crystal phases in the surfactant precursor solution. Subsequent formation of M41S silica framework occurred due to migration and polymerization of silicate

ions into the aqueous region. The second alternative pathway postulated self-assembly of liquid crystal like structures due to mutual interaction between dissolved silica and surfactant species.

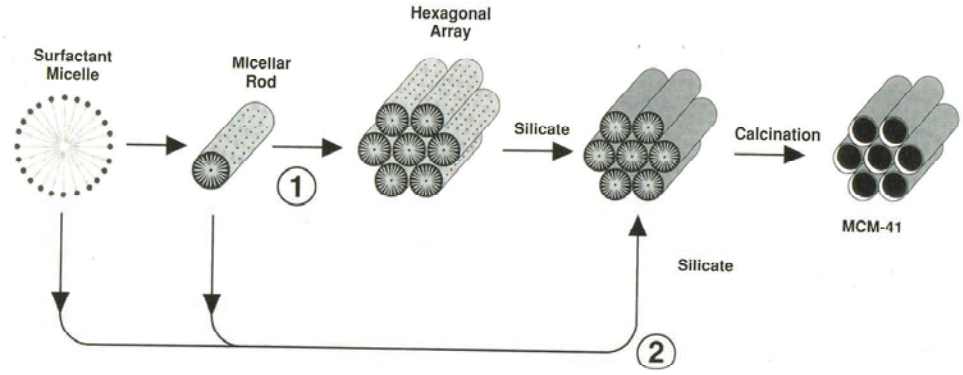

Fig. 1. 2. Liquid crystal template mechanism for the formation of MCM-41.

The second mechanism has been proposed based on the observance of a layered silica/surfactant phase upon mixing of the reactants. In this mechanism Stucky et al., carried out more detailed analysis of this phenomenon and described as cooperative mode of synthesis of mesostructure that involved the following three processes: multidentate binding of silicate oligomer to the cationic surfactant, preferred silicate polymerization in the interfacial region, and charge density matching between the surfactant and the silicate. This reasoning led to a two-step path way to M41S: precipitation of silica-surfactant and silica polymerization [78]. The mechanism pathway is also shown in Fig. 1.3. Polymerization comprises three processes, which proceed simultaneously. First, silicate anions bound to the surface of micelles polymerize to form polyanions (intramicellar polymerization). Second, micelles partly covered with silicate poly anions are gradually arranged into a regular hexagonal array through intramicellar silicate condensation. Free silicate anions or polyanions provide further building material for the formation of the silica walls between the micelles. Davis et al. identified silica-clad rod like aggregates in the synthesis mixture by ^{14}N NMR. The hexagonal MCM-41 could thus arise by close packing of the silicate-surfactant rods [79].

The synthesis parameters (e.g., temperature, pH, compositions of reaction gel) are found to exert key influence on both the surfactant behavior and the distribution of silicate species.

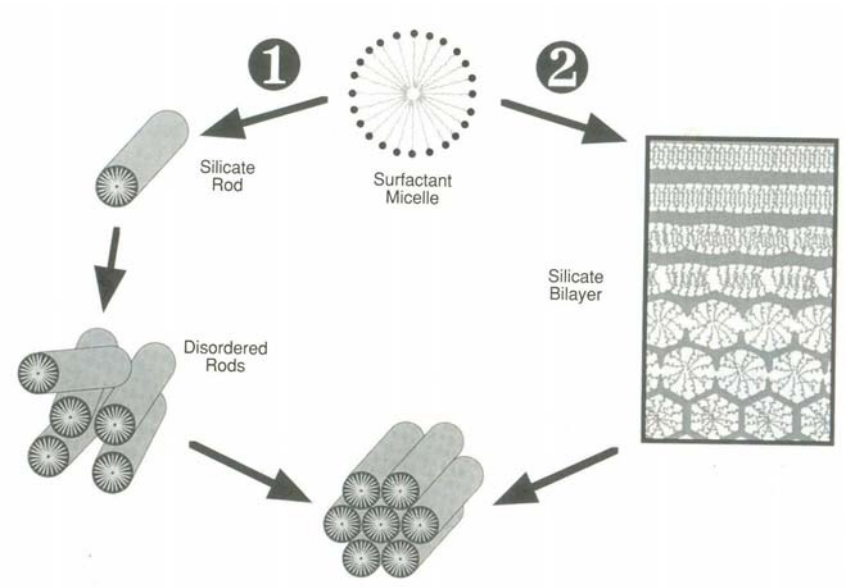

Fig. 1. 3 Mechanistic pathways by (1) stacking of silicated surfactant rods and (2) via formation of an initial lamellar intermediate.

The formation of these materials can be viewed as the interface chemistry between the surfactant and inorganic species (Fig.1.2). The concept of synthesizing mesoporous materials by exploiting surfactant properties has been expanded from original positive surfactant and anionic silicate. These include positive inorganic oxide and negative surfactant, ionic inorganic species with similarly charged surfactant, which is mediated by counter ions of opposite charges, as well as neutral surfactant [80].

1.11. Organo functionalized mesoporous materials

The mesoporous MCM-41 materials add a new dimension due to their large and variable pore diameters. Grafting of functional organosilanes by using surface hydroxyl groups as anchor points has been widely used in the field of catalysis. Important applications of these modified and functionalized systems are heterogeneous catalysis and photocatalysis

involving bulky grafted catalysts and/or the conversion of large substrates. Other potential applications include ion exchange and separations, removal of heavy metals, chromatography, stabilization of quantum wires, stabilization of dyes, and polymer composites [81,82]. The introduction of functional organic groups is usually performed through attachment of silane-coupling agents to mesoporous walls of previously synthesized and calcined materials. The functional group is either directly incorporated in the silane-coupling agent or it is grafted onto it in a second or further reaction step. Co-condensation of reactive species during the mesopores synthesis is a method to incorporate functionality into the walls of the channel system [83,84]. Macquarrie et al., and Brunel et al., have detailed the covalent attachment of basic function such as amino group on the MCM-41 surface which can be either used as base catalysts or used as an anchor point for asymmetric ligands assembly [85,86]. Surface modification techniques are enjoying a renewed interest, and it is clear that the pore walls of mesoporous materials are easily modified with either purely inorganic or with hybrid, semi-organic functional groups and can be successfully used as catalysts for green chemistry [87].

1.12. Physico-chemical characterization

Characterization of the catalysts and catalysis process by means of analytical techniques is far most important to know about the properties of the catalysts. By proper characterization studies, it is possible to propose models of the systems and according to the needs one can design the properties of the system associated with structural or functional modules. Table. 1.3 show some of the characterization techniques frequently utilized to determine the structure and composition of catalysts.

Table 1.3. Physico-chemical characterization techniques, basis and information.

Analysis method	Physical basis	Information
Infra red spectroscopy (FT-IR)	Vibrational excitation of surface atoms by adsorption of infrared radiation	Structure and bonding of adsorbates
X-ray diffraction (XRD)	Monochromatic beam of X-rays of wavelength λ, incident on a sample made of small crystallites, will be diffracted by sets of planes of high atomic concentrations.	Crystallinity of the samples, unit cell parameter, particle size, composition, etc.,
X-ray photoelectron spectroscopy (XPS)	Energy distribution of electrons that are emitted from the catalyst due to photoelectric effect	Composition at the surface, valence and binding energy of an atom.
Ultra violet-visible adsorption spectroscopy (UV-vis)	Electronic excitation of atoms or molecules by adsorption of radiation in the ultra violet-visible region.	Analyses of numerous organic and inorganic species exhibit electronic transitions.
Electron microscope (TEM, SEM)	Interaction of electron with matter	Morphology, particle size and compositions.
Thermogravimetric analysis (TGA/DTA)	Change in weight of a system under examination as the temperature is increased at a predetermined and preferably at a linear rate/Measuring of thermal effects associated with physical and chemical changes by a differential method	Determination of compositions of complex mixture, purity and thermal stability associated with physical/ chemical changes with respect to temperature.
Adsorption/desorption of gases at low temperature	Adsorptions of gaseous molecules or liquids at lower temperature and high pressure and desorption of the same at decreased pressure.	Surface area pore size distribution and pore volume of solid materials.
Temperature programmed adsorption/desorption (TPD)	Adsorption of base over the acid sites and desorption of the same at elevated temperatures.	Nature of acid sites and acid strength.
Chemical characterization of functional groups (NMR)	Change in the direction of nuclear spin quantum number in the presence of strong magnetic field.	Structural determination by means of coupling, decoupling, co-ordination position of an atom/element

1.13. Acylation reactions of aromatics

Friedel-Crafts acylation reactions are widely used in the manufacture of arylketones, which are of interest in the synthesis of a large number of fine chemicals such as drugs, fragrances, dyes, and pesticides [88]. This process has been carried out in industry by working under batch conditions using acyl halides as acylating agents and homogeneous Lewis acids such as anhydrous metal halides ($FeCl_3$, $FeBr_3$, $SbCl_5$, $TiCl_4$, $ZrCl_4$) as catalysts [89]. Conventionally, in the Friedel-Crafts ketone synthesis, homogeneous Lewis acid catalysts such as $AlCl_3$, BF_3 and HF have been used [90]. However Lewis acids must be used in higher than stoichiometric amounts, and the catalyst must be destroyed at the end of the reaction with a significant production of undesirable wastes [91]. In order to overcome all these difficulties of Lewis acid catalysts, several other acid catalysts such as iron sulfate [92], iron oxide [93], heteropoly acids [94], trifluromethane sulfonicacids [95] have been used as alternate catalysts. Various metal salts supported on zeolites and clays have also been reported for Friedel-Crafts reactions [96]. Besides, the use of solid acids such as zeolites enables one to beneficially use their shape selective properties (molecular sieving mechanism) to obtain the desired products. Zeolite catalysts and sulfated zirconia have been studied extensively for acylation of aromatics [9].

1.14. Alkylation reactions of aromatics

Electrophilic alkylation of aromatics can be carried out by variety of reactants such as olefins, alcohols, and halogenated hydrocarbons [7]. Alkylation of aromatics is a good example of reactions where the diffusion and transition shape selectivity play a predominate role in controlling the selectivity of zeolites catalysts. Further more, it shows that depending on the size of reactant and product molecules, shape selectivity applies to either medium- or large pore size zeolites, and selective alkylation process have developed using both type of

zeolites. Recently isopropylation of xylenes and ethyl benzene have been studied thoroughly with medium and large pore zeolites in our lab [35]. Many solid bases have recently been found useful in the production of alkylated products. Several alkali doped silica, zeolites, mesoporous silica have been recently reported for base catalyzed alkylation reactions [38-40, 86, 97]. Recently, Macquarrie et al have reported KF supported on natural phosphate as a green base catalyst [98]. Base catalyzed selective side chain monoalkylation of methylene active compounds is important industrial process for the formation of intermediates [99-101]. Alkali metal carbonates and organic bases have been studied in the selective monomethylation of arylacetonitriles and methyl aryl acetates in detail under batch wise conditions [102, 103].

1.15 Aldol condensation of ketones

A condensation reaction is a molecular transformation that produces a small molecule and two large molecules join together produces an even large one. Self-condensation between the same molecules also produces a condensed bigger molecule. Condensation reactions are important as condensed bigger molecule serve as the intermediates for many kinds of substances, include, dyes, flavors, fragrances, polymers and drug intermediates. Aldol condensation reaction between aldehydes and ketone is one such important condensation in which an intermediate having alcohol and ketone functional groups formed during reaction eliminates a water molecule to give α-β-unsaturated ketone. There are two hot spots for reactivity in aldehyde and ketones: the carbonyl carbon is subject to addition reaction by nucleophiles and additionally the α carbon adjacent to the carbonyl carbon can be deprotonated by a base and made into a nucleophile. The protons on an sp^3 carbon α to a carbonyl group are 30 orders of magnitude more acidic than an sp^3 carbon of an ordinary hydrocarbon. Resonance will explain it. Normally in base catalyzed condensation, sodium

hydroxide, the catalyst is highly corrosive. An intermediate for betaine-30, an important dye, which shows different colors with different solvents, has been prepared by an acid-catalyzed (con. H_2SO_4) condensation reaction between acetophenone and chalcone [104]. Cation exchange resins such as Amberlyst-15 have been studied for the condensation reactions of phenols with ketone [105-107].

1.16. Heterogeneous palladium catalysts

Palladium catalysis has achieved the status of an indispensable tool for both common and state-of-the-art organic synthesis Among the basic types of palladium-catalyzed transformations, the Heck reaction and related chemistry occupy a special place and so it is considered as a sharpening stone of palladium catalysis [108-109]. Palladium complexes with or without phosphine ligands can catalyze the Heck reaction. The phosphine-assisted approach is the classical and well-established method, which gives excellent results in a majority of cases. Palladium catalyzed homogeneous reactions are often preferred for laboratory scale preparations and the majority of mechanistic elucidations and optimization studies have been carried out in solution phase. Frequently, however, problems are encountered when taking an optimized laboratory procedure and scaling it up. An obvious alternative is the use of heterogeneous catalysis where a polymeric ligand is employed. Such catalysts have clear advantages over their homogeneous counterparts. The catalyst is easily separated from the reaction medium, and leaching into the reaction medium is often reduced. Heterogeneous catalytic systems, which include polymer/dentrimer, supported palladium catalysts [110,111], palladium on carbon [112,113], palladium supported metal oxides [114], clays [115] molecular sieves [116-118] and metal complexes of Ni, Co, Cu, Mn [119].

The discovery of Hermann and Beller et al. of the unique catalytic activity of a well known dimeric complex (palladacycle) $Pd_2(P(o\text{-}Tol)_3)_2(\mu\text{-}Oac)_2$, as is now obvious, has set a

milestone in palladium catalysis [120]. The parental structure, which is now often referred to as Hermann's catalyst (*hc*) is definitely one of the most convenient forms of palladium complexes applied in homogeneous catalysis. Even if the palladacycle would have no specific properties but was equivalent to the mixture of palladium salt and phosphine, as is indeed the case in e.g., catalytic amination, it still would deserve a place in the first row of catalysts due to exceptional ease of handling [121]. Phosphine ligands are expensive, toxic and unrecoverable. In large-scale applications on industrial scale, the phosphines might be a more serious economical burden than even palladium itself, which can be recovered at any stage of production or from wastes. Palladium complexes incorporating cyclopalladated phosphines, phosphinite, chelating diphosphines, carbene ligands and dimethylglycine have also been reported [122-127]. Recently, silica supported imines and oxime based palladacycle catalyst anchored on MCM-41 have been studied as an excellent mechanistic probe in the Suzuki reaction [128,129].

1.17. Objectives of the thesis

The present work aims at the design and development of solid catalysts for selective acylation/alkylation of aromatics, self-condensation of acetophenone and C-C coupling reactions. In the first phase, microporous molecular sieves have been synthesized and modified according to the requirement and studied for acylation/alkylation and condensation reactions. Friedel-Crafts acylation/alkylation reactions of aromatics to synthesize aromatic ketones/alkyl aromatics are fundamental reactions in organic synthesis, and numerous industrial process are still running with hazardous, homogeneous Lewis acid catalysts which are non-recommendable. Recently, zeolite beta has been commercialized for the synthesis of arylketones from activated aromatics. The development of new catalytic process using solid catalysts is becoming increasingly interest. With the ever growing environmental and

economic concerns, the present study comprises the following: selective acylation of deactivated and hindered bulky aromatic molecule, alkylation of alkyl aromatics with alcohol as an alkylating agent, solvent free self-condensation reaction of acetophenone to α, β-unsaturated ketone, selective monomethylation of methylene active compounds with dimethylcarbonate as an alkylating agent over solid base catalysts, and design and development of heterogeneous palladacycle catalyst for C-C coupling reactions.

The following objectives have been set for the present study:

- To synthesize, modify, and characterize zeolite catalysts such as beta, Na-Y, Na-X, ZSM-5, Mordenite, and K-L, metal oxides such as sulphated zirconia, and sulphated titania.
- To synthesize, modify and characterize mesoporous materials such as Na-Al-MCM-41, NH_2-Si-MCM-41, NH_2-Na-Al-MCM-41, and Cl-MCM-41.
- To synthesize palladacycle catalysts from organofunctionalised MCM-41 materials and characterize the same.
- To evaluate the catalytic activity of the acidic zeolites in the benzoylation of chlorobenzene and biphenyl, and isopropylation of isobutylbenzene reactions.
- To evaluate the catalytic activity of sulphated zirconia, sulphated titania in the self-condensation reaction of acetophenone and compare activity with zeolite beta.
- To evaluate the catalytic activity of basic zeolites, NH_2-Si-MCM-41, and NH_2-Na-Al-MCM-41 catalysts in the monomethylation reaction of phenylacetonitrile.
- To evaluate the catalytic activity of palladacycle catalysts in the C-C coupling reactions such as Heck reaction, and homoaryl coupling reactions.
- To study the regenerability of all the catalytic systems.

1.18. Outline of the thesis

The present work has been sequentially placed under seven chapters for a thesis entitled "Synthesis, Characterization of Microporous and Organo-Functionalized Mesoporous Materials and their Applications in Fine Chemicals Synthesis" as follows:

CHAPTER I: INTRODUCTION

This chapter presents an over view of various physical and chemical aspects of microporous and mesoporous molecular sieve materials. The different characteristic properties of zeolites include shape selectivity, formation mechanisms, acidity and basicity etc., have been discussed. The mechanisms for the formation of mesoporous materials have been discussed. Detailed literature survey over synthesis aspects, characterization techniques, and different catalytic applications has been given. The scope and objectives of the present work are outlined at the end of this chapter.

CHAPTER II: SYNTHESIS AND CHARACTERIZATION

This chapter describes the synthesis of various microporous and mesoporous materials synthesized during this investigation and characterization of all the samples by XRD, surface area measurements, diffuse reflectance UV-Vis spectroscopy, FT-IR spectroscopy, solid state MAS NMR spectroscopy, SEM and chemical analysis by EDX, ICP-OES analysis, CHN elemental analysis, ESCA (XPS), TEM, and thermo gravimetric analysis is discussed. This includes:

1. Synthesis and characterization of zeolite beta, ZSM-5, and K-L.
2. Synthesis and characterization of sulphated zirconia, and sulphated titania.
3. Synthesis and characterization of NH_2-Na-Al-MCM-41.

4. Synthesis and characterization of Cl-MCM-41, NH_2-Si-MCM-41, and palladacycle-MCM-41 catalysts.

CHAPTER III: ACYLATION REACTIONS OF AROMATICS

This chapter deals with catalytic studies of the H-forms of zeolites such as H-beta, H-Y, RE-Y, H-mordenite, and H-ZSM-5 in the selective benzoylation reaction of deactivated and hindered bulky aromatic molecule. Benzoylation of biphenyl and chlorobenzene over different zeolite catalysts have been presented along with different optimization studies include effect of catalyst concentration, reactant/acylating agent molar ratio, reaction temperature, and effect of different acylating agent over zeolite beta. Recycling studies over zeolite beta have also been discussed.

CHAPTER IV: ALKYLATION REACTIONS OF AROMATICS

This chapter deals with isopropylation of isobutyl benzene with isopropyl alcohol over acidic zeolites. Effect of reaction temperature, reactant/alkylating agent molar ratio, catalyst concentration, and recycling studies over zeolite beta is detailed. Side chain mono-methylation of phenylacetonitrile (PAN) has been studied over different basic zeolites; mesoporous Na-Al-MCM-41, K-exchanged Na-Al-MCM-41 and 3-aminopropyltiethoxysilane (APTES) functionalized MCM-41 catalysts. Further optimization studies over NH_2-Na-Al-MCM-41 catalyst such as effect of catalyst concentration, reactants molar ratio, reaction temperature in the monomethylation of PAN reaction has been detailed. Recycling studies have been discussed in this chapter.

CHAPTER V: SELF-CONDENSATION OF ACETOPHENONE

This chapter deals with the acid catalyzed self-condensation of acetophenone to dypnone. Activity of sulphated zirconia is compared with sulphated titania and zeolite beta. Further optimization studies including recycling study over sulphated zirconia is presented along with the mechanism of the formation of α, β-unsaturated ketone (dypnone) from acetophenone.

CHAPTER VI: PALLADACYCLE-MCM-41 CATALYSTS FOR C-C COUPLING REACTIONS

This chapter deals with the bottom up design of palladacycles over MCM-41 walls starting from incorporating 3-chloropropyltriethoxysilane along with the silane-coupling agent. Various studies such as effect of organic silane concentration, different Pd sources, different palladation conditions (base, temperature, solvent, etc.), and different ligand ($-NH_2$, -OH) to attain better results of palladation are discussed with their characterization and C-C coupling reactions (Heck, and home-aryl coupling) over the synthesized catalysts in this chapter.

CHAPTER VII: CONCLUSIONS

The summary and conclusions of the present work is drawn in this chapter. The arrival at the earlier set scope and objectives of thesis have been discussed.

1.19. References

1. Handbook of Heterogeneous Catalysis, Ed. G. Ertl, H. Knözinger, J. Weitkamp, Wiley-VCH, Weiheim, 1997.

2. J.M. Thomas, principles and Practice of Heterogeneous Catalysis, VCH, Weinheim, 1997.

3. G.Parshall, S.D. Ittel, Homogeneous Catalysis: The Applications and Chemistry of Soluble Transition-Metal Complexes; 2nd ed. John Wiley & Sons, New York, 1992.

4. B.C. Gates, Catalytic Chemistry, John Wiley & Sons, New York, 1992,310.

5. E. Santaniello, P. Ferraboschi, P. Grisenti, A. Manzocchi, Chem. Rev. **92** (1992) 1071.

6. P.B.Venuto, P. S. Landis, Adv. Catal. **18** (1968) 259.

7. P.B. Venuto,Micropor. Mater. **2** (1994) 297.

8. K.Tanabe, W.F. Hoelderich, Appl. Catal. A: Gen. **181** (1999) 399.

9. A. Corma, Chem. Rev. **95** (1995) 559.

10. N. Mizuno, M. Misono, Chem. Rev. **98** (1998) 199.

11. M. Estermann, L. B. McCusker, C. Baerlocher, A. Merrouche, H. Kessler, Nature **352** (1991) 320.

12. W.F. Hoelderich, Stud. Surf. Sci. Catal. **75** (1993) 127; Catal. Today **62** (2000) 115.

13. A.F. Cronstedt, Kongi. Svenska Vetenskaps Acad. Handlinger, **17** (1756) 120.

14. J.M. Newsam, Science **231** (1986) 1093.

15. J. Warzywoda, R.W. Thompson, Zeolites **11** (1991) 577; D.H. Olson, J. Phys. Chem. **74** (1970) 2758.

16. J. L. Schlenker, W.J. Rohrbaugh, P. Chu, E.W. Valyocsik, G.T. Kokotailo, Zeolites **5** (1985) 355; H.van Koningsveid, J.C. Jansen, H. van Bekkum, Zeolites **10** (1990) 235.

17. R.M. Barrer, J. Chem. Soc. (1948) 2158; G.J. Kim, W.S. Ahn, Zeolites **11** (1991) 745.

18. R.M. Dessau, J.L. Schlenker, J.B. Higgins, Zeolites **10** (1990) 522; R.Bialek, W.M. Meir, M.E. Davis, Zeolites **11** (1991) 438.

19. E.M. Flanigen, Stud. Surf. Sci. Catal. **58** (1991) 1; B. M. Lok, C.A. Messina, R. L. Patton, R. T. Gajek, T.R. Cannan, E.M. Flanigen, J. Am. Chem. Soc. **106** (1984) 6092.

20. M.E. Davis, C. Montes, P.E. Hathaway, J.M. Garces, stud. Surf. Sci. Catal. **49** (1989) 199; Q.Huo, R. Xu, S. Li,Z. Ma, J.M. Thomas, R.H. Jones, A.M. Chippendale, J. Chem. Soc. Chem. Commun. (1992) 875.

21. J. Dwyer, Chemistry and Industry, (1984) 258.

22. R.S. Hansford, Ind. Eng. Chem. **39** (1947) 849; J.B. Peri, J. Catal. **41** (1976) 227.

23. D. Barthomeuf, Mat. Chem. Phys. **17** (1987) 49.

24. W.M. Meir, D.H. Olson, C. Baerlocher, (1996) atlas of Zeolite Structure types, 4th edn. Elsevier, London.

25. A.Redondo, P.J. Hay, J. Phys. Chem. **97** (1993) 11754.

26. R.A. van Santen, G.J. Kramer, W.P.J.H. Jacobs, Theory of Brønsted acidity in zeolites. In: R.W. Joyner, R.A. van Santen (eds) Elementary reaction steps in heterogeneous catalysis. Kluwer Academic Publishers, (1993) 113.

27. H.G. Karge, Stud. Surf. Sci. Catal. **65** (1991) 133.

28. R.L. Wadlinger, G.T Kerr, E.J. Rosinski, US Patent 3 308 069, 1967.

29. M.M. J. Treacy, J. M. Newsam, Nature **332** (1988) 249; J.B. Higgins, R.B. LaPierre, J.L. Schlenker, A.C. Rohrman, J.D. Wood, G.T. Kerr, W.J. Rohrbaugh, Zeolites **8** (1988) 446.

30. P. Ratnasamy, R.N. Bhat, S.K. Pokhriyal, S.G. Hegde, R. Kumar, J. Catal. **119** (1989) 65.

31. L. Boretto, M.A. Camblor, A. Corma, J. Perez-Pariente, Appl. Catal. A: Gen. **82** (1992) 37.

32. I. Kirisci, C. Flego, G. Pazzuconi, W.O. Parker, R. Millini, C. Perego, G. Bellussi, J. Phys. Chem. **98** (1994) 4627.

33. M.Sun, J. Sun, Q. Li, Chem. Lett. (1998) 519.

34. A.Corma, A. martinez, P.A. Arroyo, J.L.F. Monteiro, E.F. Sousa-Aguiar, Appl. Catal. A: Gen. **142** (1996) 139.

35. C.R. Patra, R.Kumar, J. Catal. **212** (2002) 216.

36. A. K. Pandey, A.P. Singh, Catal. Lett. **44** (1997) 129; T.Jaimol, P.Moreau, A.Finiels, A.V.Ramaswamy, A.P.Singh, Appl. Catal. A: Gen. **214** (2001) 1

37. V.D. Chaube, P.Moreau, A.Finiels, A.V.Ramaswamy, A.P.Singh, J. Mol. Catal. **174** (2001) 255; Catal. Lett. **79** (2002) 89.

38. H. Hattori, Chem. Rev. **95** (1995) 537; R.J. Davis, J. Catal. **216** (2003) 396.

39. D. Barthomeuf, Catal. Rev. Sci. Eng. **38** (1996) 521.

40. Z.-H. Fu, Y. Ono, J. Catal. **145** (1994) 166.

41. W.S. Wieland, R.J. Davis, J. M. Garces, J. Catal. **173** (1998) 490.

42. H. Tsuji, F. Yagi, H. Hattori, K. Kita, Stud. Surf. Sci. Catal. **75** (1992) 1171.

43. P.E. Hathaway, M.E. Davis, J. Catal. **116** (1989) 263.

44. H.Tsuji, F.Yagi, H. Hattori, Chem. Lett. (1991) 1881.

45. J.C. Kim, H.-X. Li, C-. Chen, M.E. Davis, Micrpor. Mater. **2** (1994) 413.

46. M.Lasperas, H. Cambon, D. Brunel, I. Rodriguez, P. Geneste, Micropor. Mater. **7** (1996) 61; K.R. Kloetstra, M.Van Laren, H. van Bekkum, J. Chem. Soc. Faraday Trans. **93** (1997) 1211.

47. Y. Ono, T. Baba, Catal. Today **38** (1997) 321; I. Rodriguez, H. Cambon, D. Brunel, M.Lasperas, J. Mol. Catal. A: Chem. **130** (1998) 195.

48. P.N. Joshi, A.N. Kotsthane and V.P. Shiralkar, Zeolites **10** (1990) 598.

49. P. Ratnasamy, A.P.Singh, C.S. Sharma, Appl. Catal. A: Gen. **135** (1996) 25.

50. R.M. Barrer, P.J. Denny, J. Chem. Soc. **1961** (1961) 983.

51. Molecular Sieves: Science and Technology, 1. Synthesis, H.G. Karge, J. Wietkamp (Eds.), Springer-Verlag, Berlin Heidelberg, Germany, 1998; Catalysis and Zeolites: Fundamentals and Applications, J. Wietkamp, L. Puppe (Eds.), Springer-Verlag, Berlin Heidelberg, New York, 1999.
52. R. Szostak, Handbook of Molecular sieves. Van Nostrand Reinhold, New York, 1992.
53. R.M Barrer, Hydrothermal chemistry of zeolites, Academic Press, London, 1982.
54. B.M. Lok, T.R. Cannan, C.A. Messina, Zeolites **3** (1983) 282.
55. M.M. Helmkamp, M.E. Davis, Annu. Rev. Mater. Sci. 25 (1995) 161; M.E. Davis, Nature **382** (1996) 583.
56. M.E. Davis, Stud.Surf.Sci.Catal. **97** (1995) 35; Knight et al. **97** (1995) 483;
57. S.L. Burkett, M.E. Davis, J. Phys. Chem. **98** (1994) 4647.
58. D.N. Theodorou, J. Wei, J. Catal. **83** (1983) 205; P.H. Nelson, A.B. Kaiser, D.M. Bibby, J. Catal. **127** (1991) 101.
59. E.G. Derouance, Z. Gabelica, J. Catal. **65** (1980) 486.
60. M. Hino K. Arata. J. Chem. Soc. Chem. Commun. (1979) 1148.
61. M. Hino K. Arata. J. Chem. Soc. Chem. Commun. (1980) 851.
62. T. Jin. M. Machida, T.Yamaguchi, K. Tanabe, Inorg. Chem. **23** (1984) 4396.
63. A. Corma, M.I. Juan-Rajadell, J. M. Lopez-Nieto, a. Martinez, C. Martinez, Appl. Catal. A: Gen. **111** (1994) 175.
64. K. Arata, Adv. Catal. **37** (1990) 165.
65. C.Y. Hsu, C.R. Heimbuch, C.T. Armes, B.C. Gates, J. Chem. Soc., Chem. Commun. (1992) 1645.
66. F.R. Chen, G. Coudurier, J.F. Joly, J.C. Vedrine, J. Catal. **143** (1993) 616.
67. T.Yamaguchi, Appl.Catal. A. Gen. **61**(1990) 1; J.M. Parera, Catal. Today **15** (1992) 481.
68. K. Arata, M. Hino, Appl. Catal. A. Gen.**59** (1990) 197.

69. G.A. Ozin, C. Gil, Chem. Rev. (1989) 1749.

70. M.E. Davis, R.F. Loba, Chem. Mater. **4** (1992) 756.

71. X.S. Zhao, G. Q. Lu, G. J. Millar, Ind. Eng. Chem. Res. **35** (1996) 2075.

72. C.T. Kresge, M.E. Leonowicz, W.J. Roth, J.C. Vartulli, J.S. Beck, Nature **359** (1992) 710.

73. J.S. Beck, J.C. Vartulli, W.J. Roth, M.E. Leonowicz, C.T. Kresge, K.D. Schmitt, C.T.W. Chu, D.H. Olson, E.W. Sheppard, S.B. McCullen, J.B. Higgins, J.L. Schlenker, J. Am. Chem. Soc. **114** (1992) 10834.

74. M.Dubois, Th. Gulik-krzywicki, B. Cabane, Langmuir **9** (1993) 673.

75. J.C. Vartulli, K.D. Schmitt, C.T. Kresge, W.J. Roth, M.E. Leonowicz, S.B. McCullen, S.D. Hellring, J.S. Beck, J.L.Schlenker, D.H. Olson, E.W. Sheppard, Chem. Mater. **6** (1994) 2317.

76. A. Corma, A. Martinez, Adv. Mater. (1995) 137.

77. C. Huber, K. Moller, T. Bein, J. Chem. Soc. Chem. Commun. (1994) 2619.

78. A. Monnier, F. Schuth, Q.Huo, D. Kumar, D. Margalose, R.S. Maxwell, G.D. Stucky, M. Krishnamurthy, P. Petroff, A. Firouzi, M. Janicke, B.F. Chmelka, Science **261** (1993) 1299.

79. C.Y. Chen, S.L. Burkett, H.X. Li, M.E. Davis, Microporous Materials **2** (1993) 27.

80. Q. Huo, D.I. Margalose, U. Ciesla, P. Feng, T.E. Gier, P. Sieger, R. Leon, P. Petroff, F. Schuth, G.D. Stucky, Nature **368** (1994) 317; P.T. Tanev, T.J. Pinnavaia, Science **267** (1995) 865.

81. K. Moller, T. Bein, Chem. Mater. **10** (1998) 2950

82. W. M. Van Rhijn, D. E. De Vos, .F. Sels, W.D. Bossaert, P. A. Jacobs, J. Chem. Soc., Chem. Commun. (1998) 317.

83. C. E. Fowler, S.L. Burkett, S. Mann, J. Chem. Soc. Chem. Commun. (1997) 1769.

84. A. P. Wight, M. E. Davis, Chem. Rev. **102** (2002) 3589.

85. D. J. Macquarrie, D.B.Jackson, J. Chem. Soc. Chem. Commun. (1997) 1781; J. H. Clark, D. J. Macquarrie, J. Chem. Soc. Chem. Commun. (1998) 853.

86. D.Brunel, Micropor. Mesopor. Mater. **27** (1999) 329.

87. X.S. Zhao, G.Q. Lu, A.K. Whittakar, G.J. Millar, J. Phys. Chem. B **101** *(*1997) 6525; K. A. Koyano, T. Tatsumi, Y. Tanaka, S. Nakata, J. Phys. Chem. B. **101** (1997) 9436.

88. H.W. Kouwenhoven, H. van Bekkum, in "Handbook of Heterogeneous Catalysis" (G.Ertl, H.Knozinger, J. Weitkamp, Eds), Vol. 5, P.2358. VCH, Weinheim, 1997; J. March, "Advanced Organic Chemistry", 4th ed. Wiley, New York, 1992.

89. G.A. Olah, "Friedel-Crafts and Related Reactions", Vols. I- IV. Wiley-Interscience, New York, 1963-1964.

90. J.I. Kroschwitz, M. Howe-Gremt, Eds. Encylopedia of Chemical technology, 4th ed. Vol. II. Wiley-Interscience, New york, p 1055; M. Aslam,K.G. Davenport, W.F. Stansbury, J. Org. Chem. 56 (1991) 5955.

91. A. Kaward, S. Mitamurd, S. Kobayashi, J. Chem. Soc. Chem. Commun. (1993) 1157; Chemistry of Waste Minimisation, J.H. Clark, ed. 1995, 522; Org. Process Res. Dev., 2 (1998) 221.

92. M. Hino, K. Arata, Chem. Lett. (1978) 325.

93. K. Arata, M. Hino, Chem. Lett. (1980) 1479.

94. K. Nomiya, Y. Sugaya, S. Sasa, M. Miwa, Bull. Chem. Soc. Jpn. **53** (1980) 2089.

95. F. Effenberger, G. Epple, Angew. Chem. Int. Ed. Eng. **11** 1972) 300.

96. D.B. Baudry, A. Dormond, F.D. Montagne, J. Mol. Cat. A: Chem. **149** (1999) 215.

97. R. Bal, K. Chaudhary, S. Sivasanker, Catal. Lett. **70** (2000) 75.

98. D.J. Macquarrie, R. Nazih, S. Sebti, Green Chemistry **4** (2002) 56.

99. Y. Ono, Appl. Catal. A: Gen. **155** (1997) 133.

100. P.Tundo, M. Selva, ChemTech **25** (1995) 31.

101. J-P. Rieu, A. Boucherle, H. Cousse, G. Mouzin, Tetrahedron **42** (1986) 4095.

102. P.Tundo, G. Malagho, F. Trotta, Ind. Eng. Chem. Res. **28** (1989) 881.

103. M. Selva, C.A. Marques, P.Tundo, J.Chem.Soc. Perkins Trans. I (1994) 1323.

104. C. Reichardt, Angew. Chem. Int. Ed. Eng. **4** (1965) 29; **18** (1979) 98..

105. G.P. Kalena, A. Jain, A. Banerji, Molecules **2** (1991) 100.

106. I. Shigeru, M.Yoshio and K.Takashi, Eur.Pat. No. 319,327 (1989).

107. G.D.Yadav, N. Kirthivasan. Appl. Catal. **154** (1997) 29.

108. W. Cabri, I. Candiani, Acc. Chem. Res. **28** (1995) 2.

109. I.P. Baletskaya, A.V. Cheprakov, Chem. Rev. **100** (2000) 3009.

110. C.M. Anderson, K. Korebelass, A.K. Awasti, J. Org. Chem. **50** (1985) 3891.

111. L.K. Yeung, R.M. Crooks, Nano Lett. **1** (2000) 14.

112. D.Savoia, C. Trombini, A.Umani-Ronchi, G. Verardo, J.Chem. Soc. Chem. Commun. (1981) 541.

113. R.L. Augustine, S.T. O'Leary, J. Mol. Catal. A: Chem. **72** (1992) 229.

114. M. Wagner, K. Köhler, L. Djakovitch, S. Weinkauf, V. Hagen, M. Muhler, Top.Catal. **13** (2000)319.

115. R.K. Ramachandani, B.S. Uphade, M.P. Vinod, R.D. Wakharkar, V.R.Chodhary, A. Sudalai, Chem. Commun. (1997) 2071.

116. L. Djakovitch, K. Köhler, J. Am. Chem. Soc. **123** (2001) 5995.

117. D.H. Bennur, A. Ramani, R.Bal, B.M. Chanda, S. Sivasanker, Catal. Commun. **3** (2002) 493.

118. B.M. Choudary, S. Madhi, N.S. Chowdari, M. L. Kantam, B. Sreedhar, J. Am. Chem. Soc. **124** (2002) 14127.

119. S. Iyer, V.Thakur, J. Mol. Catal. A: Chem. **157** (2000) 275.

120. W.A. Hermann, C. Brossmer, K. Ofele, C.-P. Reisinger, T. Priermeir, M. Beller, H.

Fischer, Angew. Chem. Int. Ed. Engl. **34** (1995) 1844.

121. J. Louie, J.F. Hartwig, Angew. Chem. **108** (1996) 2531.
122. M. Beller, H. Fischer, W.A. Hermann, K. Ofele, C. Brossmer, Angew. Chem., Int. Ed. Engl. **34** (1995) 1848.
123. M. Beller, H. Fischer, K. Kuhlein, C.-P. Reisinger, W.A. Hermann, J. Organometal. Chem. **520** (1996) 257.
124. W. A. Hermann, M. Elison, J. Fischer, C. Kocher, G. R. J. Artus, Angew. Chem. Int. Ed. Engl. **34** (1995) 1844.
125. B.L. Shaw, S.D. Perera, E. A. Staley, Chem. Commun. (1998) 1863.
126. F. Miyazaki, K. Yamaguchi, M. Shibasaki, Tetrahedron Lett. **40** (1999) 7379.
127. M. T. Reetz, E. Westermann, R. Lohmer, G. Lohmer, Tetrahedron Lett. **39** (1998) 8449.
128. R.B. Bedford, C.S. J. Cazin, M. B. Hursthouse, M. E. Light, K.J. Pike, S. Wimperis, J. Organometal. Chem**. 633** (2001) 173.
129. C. Baleizao, A.Corma, H. Garcia, A. Leyva, Chem. Commun. (2003) 606.

2.1. Synthesis of catalysts

Na-X and Na-Y were obtained from Laporte Inorganics, Cheshire, UK. Zeolites ZSM-5 and beta were synthesized by following the procedures described in the literature [1, 2]. Syntheses of the zeolites were carried out in stainless steel autoclaves under hydrothermal conditions. Autoclaves were cleaned with aqueous hydrofluoric acid (40 wt.%) and polished with a carbon brush, prior to the synthesis. Typical synthesis procedures for the catalysts and the materials used in the study are presented here.

2.1.1. Materials

The materials used in the synthesis of zeolites, sulphated zirconia, sulphated titania, mesoporous materials and palladacycles along with their purity are summarized in Table 2.1.

Table 2.1. Specification of the materials used in the synthesis

Reagent and source	Chemical formula	Purity
Sodium hydroxide, s.d. Fine Chemicals., India	NaOH	97 %
Potassium hydroxide, s.d. Fine Chemicals	KOH	85 %
Catapal B, Vista Chem., Oklahoma.	Al_2O_3	65 %
Sodium aluminate	½(Na_2O. Al_2O_3)	
Tetraethyl orthosilicate, Aldrich, USA (TEOS)	$(C_2H_5O)_4Si$	98 %
3-Aminopropyltriethoxysilane, Lancaster, UK (APTES)	$(C_2H_5O)_3Si(CH_2)_3NH_2$	98 %
3-Chloropropyltriethoxysilane, Aldrich (ClPTS)	$(C_2H_5O)_3Si(CH_2)_3Cl$	98 %
3-mercaptopropyltrimethoxysilane, Aldrich (MPTS)	$(CH_3O)_3Si(CH_2)_3SH$	95 %
Ammonium nitrate, LOBA Chemie, India.	NH_4NO_3	98.5 %
Tetraethylammonium hydroxide, Aldrich. (TEOH)	$(C_2H_5)_4NOH$	35 wt.% aq. solution
Tetramethylammonium hydroxide, LOBA Chemie, India. (TMAOH)	$(CH_3)_4NOH$	25 wt.% aq. solution

Fumed silica (for beta synthesis), Sigma, USA.	SiO_2	99.8 %
Aluminium sulphate, LOBA Chemie.	$Al_2(SO_4)_3$, $16H_2O$	98 %
Potassium nitrate, LOBA Chemie.	KNO_3	99 %
Cesium nitrate, Aldrich.	Na_2SiO_3	28.9 %
Sulfuric acid, s.d. Fine Chemicals.	H_2SO_4	98 %
Nitric acid, s.d. Fine Chemicals.	HNO_3	70 %
Hydrochloric acid, s.d. Fine Chemicals.	HCl	35%
Methanol, s.d Fine Chemicals.	CH_3OH	98 %
Tetrapropyl ammonium bromide (TPAB), Aldrich	$(CH_3CH_2CH_2)_4NBr$	98 %
Cetyl trimethylammonium bromide, Loba Chemie. (CTMAB)	$CH_3(CH_2)_{15}N(CH_3)_3$ Br	98 %
Zirconiumoxychloride, Aldrich	$ZrOCl_2$. $8H_2O$	98 %
Titanium isopropoxide	$Ti(OCH(CH_3)_2)_4$	80 %
Ammonium hydroxide, s.d. Fine Chemicals.	NH_4OH	28 wt.% aq. solution
Palladium chloride, Loba Chemie.	$PdCl_2$	
Palladium acetate	$Pd(Oac)_2$	

2.1.2. Zeolite H-beta/K-beta

In a typical synthesis of beta, 0.5 g NaOH, 0.3 g KOH and 18.4 g tetraethyl ammonium hydroxide were taken in a 250 mL polypropylene beaker to which 6 g fumed silica and 10 mL water were gradually added and the gel was stirred for 1 h. 2.1 g aluminium sulphate in 15 mL deionized water was added to the gel over a period of 30 min after which the stirring was further continued for 1 h. 11 mL of deionized water was further added to the resulting gel. This final gel with a pH 12.5 was transferred into a stainless steel autoclave and subjected to hydrothermal treatment at 413 K. Full crystallinity was achieved in 7 days. The

zeolite beta was then separated from the mother liquor, washed with deionized water, dried at 383 K for 12 h and calcined at 783 K for 16 h.

The resultant Na-form of beta was thrice NH_4^+-exchanged using the following conditions: NH_4NO_3= 1 M, 10 mL NH_4NO_3 per gram of zeolite, 353 K, 6 h exchange run, pH~7-8 and calcined at 823 K for 8 h to get the protonic form.

K-beta was prepared by three exchanges of the calcined beta sample with aqueous potassium nitrate solution (1 M; solid/solution (g/mL)= 1:10) for 8 h at 353 K.

2.1.3. Zeolite H-ZSM-5

Zeolite ZSM-5 was synthesized as per the procedure described in the literature. Appropriate amounts of aluminium sulphate and sulphuric acid were dissolved in distilled water to yield solution A. A calculated quantity of tetrapropyl ammonium bromide (TPAB) was added to a solution of sodium silicate of required strength to get a solution B. The solutions A and B were then mixed in a stainless steel autoclave with continuous stirring to get a gel, which had the molar composition as follows:

4.38 $(TPA)_2O$: 27.6 Na_2O : Al_2O_3 : 44.2 SiO_2 : 32.62 H_2O.

The autoclave was then tightly closed and kept at the desired temperature (453 K) under autogenously developed pressure for about 24 h. The reactor was cooled and the contents were filtered, washed with deionized water, and then dried at 393 K overnight. It was then calcined at 823 K for 8 h to decompose the organic template. Thus, Na-ZSM-5 was obtained.

The H-form of the sample was obtained by exchanging it thrice with 1 M NH_4NO_3 solution at 353 K to get NH_4-ZSM-5, which was then calcined at 823 K for 8 h to get H-ZSM-5.

2.1.4. Zeolite K-X, Cs-X, K-Y, Cs-Y, H-Y and RE-Y

Na-X and Na-Y were converted to their respective K-forms by repeated (three times) exchanges with aqueous 1 M solution of KNO_3 in which 5 g of the sample was treated with 50 mL of the solution at 353 K with stirring for 8 h, filtered and then dried at 423 K to get the catalysts K-X and K-Y.

Cs-X and Cs-Y were obtained by treating Na-X and Na-Y with 0.1 mol $CsNO_3$ solution (two times) at 353 K with stirring for 8 h and then dried at 423 K to get Cs-X and Cs-Y catalysts.

H-Y was prepared from Na-Y by three ion exchanges with 1 M aqueous solution of NH_4NO_3 (1 M; solid/solution (g/mL) = 1:10, 8 h) and the resulting sample was then calcined at 773 K for 12 h to get the H-form.

RE-Y was prepared from Na-Y by exchange with 1 M NH_4NO_3 (three exchanges, 353 K, 8 h) and thus the resulting NH_4-Y was treated with 5 % rare earth nitrate solution followed by the analogous procedure employed for NH_4-Y exchange.

2.1.5. Zeolite K-L

The synthesis of zeolite K-L was carried out according to the literature procedure [3]. In a typical procedure, 8.96 g of KOH and 1.55 g of Catapal B were taken in a 250 mL polypropylene beaker to which 20 mL warm, deionized water was added and the gel was stirred for half an hour. 12.44 g of fumed silica in 15 mL warm deionized water was added gradually under stirring and the resulting gel was stirred for 1 h. The gel was then transferred in a stainless steel autoclave and subjected to hydrothermal treatment at 413 K. Full crystallinity was achieved in 64 h. The catalyst was then removed from the autoclave by filtration, washed with deionized water, dried at 383 K for 12 h and the resulting catalyst was then subjected to characterization.

2.1.6. Sulfated zirconia

Zirconium hydroxide was obtained by hydrolyzing $ZrOCl_2.8H_2O$ with aqueous ammonia in the pH range of 8-9 at a temperature of 60-70°C; aqueous ammonia solution (28%) was added drop wise with stirring into 50 g of $ZrOCl_2.8H_2O$ dissolved in 1 l of distilled, hot water. The precipitated solution was kept at 60-70°C for 3 h. The precipitate was washed several times with hot water until the filtrate was negative to silver nitrate solution and finally dried at 110°C. Dried sample was then stirred with 1N sulfuric acid (2 g / 30 mL) for 2 h and filtered. After drying, the sample was calcined at 823 K for 4 h in the flow of air.

2.1.7. Sulfated titania

150 mL of titanium isopropoxide solution was added into 1 l of distilled water with stirring. Addition of 30 % nitric acid solution dissolved the white precipitate, which formed. Ammonium hydroxide solution was added into the aqueous solution with stirring until the pH of the solution reached 8. The precipitate was kept for 3 h and filtered. After filtration the precipitate was washed and dried. The dried sample was then subjected to sulfation as above and calcined as described earlier.

2.1.8. Si-MCM-41

All the mesoporous materials were synthesized by reflux method following the procedure by Melo et al [4]. The molar composition of the synthesis mixture was as follows:

$1SiO_2$: 0.125 $(CTMA)_2$ O: 0.15 $(TMA)_2$ O: 0.018 Na_2O: 120 H_2O: 5 MeOH

Si-MCM-41 was synthesized by a reflux method at 373 K: TEOS (0.1 mol, 20.8 g) in methanol (16.9 g) was added drop wise for 20 min. with stirring to an aqueous solution of TMAOH (0.03 mol, 10.9 g), and CTMAB (0.025 mol, 9.1 g). The mixture was stirred at room temperature for 4 h then transferred into a glass reactor and refluxed at 373 K for 48 h. The

product was filtered, washed with water and dried at 393 K overnight. The organic surfactant molecules were removed by calcination at 800 K for 10 h under static air.

2.1.9. Na-Al-MCM-41 and K-Na-Al-MCM-41

The molar composition of the synthesis mixture was as follows: $1SiO_2$: 0.018 Al_2O_3: 0.125 $(CTMA)_2$ O: 0.15 $(TMA)_2$ O: 0.018 Na_2O: 120 H_2O: 5 MeOH

Na-Al-MCM-41 was synthesized by a reflux method at 373 K: TEOS (0.1 mol, 20.8 g) in methanol (16.0 g) was added drop wise for 20 min. with stirring to an aqueous solution of TMAOH (0.03 mol, 10.9 g), and CTMAB (0.025 mol, 9.1 g) followed by the addition of aqueous sodium aluminate solution. The mixture was stirred at room temperature for 4 h then transferred into a glass reactor and refluxed at 373 K for 48 h. The product was filtered, washed with water and dried at 393 K overnight. The organic surfactant molecules were removed by calcination at 800 K for 10 h under static air.

K-exchanged Na-Al-MCM-41 (K-Na-Al-MCM-41) was prepared by ion exchange of calcined Na-Al-MCM-41 with 1M KNO_3 solution (20 mL/g) at 353 K for 6 h. K-exchanged catalyst was dried at 393 K overnight and activated at 573 K for 5 h.

2.1.10. NH_2-Si-MCM-41

The molar composition of the synthesis mixture was as follows: (1-x) TEOS: xAPTS: 0.125 $(CTMA)_2O$: 0.15 $(TMA)_2O$: 120 H_2O: 5 MeOH. Co-condensation of tetraethylorthosilicate (TEOS), and 3-aminopropyltriethoxysilane (APTS) in presence of organic surfactant molecules has been done using the following procedure. TEOS (0.095 mol, 19.8 g) and APTS (0.005 mol, 1.1 g) in methanol (0.5 mol, 16.0 g) was added drop wise for 20 min with stirring to an aqueous solution of TMAOH (0.03 mol, 10.9 g) and CTMAB (0.025 mol, 9.1 g). The mixture was stirred at room temperature for 4 h then transferred into a glass reactor and refluxed at 373 K for 48 h. The product was filtered and washed with water

and dried at 393 K overnight. The organic surfactant molecules were removed from the material by refluxing with acid solvent mixture (100 mL methanol+ 5 mL HCl/ g of solid material) at 343 K for 24 h. From C, H, N elemental analysis the APTS loading was found to be 7.5 wt.%.

2.1.11. NH_2-Na-Al-MCM-41

The molar composition of the synthesis mixture was as follows: (1-x)TEOS: xAPTS: 0.018 Al_2O_3: 0.125 $(CTMA)_2O$: 0.15 $(TMA)_2O$: 0.018 Na_2O: 120 H_2O: 5 MeOH. The number x has been varied between 0.05 and 0.3. Co-condensation of TEOS, APTS and sodium aluminate in presence of organic surfactant molecules has been done by following the procedure. TEOS (0.095 mol, 19.8 g) and APTS (0.005 mol, 1.1 g) in methanol (0.5 mol, 16.0 g) was added drop wise with stirring to an aqueous solution of TMAOH (0.03 mol, 10.9 g) and CTMAB (0.025 mol, 9.1 g) followed by the addition of aqueous sodium aluminate solution. The mixture was stirred at room temperature for 4 h then transferred into a glass reactor and refluxed at 373 K for 48 h. The product was filtered and washed with water and dried at 393 K overnight. The organic surfactant molecules were removed from the material by refluxing with acid solvent mixture (100 mL methanol+ 5 mL HCl/ g of solid material) at 343 K for 24 h.

2.1.12. Cl/OH-MCM-41

The molar composition of the synthesis mixture was as follows: (1-x)TEOS: xClPTS: 0.125 $(CTMA)_2O$: 0.15 $(TMA)_2O$: 90 H_2O: 10 MeOH. The number x has been varied between 0.05 and 0.3. Co-condensation of TEOS and 3-chloropropyltriethoxysilane (ClPTS) in the presence of organic surfactant molecules has been done for obtaining uniformly distributed organo functionalized mesoporous materials. In a typical synthesis procedure, 11.2 g of CTMAB were dissolved in a mixture of 13.5 g of TMAOH and 150 g deionised water, in

a 250 mL polypropylene beaker. A mixture of 18.0 g of TEOS, 0.84 g ClPTS in methanol was added to this solution. The obtained gel was stirred at room temperature vigorously for 6 h to evaporate the alcohol, and then the reaction mixture was introduced along with the remaining portion of water (66 g) into 500-mL round bottomed flask which was heated at 373 K for 48 h with stirring. The solid products were recovered by filtration, washed and dried at 373 K. The surfactant was removed by stirring 1.0 g of the dried sample with a solution of 5 mL of HCl (35 wt%) in 100 mL of methanol at 338 K for 24 h (Cl-MCM-41).

Chlorine groups in Cl-MCM-41 samples were hydrolyzed into hydroxyl groups by treating the extracted sample with aq. methanol solution (10 mL of H_2O and 10 mL of MeOH/ g sample) at 338 K for 2 h. The hydrolyzed material (OH-MCM-41) is then filtered and dried at 373 K overnight.

2.1.13. Cl/OH-SiO_2

ClPTS functionalised silica was obtained by one step, base catalyzed procedure to obtain 20 wt.% of ClPTS in dry sample. The molar ratio of the compound was $0.9SiO_2$:0. 1ClPTS: 8EtOH: $3H_2O$:0. $008NH_3$. Wet gel was prepared as follows. First two solutions were prepared at room temperature: solution A contained TEOS, ClPTS and half of the total ethanol content whereas solution B consisted of remaining ethanol, water, and ammonium hydroxide. The solution A was added to B under stirring and the resulting sol was heated to 50°C. The gelation took place in 1 h. The resulting alcogel was dried slowly under cover at room temperature to obtain 3-chloropropyl triethoxysilyl functionalised silica materials (Cl-SiO_2). The Cl-SiO_2 was treated with aqueous methanol for 2 h to convert all the Cl groups into OH groups (OH-SiO_2).

2.1.14. Palladacycle (PdOMS/Pd-SiO_2/Am-PdMS)

Palladation was carried out over the samples OH-M/OH-SiO_2/Am-MCM-41 with the palladation reagent, either Li_2PdCl_4, NaOAc in methanol/acetone or Pd $(OAc)_2$ in $CHCl_3$ either at reflux temperature or at room temperature for 24 h [5] to get PdOMS/Pd-SiO_2/Am-PdMS. After palladation, the grey colour material was washed thoroughly with aqueous methanol to remove all unreacted palladium salt and the inorganic base. Different concentration of Li_2PdCl_4 has been used for the palladation of OH-M to get different concentration of Pd loaded catalysts.

2.2. Physico-chemical characterization

2.2.1. X-ray diffraction (XRD)

The structure of a crystal can be determined using the technique of X-ray diffraction (XRD). X-rays have wavelength in the Å range, are sufficiently energetic to penetrate solids and are well suited to probe their internal structure. It is used to identify the bulk phases, degree of crystallinity, unit cell parameters and to estimate particle size [6].

In XRD, X-rays are generated by bombarding a metal target (often copper) with high-energy electrons inside a vacuum tube. Then X-rays are directed at the crystal surface. The crystal mount is rotated so that incident X-rays can be oriented with respect to these crystallographic axes. While most of the X-rays pass straight a small amount of radiation are diffracted by atoms in a periodic lattice. The scattered monochromatic X-rays that are in phase give constructive interference. The detector records the pattern of diffracted light to give diffraction pattern. To observe a diffraction signal, the diffracted light must interfere constructively. For this, the crystal plane must be oriented with respect to the incident rays, so that the path difference is equal to integrated multiple of the wavelength of X-ray radiation.

One can derive lattice spacings, d, by measuring the angles, 2θ, under which constructively interfacing X-rays with wavelength, λ, leave the crystal, by using Bragg relation:

$$n\lambda = 2d \sin\theta \; ; \quad n = 1,2,\ldots$$

The XRD pattern of a powdered sample is measured with a stationary X-ray source (usually Cu Kα) and a movable detector, which scans the intensity of the diffracted radiation as a function of the angle 2θ between the incoming and the diffracted beams. When working with powdered samples, an image of diffraction lines occurs because a small fraction of the powder particles will be oriented such that by chance a certain plane (*hkl*) is at the right angle with the incident beam of constructive interference. Synthesized catalysts were characterized by X-ray diffraction using a Rigaku Miniflex powder diffractometer on finely powdered samples using Cu-K_α radiation and 45 kV and 40mA. The scans were done at 1° per minute for low angle scanning and 4° per minute for microporous zeolites and sulphated zirconia. The XRD patterns were recorded for 2θ's between 1.5 and 50° for mesoporous materials; 5 and 50° for microporous materials.

2.2.2. Chemical composition by EDAX, ICP-OES and CHN analysis

The compositions of zeolites were analyzed by EDAX. Inductively Coupled Plasma-Optical Emission Spectra (ICP-OES) determined the palladium content in the materials on a Perkin-Elmer P1000 instrument. An average of two analyses was done to calculate average concentrations of Pd in the samples. Samples for ICP analyses were prepared by dissolving 0.05 g of sample in approximately 5 mL of HF and subsequently with 5 mL of aqua regia and then diluting to 50 mL with double deionized water (DDW). Analysis of the organic content present in the catalysts was carried out using a Carlo-Erba CHN analyzer.

2.2.3. Surface area (BET) and Pore size distributions (BJH)

The most common method of measuring surface area, pore volume and pore size distribution of a catalyst (solid material) is developed by Brunauer, Emmett and Teller using nitrogen as adsorbent. Measurement of the amount of nitrogen gas adsorbed or desorbed is the most commonly used procedure for determining the pore size distribution of mesopores. Adsorption of nitrogen was carried out at 77 K using a NOVA 1200 (Quantachrome) instrument. The sample was evacuated at 673 K for 2 h under high vacuum (10^{-6} mm). The anhydrous weight of the sample was measured. The sample was then cooled to 94 K using liquid nitrogen and then allowed to adsorb nitrogen gas. Surface area of the sample was calculated by using BET method.

For a multiplayer adsorption the heat of adsorption for all layers except the first layer is assumed to be equal to the heat of liquefaction of the adsorbed gas. So the BET equation comes for summation over an infinite number of adsorbed layers. The general form of the BET equation may be written as follows:

$1/V_{ads}(P_0-P) = 1/V_mC + [C-1/V_mC]\ P/P_0$ ---------- {eq. 1}

Where,

V_{ads} = volume of the gas adsorbed at pressure P,

P_0 = saturated vapour pressure,

V_m = volume of the gas adsorbed for monolayer coverage,

C = BET constant

By plotting left side of equation 1 against P/P_0, a straight line is obtained with a slope of $C-1/V_mC$ and an intercept $1/V_mC$. The BET surface area is calculated using the formula

$S_{BET} = X_M.N.A_M.10^{-20}$

Where, N is the Avagadro's number, A_M is the cross-sectional area of the adsorbate molecule (N_2, 16.2 $Å^2$) and X_M is the moles of N_2 adsorbed.

Pore size distribution was obtained by using BJH pore analysis applied to the desorption branch of the nitrogen adsorption/desorption isotherm.

2.2.4. Fourier transform infrared spectra (FT-IR)

FT-IR is used to determine a variety of materials property including structural details and functional groups confirmation, strength and distribution of acid sites in porous materials. Infrared spectroscopy is the measurement of the wavelength and intensity of absorption of middle IR by a sample. Middle IR light (400-4000cm^{-1}) is energetic enough to excite molecular vibration to higher energy levels. The wavelengths of IR absorption bands are characteristic of specific types of chemical bond and IR spectroscopy finds its greatest utility for the identification of organic and organo metallic molecules.

Infrared spectra of the solid samples diluted in KBr were recorded at room temperature in the transmission mode, in the range 4000 to 450 cm^{-1} at 4 cm^{-1} resolutions, using Spectra One spectrometer.

2.2.5. Thermal studies

Thermal methods of analysis may be defined as those techniques in which changes in physical and/or chemical properties of substances are measured as a function of temperature. Two important thermal analytical techniques are thermogravimetry (TGA) and differential thermal analysis (DTA). Thermogravimetric analysis is a valuable technique for the assessment of the purity of the materials. Many material especially silica, absorb appreciable amount of water when exposed to atmosphere. TG date can show the extent of this absorption and hence most suitable drying temperature for a given reagent may be determined. Organic matter which are burn out can be clearly seen from TG plot in terms of weight loss at corresponding temperature ranges. These data can be useful for knowing the chemical stability of the organic matter anchored into the inorganic materials. Differential thermal

analysis gives information about thermal stability against decomposition, fusion, and phase changes.

Thermal analyses were performed using a Mettler Toledo 851^{e} instrument, from 303 to 1173 K at a heating rate of 20 K min^{-1} under air flow.

2.2.6. Electron microscopy (SEM/TEM)

Electron microscopes are instruments, which uses beam of highly energetic electrons to create magnified images of tiny crystals or particles. An electron gun emits a beam of high-energy electron that travels through a series of magnetic lenses, which focus the electrons to a very fine spot or sample. Interactions occur inside the irradiated sample. The electrons emitted from each point of the sample form the final image. The striking electrons may remain unscattered and transmitted through the specimen (TEM) or may be elastically scattered (without loss of energy) or may be inelastically scattered (SEM) producing low energy secondary electrons. The main difference between SEM and TEM is that SEM sees contrast due to the topology of a surface, whereas TEM projects all information in a two dimensional image, which however, is of sub nanometre resolution.

Scanning Electron microscope (SEM) has been used particularly to examine the topology and morphology of the sample. It is used for thick specimen. The incoming beam of electrons interacts with sample inelastically and causes ionisation of the electron in the sample atom. These ionised electrons are termed as ‘secondary electrons’. The detector detects either secondary electron or back-scattered electrons as a function of the position of the primary beam. The secondary electrons have low energies (10-50 eV) and originate from the surface region of the sample whereas back-scattered electrons come from deeper and carry information on the composition of the sample, because heavy elements are more efficient

scatterers and appear brighter in the image. The SEM micrographs of the samples were obtained in a Leica Steroscan 440 instrument.

Transmission electron microscope uses thin specimens in which the unscattered transmitting electrons provide the image. TEM provide information about the size, shape and arrangement of particles in specimen. In TEM, a high intensity primary electron beam passes through a condenser to produce parallel rays, which impinge on the sample. As the attenuation of the beam depends on the density and the thickness, the transmitted electrons form a two-dimensional projection of the sample mass, which is subsequently magnified by the electron optics to produce a so-called bright field image. The pore structures are also seen through TEM images. Transmission electron micrographs were recorded using a JEOL JEM-1200EX transmission electron microscope operating at 100 kV.

2.2.7. Solid-state NMR studies

Solid-state Nuclear Magnetic Resonance (NMR) analysis covers a wide range of applications that cannot be addressed by liquid state experiments. In solution NMR, spectra consist of a series of very sharp transitions due to averaging anisotropic NMR interactions by rapid random tumbling. By contrast, solid-state NMR spectra are very broad as full effects of anisotropic or orientation dependent interactions are obtained in the spectrum. High resolution ^{13}C NMR spectra of materials are obtained by using well established techniques of high power decoupling magic angle spinning to remove chemical shift anisotropic and cross polarization to improve sensitivity and so avoiding long relaxation delay.

Solid-state ^{13}C CPMAS spectra have been recorded on a Bruker DRX-500 NMR spectrometer spun at high speeds (3 –14 kHz) in order to allow acquisition of NMR spectra with sufficient resolution to allow chemical determinations to be made.

2.2.8. X-ray photoelectron spectra (XPS) studies

XPS is based on the photoelectric effect. Routinely used X-ray sources are Mg Kα (hν=1253.6 eV) and Al Kα (hν=1486.3 eV). In XPS one measures the intensity of photoelectrons N(E) as a function of their kinetic energy E_k. Because a set of binding energies is characteristic for an element, XPS can be used to analyze the composition of samples. Binding energies are not only element specific but contain chemical information as well: the energy levels of core electrons depend on the chemical state of the atom. Photoelectron peaks are labeled according to the quantum numbers of the level from which the electron originates. An electron coming from an orbital with main quantum number n, orbital quantum number l (0,1,2,3,.. indicated as s,p,d,f,..) and spin quantum number s (+1/2 0r –1/2) is indicated as nl_{l+s}. Almost all photoelectrons used in the laboratory XPS have kinetic energy in the range of 0.2 to 1.5 keV, and probe the outer layer of the catalyst.

X-ray photoelectron spectra (XPS) were obtained using a VG Microtech Multilab-ESCA-3000 spectrometer equipped with a twin anode of Al and Mg. All the measurements are made on as received powder samples using Mg Kα X-ray at room temperature. Base pressure in the analysis chamber was 4 x 10^{-10} Torr. Multichannel detection system with nine channels is employed to collect the data. The overall energy resolution of the instrument is better than 0.7 eV, determined from the full width at half maximum of 4f7/2 core level of gold surface. The errors in all BE (binding energy) values were with in ±0.1 eV.

2.2.9. UV-vis spectra

Absorption bands in the visible and ultra violet regions have proved interesting for study. The location of electronic band depends on the energy involved in electronic transitions responsible for absorption. When the energy involved in the electronic transition is

large, the adsorption will take place primarily in ultra violet. With smaller energies, however, the absorption will occur in the near ultra or in the visible light region.

The diffuse reflectance UV-vis spectra in the 200-800 nm ranges were recorded with a Shimadzu UV-2101 PC spectrometer equipped with a diffuse reflectance attachment using $BaSO_4$ as a reference.

2.2.10. X-ray fluorescence Spectroscopy (XRF)

Silica to alumina ratios of the samples were verified by XRF using a wavelength dispersive X-ray spectrometer (Rigaku, 3070) with rhodium target energized at 45 KV and 40 MA. The borate fusion technique was applied for sample preparation. For the calibration of silica and alumina, a pentaerythrital (PET) crystal was used. For the analysis Kα lines were selected and pulses were collected for 40 s using flow-proportional detector. A background correction was applied.

2.2.11. Acidity measurement

The acidity and the acid strength distribution of the zeolites were measured by the temperature programmed desorption (TPD) of ammonia [7-9]. The sample 20-30 mesh size (~ 1.0 g) was activated in a flow of N_2 at 773 K for 6 h and cooled to room temperature. NH_3 gas (25 mL/min) was then passed continuously for a period of 30 min, then the physically adsorbed NH_3 was desorbed by passing N_2 for 15 h (15 mL/min). Acid-strength distribution was obtained by raising the temperature with a ramping rate of 10^0 C /min, from 303 to 773 K in a number of steps in a flow of N_2 (10 mL/min). The NH_3 evolved was trapped in HCl solution and titrated with a standard NaOH solution. The higher the temperature required for desorption the stronger is the acidity of that portion of acid sites. It gives quantitative (total number of acid sites either Brönsted or Lewis) information about acid sites.

2.2.12. Catalysis and analysis of products

Anhydrous AR grade chemicals were used without further purification. The liquid phase reaction was carried out in a 50 mL two necked flask attached to a condenser and a septum. The temperature of the reaction vessel was maintained using an oil bath. The reaction mixture was magnetically stirred and heated to the required temperature at atmospheric pressure. The product samples were withdrawn at regular intervals of time and analyzed periodically on a gas-chromatograph (HP 6890) equipped with a flame ionization detector and a capillary column (5 μm thick cross-linked methyl silicone gum, 0.2 mm x 50 m long). The products were also identified by injecting authentic samples and GCMS (Shimadzu 2000 A) and ^{1}H-NMR analysis.

Autogenously pressure-developing alkylation reaction was carried out in a 250 mL stainless Parr autoclave equipped with a stirrer and a temperature controller. The reaction mixture was flushed with nitrogen before heating to required temperature.

The percentage conversion of reactant is defined as the total percentage of reactant transformed. The rate of reactant conversion (TOF) was calculated as the moles of reactant converted per second per mol of active site. The selectivity to a product is expressed as the amount of a particular product divided by the amount of total products and multiplied by 100.

2.3. Results and Discussions

The X-ray diffraction pattern of all the synthesized as well as modified zeolites matched with those in the literature (Fig 2.1 and Fig.2.2). In addition, the crystallinity and phase purity of the zeolite samples as well as the absence of any amorphous matter within the pore structure were confirmed by XRD. Also, the XRD examination gave no evidence of structure damage or change of the zeolite as a result of various treatments. XRD pattern of sulphated zirconia and sulphated titania match with the reported XRD pattern (Fig. 2.3). The

surface area and scanning electron micrographs showed the absence of amorphous matter inside the channels and on the external surface of the zeolites, respectively.

Table 2.2a. Properties of acidic zeolites

Catalyst	SiO_2/Al_2O_3 molar ratio	Crystal size (μm)	Surface area[a] (m^2/g)	NH_3 chemisorbed at 303 K (mmol/g)
H-ZSM-5	41.0	0.4	413	1.23
H-mordenite	22.0	1.0	552	0.71
H-beta	26.0	0.5	645	0.75
H-Y	4.1	1.0	615	1.45
H-RE (70.6)Y[b]	4.1	1.0	659	0.74

[a] N_2 adsorption
[b] The percentage of RE^{3+} exchange in H-Y is given in the parenthesis.

Table 2.2b Acid sites distribution

Zeolites	NH_3 desorbed (mmol/g) at different temperature (K)					NH_3 chemisorbed at 303 K (mmol/g)
	303-353	353-433	433-513	513-653	653-773	
H-ZSM-5	0.55	0.16	0.05	0.26	0.21	1.23
H-mordenite	0.20	0.17	0.15	0.12	0.07	0.71
H-beta	0.14	0.24	0.05	0.16	0.16	0.75
H-Y	0.29	0.55	0.49	0.11	0.01	1.45
H-RE (70.6)Y	0.17	0.10	0.26	0.11	0.10	0.74

All the zeolite samples consisted of particles of about 0.2 – 1.0 μm size. The properties as well as chemical composition of the zeolites used in the present study as

obtained by a combination of wet chemical analysis and atomic absorption spectroscopy (AAS) and X-ray fluorescence spectroscopy (XRF) are reported in Table 2.2a and Table 2.3.

The results of the stepwise thermal desorption of ammonia from the zeolite catalysts are presented in Table 2.2b. Though, TPD of ammonia, do not reveal the qualitative information about the acid sites, (whether Lewis or Bronsted), this method can suggest the weaker/stronger nature of acid sites depending upon the desorption range. Zeolite H-ZSM-5 and H-Y having SiO_2/Al_2O_3 ratio 40 and 4.1, respectively, show acid sites concentration nearly similar (>1.2 mmol/g). H-mordenite, H-beta, and RE-Y show acid site concentration nearly similar (~0.7 mmol/g). H-Beta catalyst exhibits higher acid strength, which was evident from higher conversion of the reactant than other zeolite catalysts, which was having higher acid sites concentration. Higher the desorption temperature of ammonia, stronger the strength of the sites present in the catalyst.

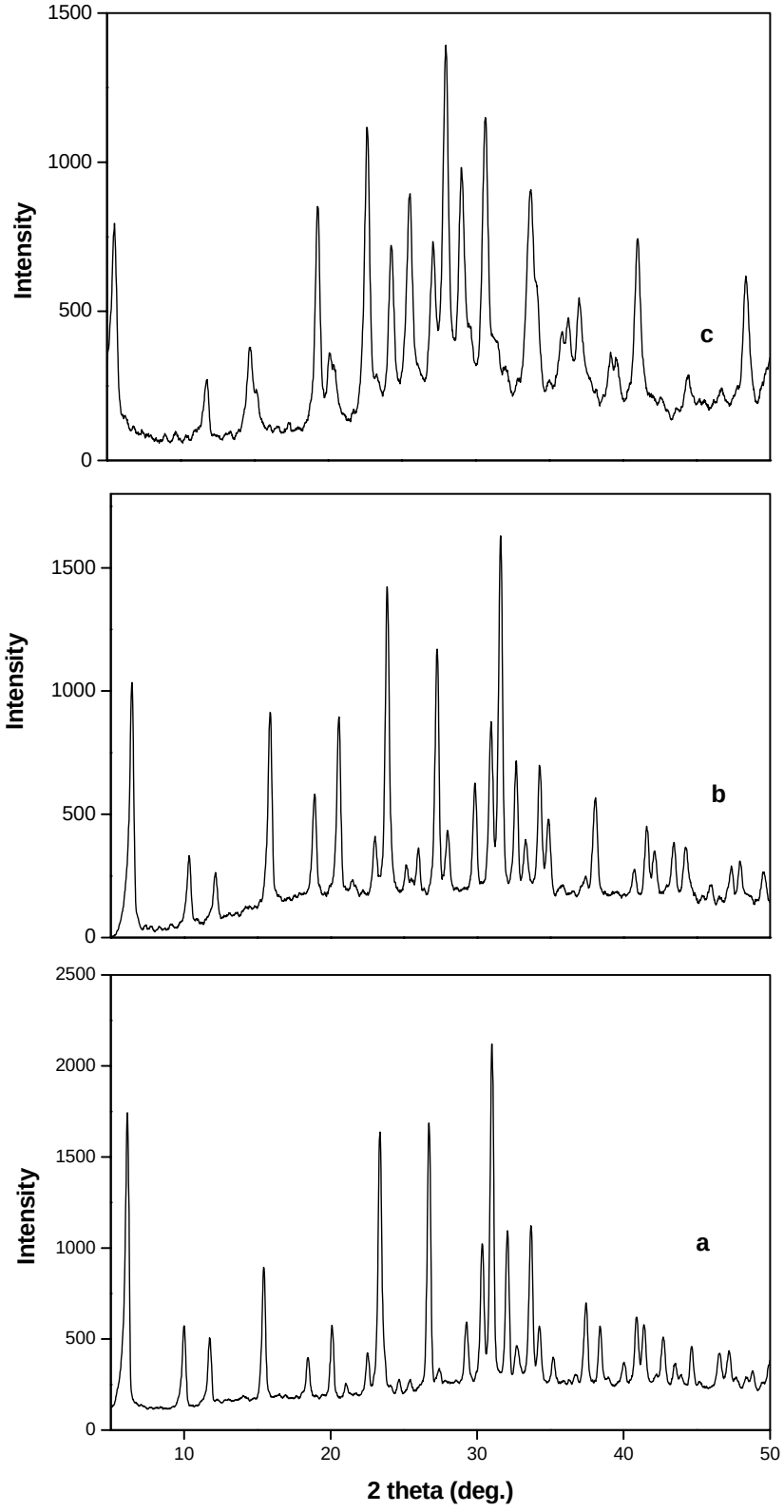

Fig. 2.1. X-ray diffractograms of zeolites (a) Na-X (b) Na-Y and (c) K-L

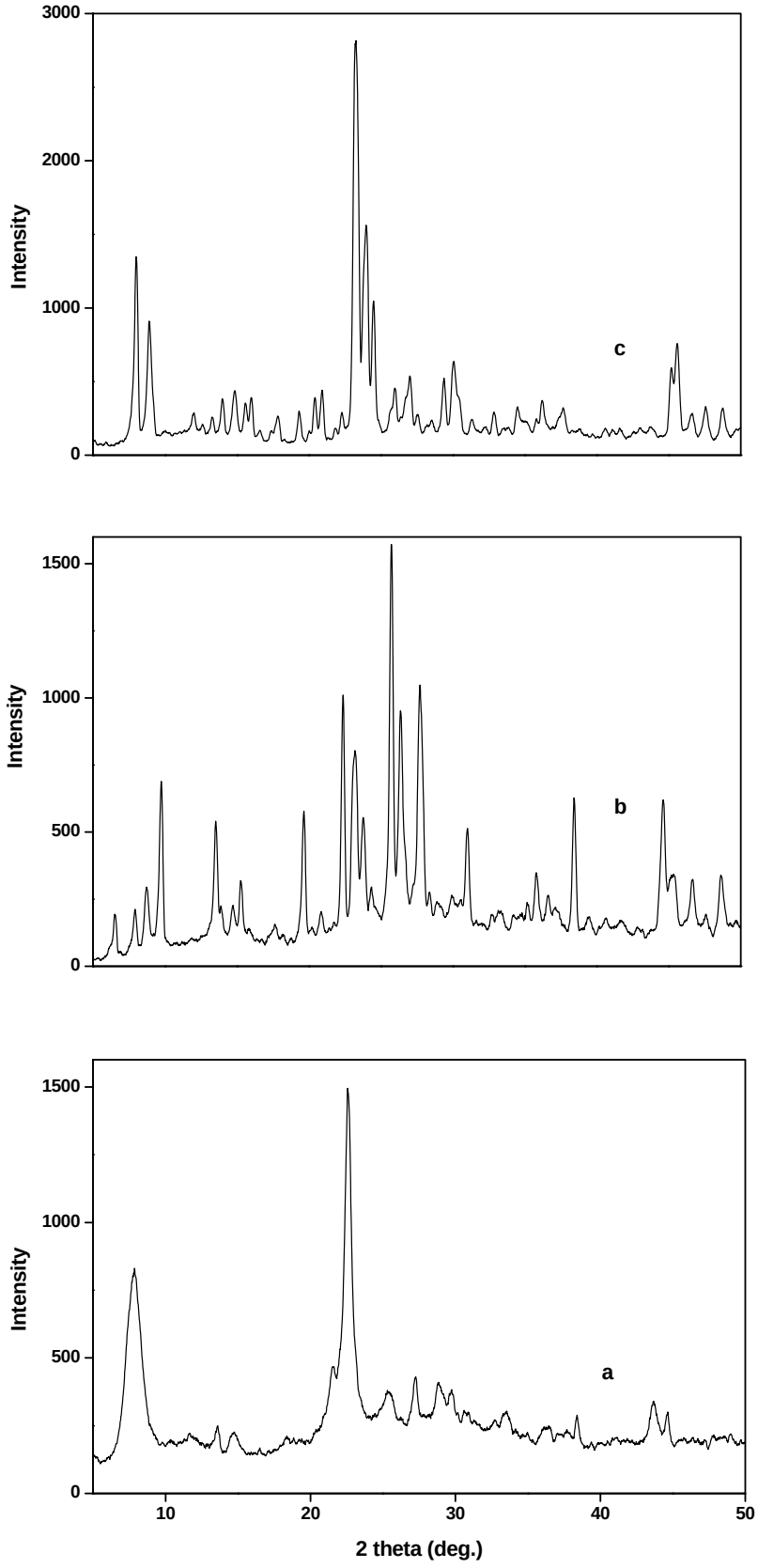

Fig. 2.2. X-ray diffractograms of zeolites (a) H-beta (b) H-mordenite and (c) H-ZSM-5

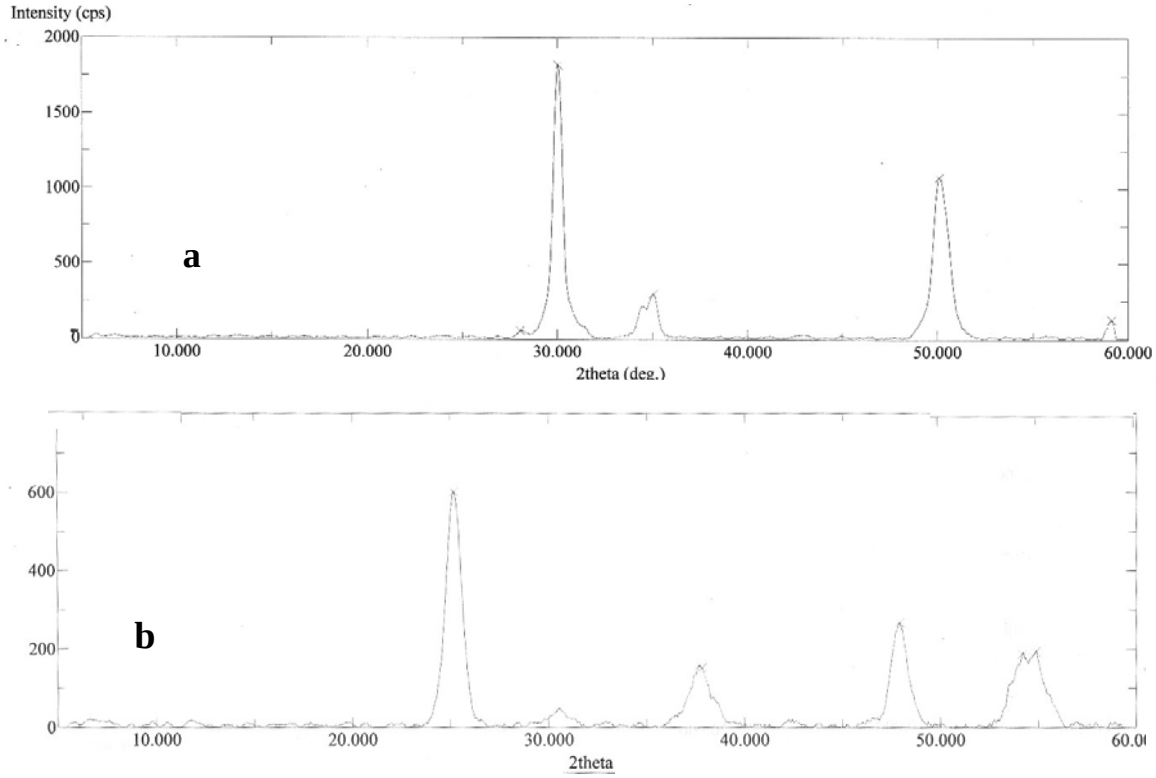

Fig. 2.3. X-ray diffractograms of (a) SO_4/ZrO_2 (b) SO_4/TiO_2

Table 2.3. Physical properties of the basic zeolites

Zeolites	SiO_2/Al_2O_3 (molar ratio)	Cation composition (wt.%)[a]			Surface area[b] (m^2/ g)	Crystal size (μm)
		H^+	Na^+	K^+		
K-X	2.4	-	7.4	92.6	615	1.0
K-Y	4.1	-	7.2	92.8	606	1.0
K-beta	26.0	9.8	4.3	85.9	743	0.5
K-L	6.8	-	1.4	98.6	215	0.2
Na-Al-MCM-41	33	-	98.2	1.8	1243	0.5
K-Na-Al-MCM-41	33	-	25.1	74.9	540	0.5

[a] Na^+ and K^+ ions were analyzed by XRF. H^+ was obtained by the difference between the Al content and the sum of the alkali metal values. Values are reported as percent of the total cation sites with Al content taken as 100%.

[b] Measured by N_2 adsorption; [c] Value in parenthesis represent the percentage of H^+ in K-L.

Fig. 2.4 shows the XRD patterns of the mesoporous catalysts, Na-Al-MCM-41, K-Na-Al-MCM-41, NH_2-Na-Al-MCM-41 (7.5) and NH_2-Si-MCM-41 (7.5). K-Na-Al-MCM-41 shows decrease in peak intensity as well as *d* spacing compared to Na-Al-MCM-41, which may be due to decrease in long-range order. Earlier studies on the influence of different alkali cations (Li^+, Na^+, K^+) on the structural properties of the gels, showed that the presence of "structure forming" Li^+ and Na^+ ions in the batch induces the formation of structural subunits, or even more complex structures inside the gel matrix, while the concentration of sub structural units is considerably lower when the gel is precipitated in the presence of 'structure breaking" K^+ ions [10]. The same fact can be anticipated here when the catalyst was ion-exchanged with KNO_3 solution, local subunits in the amorphous MCM-41 walls get degraded with K^+ ions. Surface area of the samples, K-Na-Al-MCM-41 was also found to be lower as compared to the parent Na-Al-MCM-41, which can be attributed to the formation of bulk potassium silicates and aluminates. The above fact was also confirmed by the elemental analysis where SiO_2/Al_2O_3 ratio decreases almost to half suggesting that potassium silicates and aluminates formed during the ion exchange. Removal of part of framework aluminum and silicon caused degradation of long-range order and surface area (Table 2.3).

3-Aminopropyltriethoxysilyl molecules are attached to the mesoporous support similarly to the self-assembled monolayers on flat surfaces by co-condensation and assembling techniques [11]. There are three types of ≡ SiOH groups over siliceous MCM-41 surface [12], e.g. isolated single, hydrogen bonded and geminal ≡ SiOH groups, of which only the single and geminal ≡ SiOH groups are responsible for active silylation. The hydrolysis of required composition of 3-aminopropyltriethoxysilane and tetraethoxysilane (0.05-0.3 and 0.095-0.7, respectively) in the presence of tetramethylammonium hydroxide enriches the mother liquor with single and geminal ≡ SiOH monomer silica species. Co-

condensation of symmetrical $Si(OH)_4$ and unsymmetrical $RSi(OH)_3$ species results to the formation of uniformly distributed organo functionalized silica.

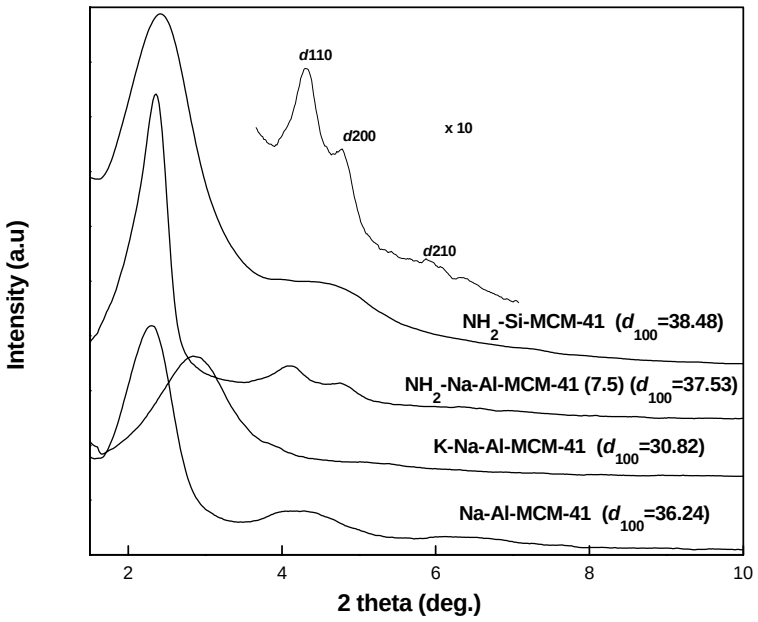

Fig. 2.4. X-ray diffractograms for various MCM-41 catalysts.

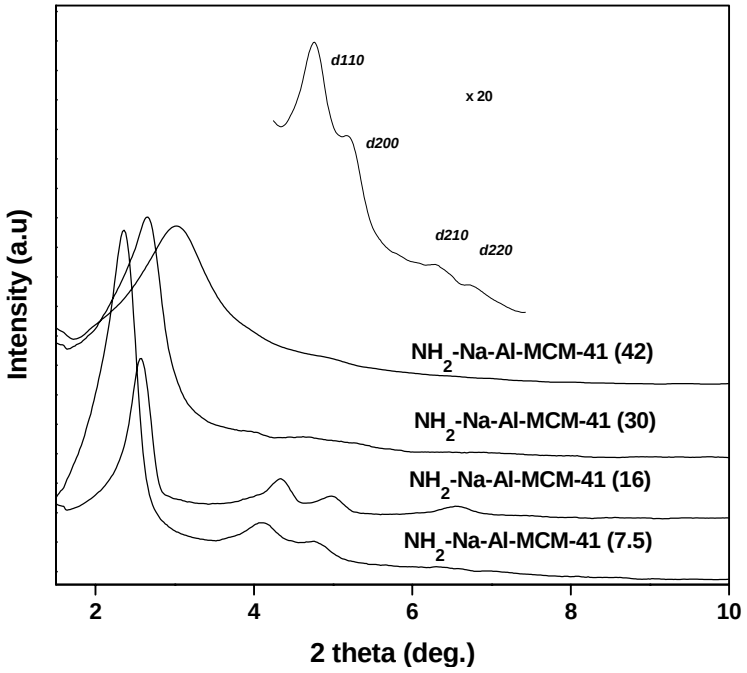

Fig. 2.5. X-ray diffractograms of various amounts of APTES functionalized Na-Al-MCM-41 catalysts.

The XRD pattern of NH_2-Na-Al-MCM-41 (7.5), NH_2-Na-Al-MCM-41 (16) show an intense peak due to d_{100} reflection, at 2θ between 2.0 and 2.5 accompanied by weaker reflections at 2θ between 4.0° and 6.5°, corresponding to the d_{110}, d_{200} and d_{210} spacing (hexagonal symmetry p6mm) which are characteristic peaks of MCM-41 [13](Fig. 2.5). It is clearly seen from the Fig. 2.5 that as the loading increases in samples, NH_2-Na-Al-MCM-41(30), NH_2-Na-Al-MCM-41 (42), the *d* value as well as peak intensity deceases proportionally indicating the reduction in pore size and long-range order. Higher the amount of organo silane loaded, larger the degradation of mesoporous structure.

MCM-41 gives type IV isotherms, typical of mesoporous solids [Fig. 2.6]. Adsorption at low pressure (p/p_0~0.35-0.45) is accounted for by a thin layer of the adsorbed gas on the walls of mesopores. The fact that the sudden increase in the volume of gases adsorbed in the range of relative pressure p/p_0 of, which is typical volume filling of mesopores by the process of capillary condensation [14]. The desorption branch of the isotherm carries more information about the degree of channel blocking than does adsorption branch, and best results are obtained from the BJH formula [15]. Surface area, 550 m^2g^{-1}, and average pore diameter, 32 Å, were found to be comparable with the earlier reported samples. The transmission electron microscope photographs of NH_2-Na-Al-MCM-41 (30) exhibits irregular mesoporous channels with diameters in the range of 3-8 nm (Fig. 2.7).

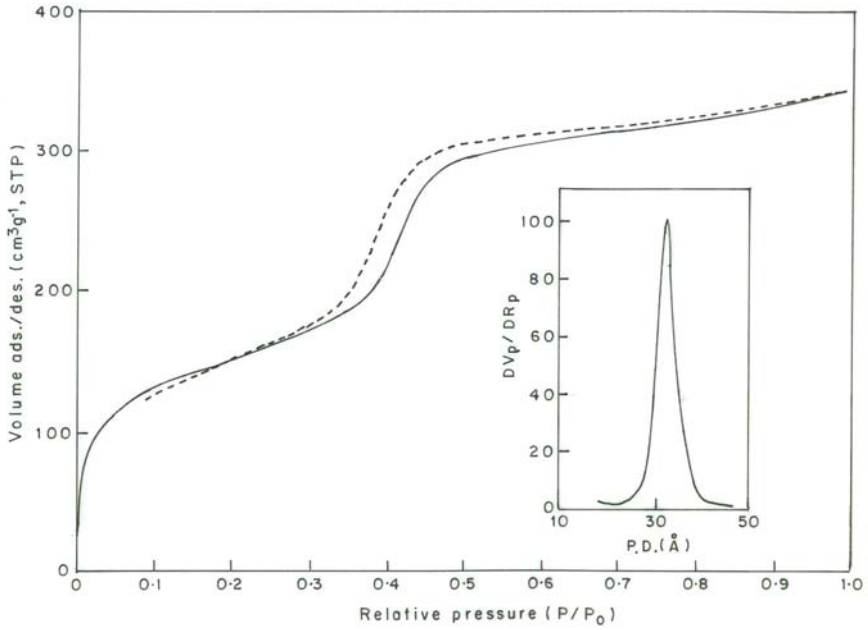

Fig. 2.6 Nitrogen adsorption-desorption isotherms and pore size distribution (inset) for NH_2-Na-Al-MCM-41 (30). Solid line: adsorption and dotted line: desorption.

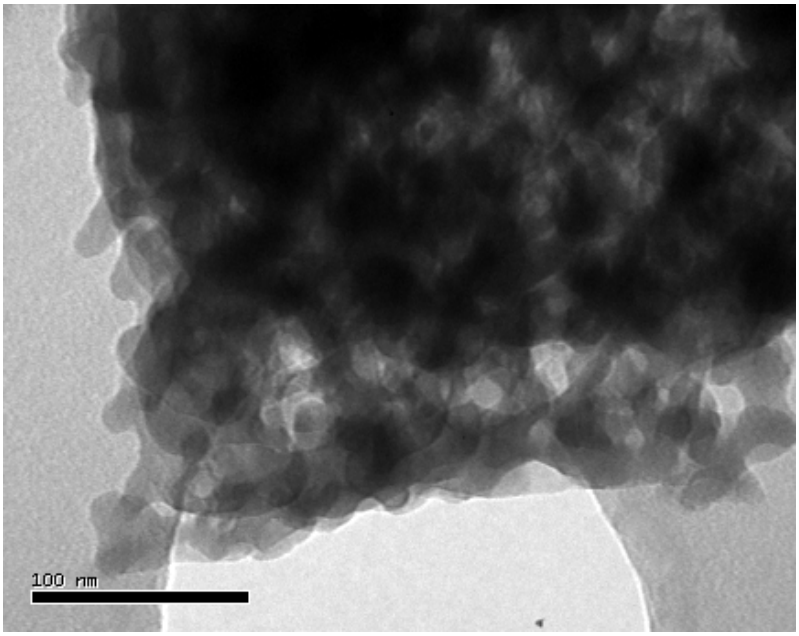

Fig. 2.7. TEM photographs of NH_2-Na-Al-MCM-41 (30)

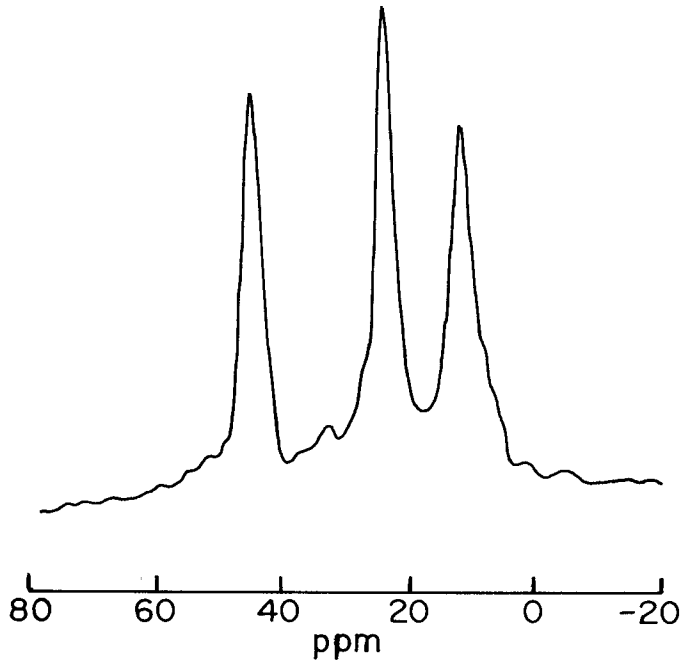

Fig. 2.8. ^{13}C CP-MAS NMR spectrum of NH_2-Na-Al-MCM-41 (30).

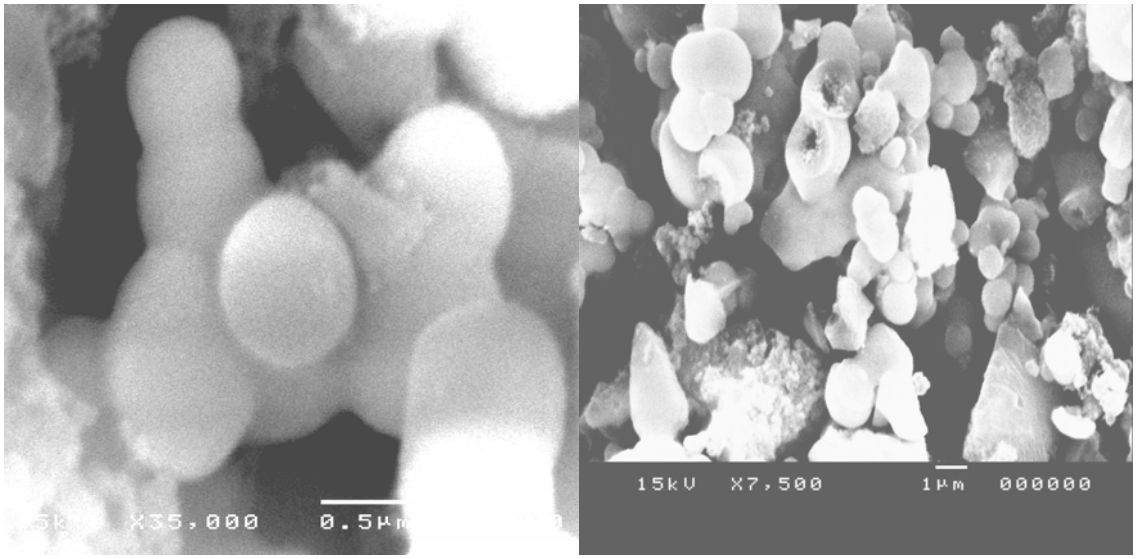

Fig. 2.9. SEM photographs of NH_2-Na-Al-MCM-41 (30).

^{13}C CP-MAS NMR spectrum of NH_2-Na-Al-MCM-41 (30) shows the characteristic of three carbons in the propyl chain anchored on the mesoporous walls (Fig. 2.8). The solid state ^{13}C CP-MAS NMR chemical shift (ppm) for NH_2-Na-Al-MCM-41(30) is found to be: ≡Si-$^{\alpha}CH_2$-$^{\beta}CH_2$- $^{\gamma}CH_2$-NH_2: $^{\alpha}$C:10.3; $^{\beta}$C: 23.7; $^{\gamma}$C:43.2. The scanning electron microscope photographs of NH_2-Na-Al-MCM-41 (30) exhibits uniform and spherical shaped crystals with crystal size, 0.2 μm. (Fig. 2. 9).

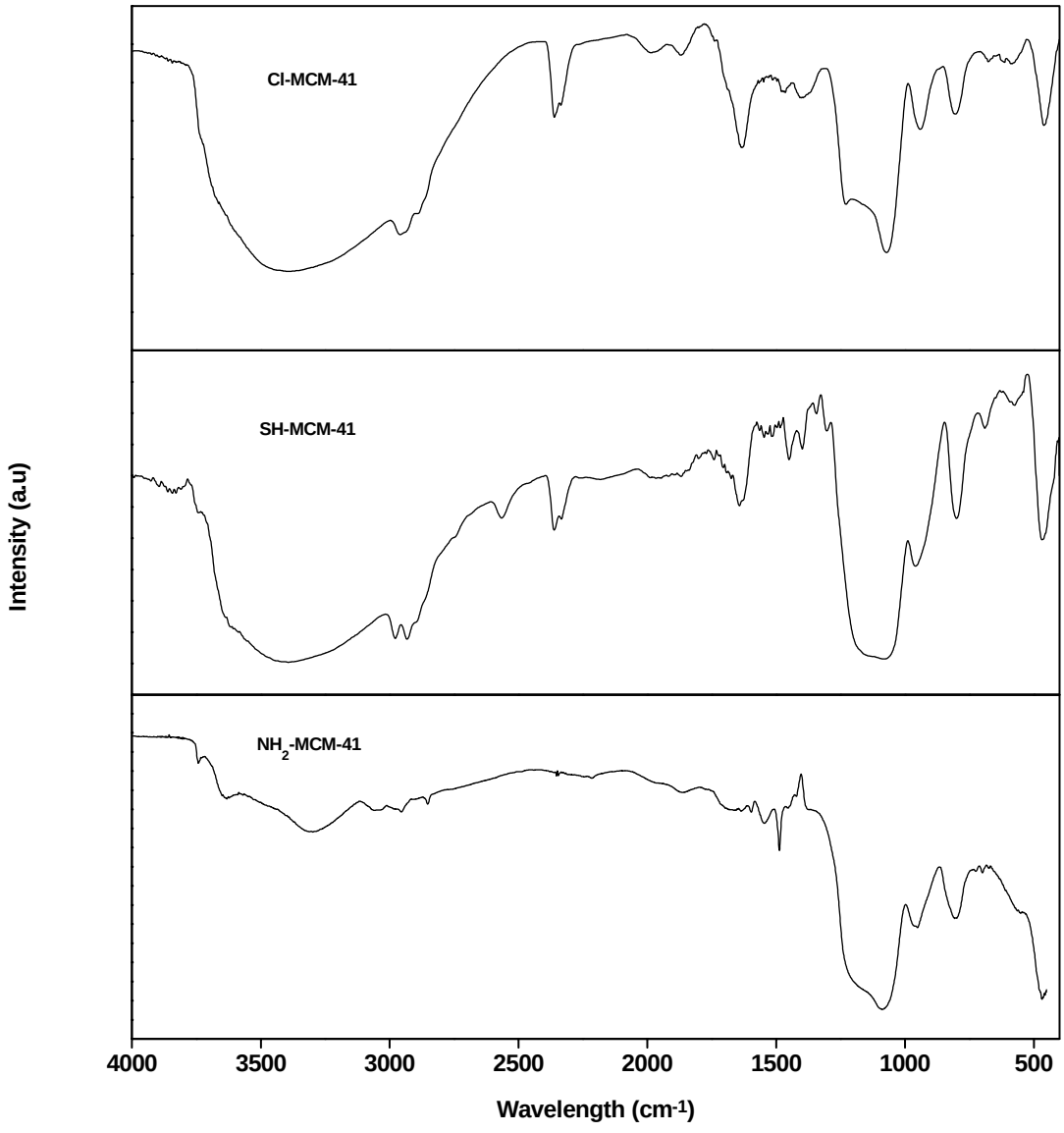

Fig. 2.10. FT-IR spectra of Cl-MCM-41, SH-MCM-41 and NH_2-MCM-41

Fig. 2.10 shows the FT-IR spectra of Cl-MCM-41, SH-MCM-41 and NH_2-MCM-41 materials. The characteristic stretching band of $–NH_2$ and –SH group is clearly seen around 3370 cm^{-1} and 2570 cm^{-1}, respectively. The stretching bands around 2800-2950 cm^{-1} in all the three samples are due to C-H bond of organo silane. Similarly the stretching bands between 800 and 1200 cm^{-1} due to mesoporous Si-O-Si bond are also clearly identified.

2.4. Conclusions

Zeolites such as Na-beta, Na-ZSM-5, and K-L have been synthesized by hydrothermal method. The commercially obtained Na-X, Na-Y and Mordenite along with the synthesized Na-beta, Na-ZSM-5 were ion-exchanged with NH_4NO_3 solution and activated at 793 K for 6 h to get respective H-forms. Na-X and Na-Y were exchanged with KNO_3 (1 M solution) and $CsNO_3$ (0.1 M solution) to get K-X, K-Y, Cs-X and Cs-Y, respectively. Synthesized zeolites were characterized by wet chemical analysis, XRD, N_2 adsorption, EDX, and SEM analysis. Mesoporous materials were prepared by reflux method. Si-MCM-41, and Na-Al-MCM-41 were used as the basic supports for organo functional groups such as APTS, ClPTS and MPTS. The attachment of organo functional molecules to the mesoporous silica walls has been achieved by the direct reaction of surface hydroxyl groups with reactive alkoxy groups of organosilanes. Fraction of organo functionalized silicon atom has been varied from 0.03 to 0.3 in the synthesis gel to get maximum concentration of organofunctionalized group inside the mesopores. It was observed that above the optimum level of concentration of organo functionalized silicon atom, there is gradual decrease in the structural integrity. The maximum fraction of organo functionalized silicon atom attached into the mesoporous silica walls were achieved up to 0.2. XRD, FT-IR, UV-vis, 13C-CPMAS NMR, SEM, TEM, N2 adsorption/desorption and thermal analysis characterized the mesoporous materials.

2.5. References

1. P. Ratnasamy, R.N. Bhat, S.K. Pokhriyal, S.G. Hegde, R. Kumar, J. Catal. **119** (1989) 65; M. A. Cambler, J. Perez Pariente, Zeolites **11** (1991) 202.
2. R.J. Argauer, G.R. Landolt, US Patent, 3 702 886 (1972).
3. P.N. Joshi, A.N. Kotsthane, V.P. Shiralkar, Zeolites **10** (1990) 598.
4. R.A. A. Melo, M.V. Giotto, J. Rocha, U.A. Urquieta-Gonzalez, Mater. Res. **2** (1999) 173.
5. V.V. Dunia, L.G. Kuz'mina, M.Y. Kazakova, O.N. Gorunova, Y.K. Grishin, E.I. Kazakova, Eur. J. Inorg. Chem. (1999) 1029.
6. J.B. Cohen, L. H. Schwartz, Diffraction from Materials, Academic Press, New York, 1977.
7. M. Chamumi, D. Brunel, F. Fajula, P. Geneste, P. Moreau, J. Solof, Zeolites **14** (1994) 283.
8. A.P. Singh and D. Bhattacharya, Catal. Lett. **32** (1995) 327.
9. A.P.Singh, D. Bhattacharya, S. Sharma, Appl. Catal. A: General **150** (1997) 53.
10. R.Aielo, F.Crea, A.Nastro, B. Subotic, F. Testa, Zeolites **11** (1991) 767.
11. J. Liu, X. Feng, G.E. Fryxell, L. Q. Wang, A.Y. Kim, M. Gong, Adv. Mater. **10** (1998) 161.
12. X.S. Zhao, G.Q. Lu, J. Phys. Chem. B **102** (1998) 1556.
13. J.S. Beck, J.C. Vartulli, W.J. Roth, M.E. Leonowicz, C.T. Kresge, K.D. Schmitt, C.T.W. Chu, D.H. Olson, E.W. Sheppard, S.B. McCullen, J.B. Higgins, J.L. Schlenker, J. Am. Chem. Soc. **114** (1992) 10834.
14. C.F. Cheng, D.H. Park, J. Klinowski, J. Chem. Soc., Faradaz Tans. **93** (1997) 193.
15. P.T. Tanev, L. T. Vlaev, J. Colloid Interface Sci., **160** (1993) 110.

3.1. Benzoylation of biphenyl

3.1.1. Introduction

4-Phenylbenzophenone is used as an important intermediate in the pharmaceutical and agrochemical industry [1]. In addition, 4-PBP is also used in the synthesis of photo chromic naphthopyran compounds for the coatings of lenses and other optical materials [2], and as a photo initiator [3]. Acylation of biphenyl with acyl halides, which is a typical example of Friedel-Crafts acylation, is generally known to proceed over the homogeneous Lewis acid catalyst $AlCl_3$. 4-PBP is prepared in 74% yield by treatment of benzoyl chloride with $AlCl_3$ in $CHCl_3$ at room temperature, followed by addition of biphenyl into refluxing solution of complex of benzoyl chloride with $AlCl_3$ [4]. Either trace amounts of $FeCl_3$, Fe acetylacetonate and salicylate, powder of Fe or $Fe_2(SO_4)_3$ catalyses the benzoylation of biphenyl, giving 61 to 84 % yield of 4-PBP with 100% selectivity at 393-448 K [5]. A detailed investigation of Friedel-Crafts reaction on biphenyl was carried out by Adam [6]. The *ortho*- and *meta*-phenylacetophenones were prepared from acetic anhydride by the low temperature Grignard procedure [7,8]. In a rather extensive investigation Silver and Lowy [9] and Long and Henze [10] have shown conclusively that acylhalides reacts with biphenyl in the Friedel-Crafts reactions to form 4-monoacetylbiphenyl and 4,4'-diacetylbiphneyl products. 4-Phenylacetophenone is also prepared by the acetylation of biphenyl with acetic anhydride in the presence of anhydrous HF and BF_3 [11]. The use of Lewis acid catalysts is fraught with problems, such as their handling, the necessity of using large amounts with substrates and separation from the products. Some catalysts are toxic. In addition, halides of iron and aluminum, being strong Lewis acids also, catalyze other undesirable reactions such as isomerization and trans-alkylation reactions. In view of the above, it was of interest to

develop a new solid catalyst for the selective synthesis of 4-phenylbenzopheneone, 4-phenylpropiophenone and 4-phenylacetophenone (Scheme 3.1).

Zeolite catalysts, due to their shape-selectivity, thermo stability, the easy separation from the products and the possibility of regeneration of the deactivated catalysts, are used extensively in the petroleum refining and petrochemical industries for various cracking, hydrocracking, isomerization, alkylation, dehydrogenation and rearrangement reactions of hydrocarbons and their derivatives [12]. The use of zeolite catalysts in the synthesis of fine chemicals is of growing importance in recent years [13]. Recently, zeolite catalysts were found to be active in the acylation of aromatics [14-29]. Acylation of biphenyl under various reaction conditions and effect of some variables on catalyst performance was investigated. The results obtained over zeolite catalyst are compared with those obtained using the Lewis acid catalyst, $AlCl_3$.

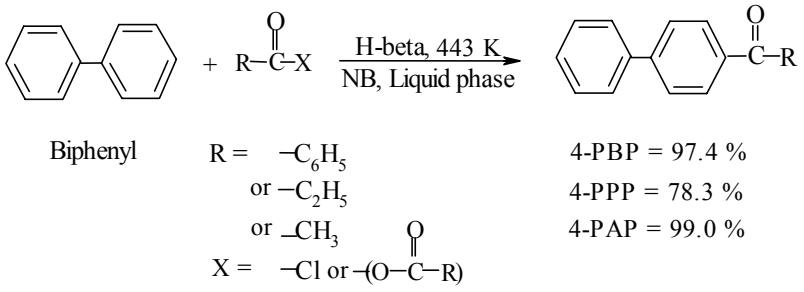

Scheme 3.1

3.1.2. Experimental

Anhydrous AR grade chemicals were used without further purification. The liquid phase acylation of biphenyl with acylating agent was carried out in a 50 ml two necked flask attached to a condenser and a septum. The temperature of the reaction vessel was maintained using an oil bath. In a typical run, to a nitrobenzene (NB) solution (20 ml) of biphenyl (10 mmol) and acylating agent (10 mmol) was added activated zeolite catalyst (0.5 g). The

reaction mixture was magnetically stirred and heated to the required temperature at atmospheric pressure.

3.1.3. Results and Discussions

3.1.3.1. Catalytic activity of various catalysts

The results of the catalytic activities in the benzoylation of biphenyl with benzoyl chloride using H-beta, H-ZSM-5, H-Y and RE-Y are depicted in Table 3.1. The results with Lewis acid catalyst, $AlCl_3$, are compared under identical reaction conditions. The main product of the reaction is 4-PBP. A small amount of 2-PBP is also observed in some cases. The activities of catalysts are compared using data after 6 h runs.

Table 3.1 Benzoylation of Biphenyl

Catalyst	Reaction time (h)	Biphenyl Conv. (%)[a]	TOF[b] (10^{-5} $s^{-1}mol^{-1}$ Al)	Product distribution[c] (%)		4-/2-[d] PBP
				2-PBP	4-PBP	
H-beta	6	41.0	31.7	2.6	97.4	37.4
	12	58.3	22.5	2.7	97.3	36.1
H-ZSM-5	6	5.2	6.0	0	100	0
	12	9.0	5.2	0	100	0
RE[e]-Y	6	3.4	0.5	0	100	0
	12	7.5	0.6	0	100	0
H-Y	6	3.2	0.5	0	100	0
	12	5.6	0.5	0	100	0
$AlCl_3$	0.5	48.6	72.1	20	80	4.0
	1	63.2	46.8	20	80	4.0

[a] Reaction conditions: catalyst (g) = 0.5; biphenyl (mol) = 0.01; benzoyl chloride (mol) = 0.01; nitrobenzene (mL)=20; reaction temperature (K) = 443; [b] TOF (turnover frequency) = moles of BP transformed per second per mol of aluminum; [c] 2-PBP = 2-phenyl-benzophenone; 4-PBP = 4-phenylbenzophenone; [d] ratio of 4-phenylbenzophenone / 2-phenylbenzophenones; [e] 70.6% RE^{3+}-exchange in NH_4-Y-zeolite

The most interesting feature of the reaction is that conversion of BP, rate of BP conversion, product distribution and 4-PBP to 2-PBP ratio depend on the type of zeolite used. As can be seen from the Table 3.1, zeolite H-beta is found to be more active than any other zeolite. The H-ZSM-5, RE-Y and H-Y are less active and have almost identical activities. The conversion of BP, rate of BP conversion and selectivity for 4-PBP over H-beta, H-ZSM-5, RE-Y and H-Y after 6 h of reaction time are found to be 41.0, 5.2, 3.4, 3.2 (%), 31.7, 6.0, 0.5, 0.5 ($10^{-5}s^{-1}mol^{-1}Al$) and 97.4, 100, 100, 100 (%), respectively. $AlCl_3$ produces 20 % 2-PBP and 80 % 4-PBP at 48.6 % conversion level of BP at 0.5 h reaction time. The 4-PBP/2-PBP ratio was found to be about ten times higher (4-/2- = 37.4) over H-beta than that of non shape-selective Lewis acid $AlCl_3$ catalyst (4-/2- = 4.0). Among the zeolites studied, H-beta revealed the highest PBP yield and rate of BP conversion, which may be attributed to its stronger acid sites (Table 2.2) as seen from NH_3 desorption experiment. With the increase the amount of strong acid sites, the conversion of BP enhances, which means that medium and strong acid sites of H-beta promoted the reaction. Being large pore and weaker acid sites, HY and RE-Y showed less PBP yield for the same reaction. The lower yield of PBP over H-ZSM-5 in the benzoylation of BP may be attributed to its pore openings being smaller than the size of the products. The catalysts used in this study, show the following decreasing order of activity after 6h of reaction time: $AlCl_3$ > H-beta > H-ZSM-5 > RE-Y ≈ H-Y. The results indicate that mainly ortho- and para- substitutions take place over zeolite H-beta, which is expected for an electrophilic aromatic substitution pathway. Acidic zeolites polarize the benzoyl chloride into an electrophile ($C_6H_5CO^+$), which attacks on the aromatic ring, resulting in the formation of phenylbenzophenones [30-32].

3.1.3.2. Influence of reaction time using zeolite H-beta

A typical reaction course according to the time is pointed out in Fig. 3.1 for the transformation of biphenyl over zeolite H-beta at 443 K. The conversion of biphenyl increased almost linearly up to 8 h of reaction time and then a marginal increase in the conversion of BP is observed. BP leads mainly to 4-PBP in 97.6% selectivity at 15 min. reaction time and remains almost unchanged up to 12 h. A small amount of 2-PBP is also observed until the end of the reaction. The results show that the reaction time influenced the conversion of BP, but did not affect the 4-PBP / 2-PBP isomer ratio to a great extent.

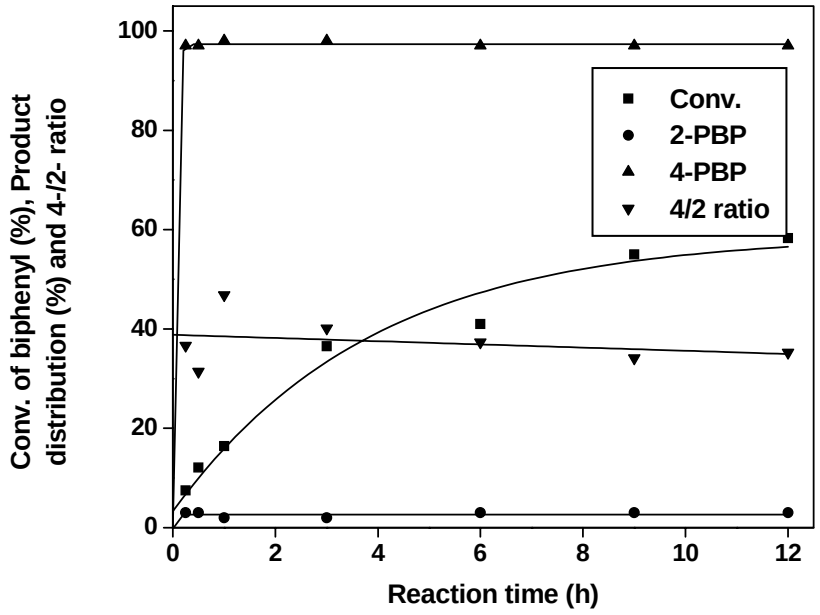

Fig. 3.1. Effect of reaction time on conversion of BP (%), product distribution (%) and 4-PBP/2-PBPP ratio using H-beta as catalyst**.** Reaction conditions: catalyst (g) = 0.5; biphenyl (mol) = 0.01; benzoyl chloride (mol) = 0.01; nitrobenzene (mL)=20; reaction temperature (K) = 443.

3.1.3.3. Influence of H-beta / BP (wt./wt.) ratio

In order to clarify the effects of catalyst concentration on the conversion of BP, rate of BP conversion and product distribution, the catalyst concentration (H-beta / BP ratio (w/w))

was increased from 0.06 to 0.49 (Fig.3.2). A sharp increase in the conversion of BP is observed when H-beta / BP (wt./wt.) ratio was raised from 0.06 to 0.19. Afterwards, a slow but steady increase in the conversion of BP is noticed in the benzoylation of BP. No change in the product distribution is seen due to the change in catalyst concentration. A marginal increase in the rate of BP conversion (TOF) is seen up to 0.19 ratio of H-beta to BP, whereas it decreases continuously and linearly due to the increase in catalyst concentration and a corresponding increase in the concentration of aluminum in the total amount of zeolite H-beta used in the benzoylation of BP. The maximum increase in the conversion of BP with reaction time is found for a H-beta / BP (wt./wt.) ratio of 0.49.

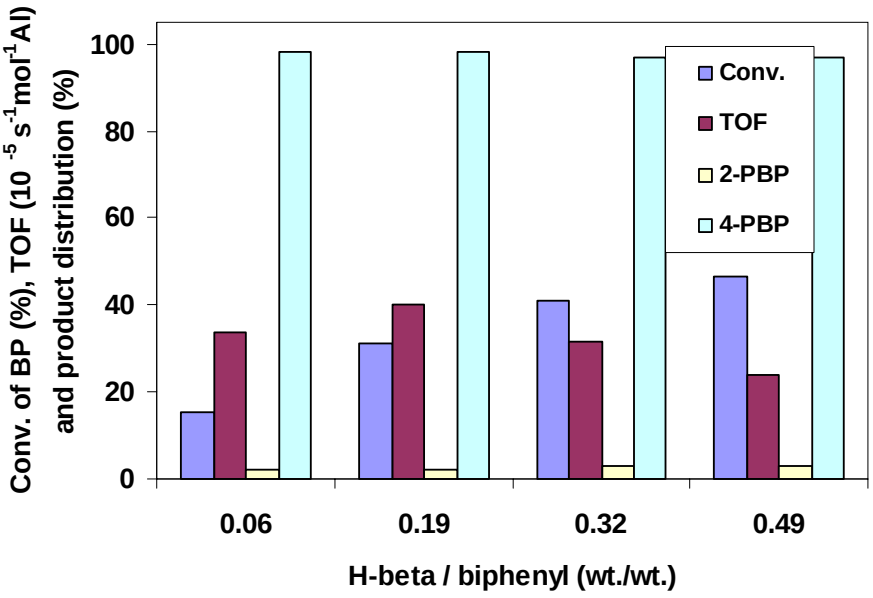

Fig. 3.2. Effect of beta/BP (wt./wt.) on conversion of BP (%), TOF ($10^{-5}s^{-1}mol^{-1}Al$) and product distribution (%). Reaction conditions: biphenyl (mol) = 0.01; benzoyl chloride (mol) = 0.01; nitrobenzene (mL)=20; reaction temperature (K) = 443; reaction time (h)=6.

3.1.3.4. Influence of reaction temperature

The effect of reaction temperature is studied on the conversion of BP, rate of BP conversion and product distribution in the benzoylation of BP. The results are depicted in Fig.

3.3. When the temperature is increased from 433 to 453 K, both the conversion of BP and rate of BP conversion increased from 6.7 to 46.4 %and 5.2 to 35.8 ($10^{-5}s^{-1}mol^{-1}Al$), respectively.

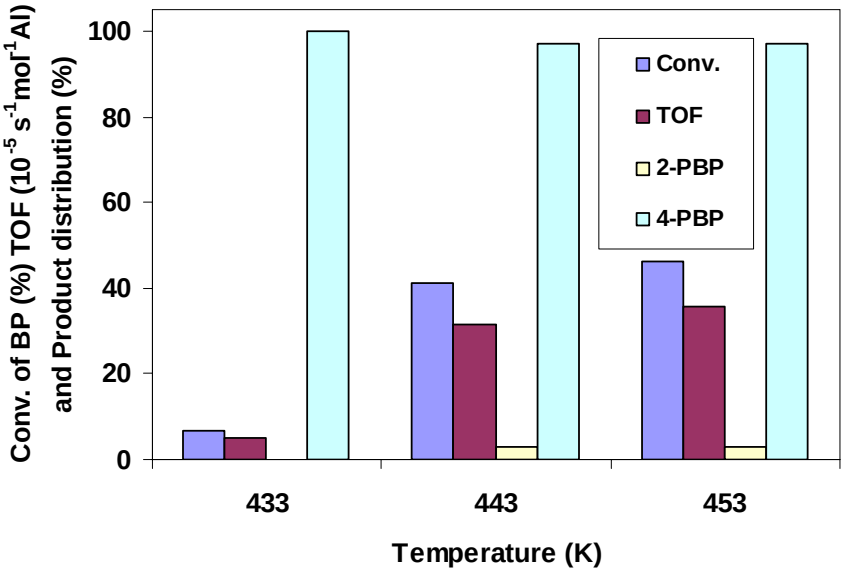

Fig. 3.3. Effect of reaction temperature on conversion of BP (%), TOF ($10^{-5}s^{-1}mol^{-1}Al$) and product distribution (%). Reaction conditions: biphenyl (mol) = 0.01; benzoyl chloride (mol) = 0.01; H-beta catalyst (g)=0.5; nitrobenzene (mL)=20; reaction time (h)=6.

However, the selectivity for 4-PBP remains nearly unchanged with the increase in reaction temperature, as shown in Fig. 3.8. The conversion of BP at various reaction temperatures over a period of 12 h using zeolite H-beta increases sharply at the initial stages of the reaction and finally reaches a relatively steady state value over all temperatures.

3.1.3.5. Influence of BOC / BP molar ratio

Figure 3.4 exhibits the effect of the BOC / BP molar ratio on the catalytic activity of H-beta. The ratio is changed while keeping the amount of biphenyl constant. The data at 443 K show that, as the BOC / BP molar ratio is increased from 0.3 to 2, the conversion of BP and rate of BP conversion increase linearly from 21.2 %and 16.4 ($10^{-5}s^{-1}mol^{-1}Al$) to 58.6% and

45.2 ($10^{-5}s^{-1}mol^{-1}Al$), respectively. In addition, the selectivity to 4-PBP is found to be unaffected over the wide range of BOC / BP ratio. The conversion of BP vs. reaction time increased with all molar ratios of BOC/BP, and the fact that the conversion of BP is also

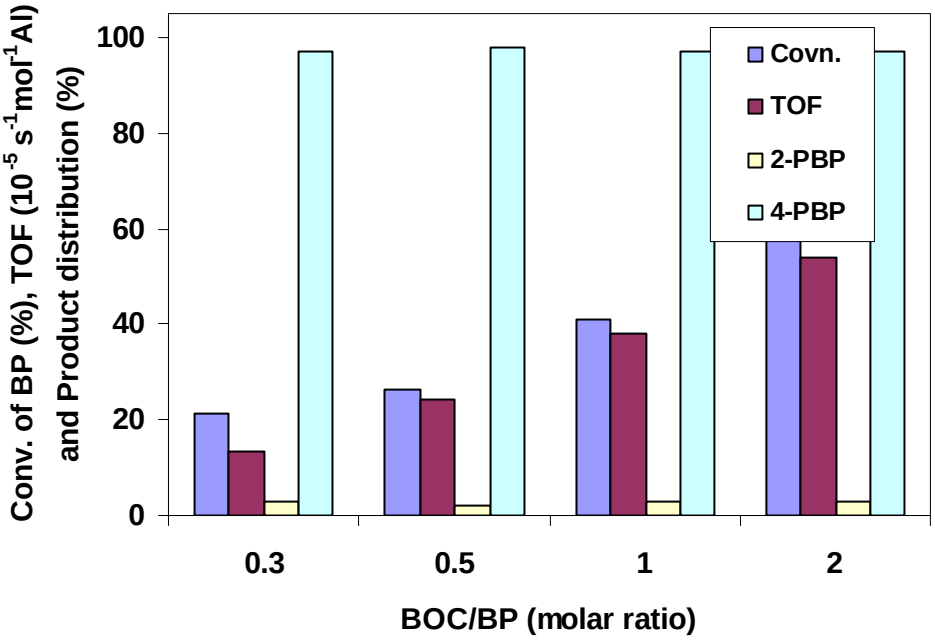

Fig.3.4. Effect of BOC/BP molar ratio on conversion of BP (%), TOF ($10^{-5}s^{-1}mol^{-1}Al$) and product distribution (%). Reaction conditions: biphenyl (mol) = 0.01; H-beta catalyst (g)=0.5; nitrobenzene (mL)=20; reaction time (h)=6; reaction temperature (K)= 443.

stabilized from an early stage till 7 h of the reaction time. A higher increase in the BP conversion with reaction time is observed when BOC/BP molar ratio of two is used in the benzoylation of biphenyl.

3.1.3.6. Acetylation, propionylation and benzoylation of biphenyl

The results of the benzoylation of biphenyl are compared at 443 K with the results of propionylation and acetylation of biphenyl using zeolite H-beta as catalysts and acyl halides (benzoyl chloride, propionyl chloride, and acetyl chloride, respectively) as acylating agents (Table 3.2). The propionylation and acetylation of biphenyl lead to the formation of 2-phenylpropiophenone (2-PPP), 4-phenylpropiophenone (4-PPP) and 2-phenylacetophenone

(2-PAP) and 4-phenylacetophenone (4-PAP), respectively. The conversion and rate of BP conversion in the acylation reactions under similar reaction conditions decrease in the following order: benzoylation > propionylation > acetylation.

Table 3.2 Influence of acylating agent

Agent	Conv. Of BP (%)[a]	TOF ($10^{-5}s^{-1}mol^{-1}$ Al)	Product distribution (%)[b]						4-/2-ratio[d]
			2-PBP	4-PBP	2-PPP	4-PPP	2-PAP	4-PAP	
C_6H_5COCl	41.0	31.7	2.6	97.4	-	-	-	-	37.4
$(C_6H_5CO)_2O$	30.3	23.4	2.0	98.0	-	-	-	-	49.0
C_2H_5COCl	11.1	8.6	-	-	21.7	78.3	-	-	3.6
$(C_2H_5CO)_2O$	10.1	7.8	-	-	0	100	-	-	0
CH_3COCl	6.7	5.2	-	-	-	-	1.0	99.0	99.0
$(CH_3CO)_2O$[e]	4.2	3.2	-	-	-	-	1.0	99.0	99.0

[a] Reaction conditions: Catalyst (H-beta) (g) = 0.5; Biphenyl (mol) = 0.01; acylating agent (mol) = 0.01; nitrobenzene (ml)=20; reaction temperature (K) = 443; reaction time (h) = 6
[b] 2-PBP = 2-Phenylbenzophenone; 4-PBP = 4-Phenylbenzophenone; 2-PPP = 2-Phenylpropiophenone; 4-PPP = 4-Phenylpropiophenone; 2-PAP = 2-Phenylacetophenone; 4-PAP = 4-Phenylacetophenone; [c] Ratio of 4-/2- isomer; [d] Reaction temperature (K) = 453.

The conversion of BP and rate of BP conversion in the benzoylation, propionylation and acetylation of biphenyl using acyl halides as acylating agents over zeolite H-beta are found to be 41.0, 11.1, 6.7 % and 31.7, 8.6 and 5.2 ($10^{-5}s^{-1}mol^{-1}$Al), respectively. The corresponding selectivity for 4-PBP, 4-PPP and 4-PAP are 97.4, 78.3 and 99.0%, respectively.

Acid anhydrides (benzoic anhydride, propionic anhydride and acetic anhydride) are also employed as acylating agents instead of acyl chlorides in the acylation of biphenyl. Acid anhydrides are also capable of acylating biphenyl. The conversion of BP and rate of BP conversion in the acylation of biphenyl with benzoic anhydride, propionic anhydride and acetic anhydride are found to be 30.3, 10.1, 4.2 %and 23.4, 7.8 and 3.2 ($10^{-5}s^{-1}mol^{-1}$Al),

respectively. The corresponding selectivity for 4-PBP, 4-PPP and 4-PAP is 98, 100 and 99%, respectively. The yield of PBP over zeolite H-beta in the acylation of biphenyl with acid chlorides and acid anhydrides decreases in the following order: Acid chlorides > Acid anhydrides.

As a function of reaction time over zeolite H-beta using various acylating agents, benzoyl chloride exhibited higher conversion of BP compared to the other acylating agents. The total conversion of BP reached 58.3% in 12 h using benzoyl chloride as benzoylating agent. Benzoic anhydride was found to be less active than BOC and only 38.3% conversion of BP is noticed after 12 h of reaction time. Other acylating agents gave much less conversion of BP. The conversion of BP after 12 h of reaction time with various acylating agents decreases in the following order: benzoyl chloride > benzoic anhydride > propionyl chloride > propionic anhydride > acetyl chloride > acetic anhydride.

3.1.3.7. Reaction mechanism

The classical Friedel-Crafts acylation is an electrophilic aromatic substitution in which an electron deficient species (electrophile) is generated by the activation of acyl chloride or acid anhydride on the protonic sites of the zeolite which then attacks the electron cloud in the aromatic ring resulting in the formation of aromatic ketones. Phenylbenzophenones are formed according to the following scheme (Scheme 3.2) [30-33]. Generally, kinetic studies reported in the literature [12] for alkylation or acylation of aromatics on acidic zeolites suggest that an Eley-Rideal mechanism is operative. According an Eley-Rideal-type mechanism, the considered reaction takes place between benzoyl chloride (BC) compulsory adsorbed on the catalyst site to form the surface electrophile and biphenyl (BP) from the liquid phase.

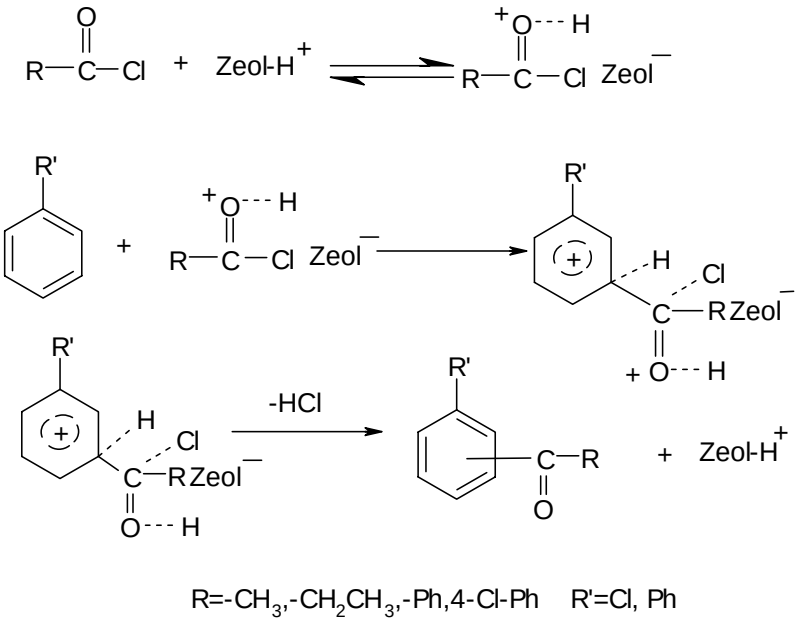

Scheme 3.2

3.1.3.8. Effect on catalyst recycling

In order to check the stability and catalytic activity of zeolite H-beta in the benzoylation of biphenyl, three reaction cycles (fresh and two cycles) were carried out using the same catalyst. The results are presented in Table 3.3. After workup of the reaction mixture, the zeolite H-beta was separated by filtration washed with acetone and calcined for 16 h at 773 K in the presence of air before use in the next experiment. Thus, the recovered zeolite after each reaction was characterized for its chemical composition by atomic absorption spectroscopy (AAS) and crystallinity by X-ray diffraction (XRD). AAS and XRD studies showed a downward trend in the content of aluminium and crystallinity of H-beta after each cycle. The 4-PBP yield decreases progressively on recycling and the conversion of BP decreases from 41 to 33.0 % when H-beta was recycled from fresh to second cycle, respectively, in the benzoylation of biphenyl. The hydrogen halide liberated during the reaction probably

promotes the extraction of aluminium to some extent from the framework positions of the zeolite H-beta. The loss of aluminium and a decrease in the crystallinity of zeolite H-beta may be attributed for the decrease in catalytic activity after each cycle. The results reported here are in good agreement with the benzoylation of aromatics using zeolite catalysts [27,32].

Table 3.3. Effect of catalyst recycling

Cycle	SiO_2/Al_2O_3 (molar ratio)	Conv. of BP (%)[a]	Product distribution (%)[b]		4-/2-ratio	H-beta crystallinity (%)[c]
			2-PBP	4-PBP		
Fresh	26.0	41.0	2.6	97.4	37.4	100
1st recycle	27.1	35.0	2.0	98.0	43.0	100
2nd recycle	33.7	33.0	3.0	97.0	37.3	92.8

[a] Reaction conditions: Catalyst (H-beta) (g) = 0.5; Biphenyl (mol) = 0.01; acylating agent (mol) = 0.01; nitrobenzene (ml)=20; reaction temperature (K) = 443; reaction time (h) = 6
[b] 2-PBP = 2-Phenylbenzophenone; 4-PBP = 4-Phenylbenzophenone.
[c] Determined by XRD.

3.1.4. Conclusions

Zeolite H-beta catalyzes the benzoylation of biphenyl efficiently and is superior to other zeolite catalysts. Higher selectivity to 4-PBP in the range of 97.4% is achieved at 41.0% conversion of BP over H-beta, whereas $AlCl_3$ gave lower selectivity to 4-PBP (80%) under similar reaction conditions. A higher strength of acid sites and medium pore size of H-beta are the responsible for the conversion of BP. The conversion of BP using zeolite H-beta increased significantly with an increase in reaction time, catalyst concentration, reaction temperature and BOC to BP molar ratio. The acetylation and propionylation of BP are also investigated along with benzoylation over zeolite H-beta catalyst with different acylating agents (BOC, benzoic anhydride, propionyl chloride, propionic anhydride, acetyl chloride,

acetic anhydride) and found that the conversion of BP decreases in the following order: benzoylation > propionylation > acetylation. The yield of 4-PBP over zeolite H-beta in the acylation of biphenyl with acid chlorides and acid anhydrides decreases in the following order: acid chlorides > acid anhydrides. H-beta was recycled two times (fresh plus two cycles) and a decrease in BP conversion is observed after each cycle, which is related to a minor dealumination of zeolite catalyst and consequently a decrease in the crystallinity of H-beta due to the formation of HCl during the reaction. The formation of acylated products of BP is explained by an electrophilic attack of acyl cation ($R\text{-}CO^{+;}$ where R = C_6H_5- or CH_3CH_2- or CH_3-) on the BP ring, whose formation is facilitated by acid sites of the zeolite catalysts.

3.2. Benzoylation of chlorobenzene

3.2.1. Introduction

4,4'-Dichlorobenzophenone (4,4'-DCBP) is used as photosensitizer and applied to the UV-curable coatings or UV-curable inks. Substituted diphenylketones are also used as intermediates for pharmaceutical and agricultural chemicals [34]. 4,4'-DCBP is usually produced by the Friedel-Crafts reactions of chlorobenzene (CB) with 4-chlrobenzoylchloride using Lewis acid catalysts such as $AlCl_3$, BF_3, $TiCl_4$, $ZnCl_2$ etc. [35-38], however, these catalysts have several disadvantages; wasting a lot of Lewis acid catalyst $AlCl_3$, because of the reaction being mostly equimolar and of the difficulty of recycling it after use, and corrosion of containers by evolved acidic gases. In order to overcome these difficulties of Lewis acid catalysts, solid acidic zeolite catalysts meet the requirement for industrial processing of organic chemicals taking into account their environmental advantage. In addition, zeolites are well known shape-selective and thermally stable materials. Here we studied for the first time the catalytic activity of a stable and recyclable H-beta catalyst in the

benzoylation of chlorobenzene with 4-ClBC at atmospheric pressure (scheme 3.3). The influence of catalyst concentration, reaction temperature, CB/4-ClBC molar ratio and recycling of H-beta is also examined on the conversion of 4-ClBC using H-beta. The results obtained over H-beta are compared with that over the $AlCl_3$.

3.2.2. Experimental

The catalytic reactions were carried out in a three necked flask (capacity, 50 ml) fitted with condenser, gas supply tube and a septum. The temperature of the reaction vessel was maintained using an oil bath. In the reaction flask, 0.044 mol of chlorobenzene and 0.3 g of zeolite (activated at 438 K for 2 h) and 0.022 mol of 4-chlrobenzoyl chloride were introduced.

The reaction mixture was stirred and heated to attain the reaction temperature (443 K) in the presence of nitrogen gas. The reaction was monitored by taking the samples of reaction mixture at suitable intervals and analyzed using a gas chromatograph (HP 6890N series) with a flame ionization detector (FID) and a 50 m x 0.2 mm capillary column of methyl silicone gum. The products were also identified by GC-MS and compared with authentic samples.

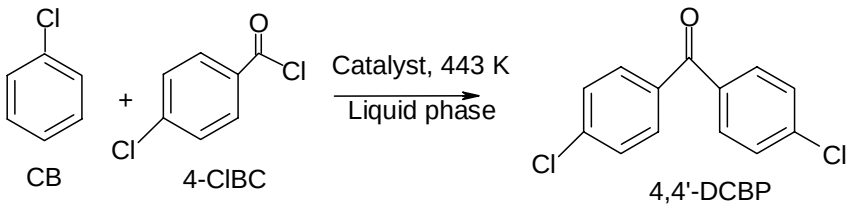

Scheme 3.3

3.2.3. Results and discussion

3.2.3.1 Influence of various catalysts

Table 3.4 lists typical values of benzoylation of chlorobenzene by 4-chlorobenzoylchloride over various acidic zeolites. The results obtained over various catalysts

are compared under identical reaction conditions with the homogeneous catalyst, $AlCl_3$. The main product of the reaction is 4,4'-dichlorobenzophenone (4,4'-DCBP). Small amounts of 2,4'-dichlorobenzophenone (2,4'-DCBP) and others (di-benzoylated products) are also detected. While 2,4'- and 4,4'-DCBP results from the aromatic substitution of CB by parallel reactions the others are obtained by the consecutive reactions of 2,4'- and 4,4'-DCBP. The activities of various zeolite catalysts are compared using data after the 4 h of the reaction time under similar reaction conditions whereas the activity and selectivity of $AlCl_3$ is compared after 1 h of reaction time owing to its higher activity and rate of reaction than that of zeolite catalysts. As can be seen from the Table 3.4, H-beta exhibits the higher catalytic activity and rate of 4-ClBC conversion (TOF = turn over frequency) among zeolite catalysts. The rate of 4-ClBC conversion (TOF) was found to be several times higher over H-beta than that of the RE-Y and H-mordenite, whereas dealuminated H-Y is found to active compared to the RE-Y and H-mordenite. The conversion of 4-ClBC over H-beta, H-Y, RE-Y and H-mordenite are found to be 19.8, 12.4, 1.5 and 1.8 wt. %, respectively.

Table 3.4 Benzoylation of chlorobenzene to 4,4'-dichlorobenzophenone

Catalyst	Conv.of 4-ClBC (wt.%)[a]	TOF ($10^{-4}s^{-1}mol^{-1}Al$) [b]	Product distribution (wt.%)[c]		
			2,4'-DCBP	4,4'-DCBP	Others
H-beta	19.8	8.4	6	88	6
H-Y	12.4	6.0	10	87	3
RE-Y[d]	1.5	0.1	7	83	10
H-Mordenite	1.8	0.6	8	85	7
$AlCl_3$ [e]	22.0	6.0	2	84	14

[a]Reaction conditions: catalysts (g) = 0.3 ; catalyst / 4-ClBC (wt./wt.) = 0.078; chlorobenzene (mole)=0.044; 4-ClBC (mole)=0.022; reaction temperature(K)=443; reaction time (h)=4 ; [b]Turnover rates are expressed as turnover frequency (TOF, moles of 4-ClBC converted s^{-1} mol^{-1} Al); [c] 2,4'-DCBP = 2,4'-dichlorobenzophenone; 4,4'-DCBP = 4,4'-dichlorobenzopheneone; Others = consecutive products; [d]70.6% RE^{3+}-exchange in NH_4-Y-zeolite; [e] reaction time (h) = 1.

The corresponding TOF (10^{-4} $s^{-1}mol^{-1}Al$) are 8.4, 6.0, 0.1 and 0.6 x 10^{-4} $s^{-1}mol^{-1}Al$, respectively. The homogeneous Lewis acid catalyst, $AlCl_3$, is found to be most active catalyst due to its strong Lewis acidity and the conversion of 4-ClBC, TOF and selectivity for 4,4'-DCBP are found to be 22.0 wt.%, 6.0 (10^{-4} $s^{-1}mol^{-1}Al$) and 84.0 wt.%, respectively. In addition, the results show that the selectivity for 4,4'-DCBP over H-beta is higher (88.0 wt.%) than the other catalysts. A higher amount of consecutive products formation is observed over $AlCl_3$ due to its non shape-selective character. From the data in Table 3.4, it is clear that that the performance of the catalyst is governed by the acidity and the structure of the zeolites.

The higher conversion of 4-ClBC and TOF over H-beta and H-Y seem to be due the fact that the H-beta exhibits the stronger Brönsted acid sites compared to the other catalysts. These results indicate that acid strength is the most important factor for the polarization of ClC_6H_5COCl (4-ClBC) into an electrophile ($ClC_6H_5CO^+$) which attacks the CB ring and produces the DCBPs (dichlorobenzophenones) [39-42] The little higher selectivity for 4,4'-DCBP over H-beta might be attributed to its peculiar pore opening (5.5 x 7.5 Å) than H-Y (7.4 Å) and H-mordenite (6.5 x 7.0 Å). The results of the preceding section have revealed that H-beta is the best catalyst for the benzoylation of chlorobenzene to 4,4'-DCBP. The influence of various parameters on the conversion of 4-ClBC and product distribution over H-beta is reported in the following section.

3.2.3.2 Influence of catalyst concentration

Figure 3.5 displays the conversion of 4-ClBC, rate of 4-ClBC conversion (TOF) and product distribution at 4 h reaction time as a function of H-beta / 4-ClBC ratio. The different ratios of H-beta / 4-ClBC ratio were obtained by varying the amount of the catalyst (H-beta, SiO_2/Al_2O_3 =26) and keeping the concentration of 4-ClBC constant. A linear increase in the conversion of 4-ClBC from 3.1 to 23.8 wt.% was observed when catalyst to 4-ClBC ratio was

increased from 0 to 0.131, respectively. The corresponding TOF decreases from 14.9 to 6.0 (10^{-4} $s^{-1}mol^{-1}Al$.) due to the increase in aluminum content when H-beta / 4-ClBC ratio was increased from 0.026 to 0.131, respectively. However, the selectivity for 4,4'-DCBP remains mostly unaffected even after the change in catalyst to 4-ClBC ratio. The yields of the products increase with the increase in the catalyst concentration due to the increase of moles of Al in the total amount of zeolite H-beta. These results indicate that with an increase in catalyst loading the conversion of 4-ClBC increases linearly because of the increase in the total number of acid sites available for the reaction.

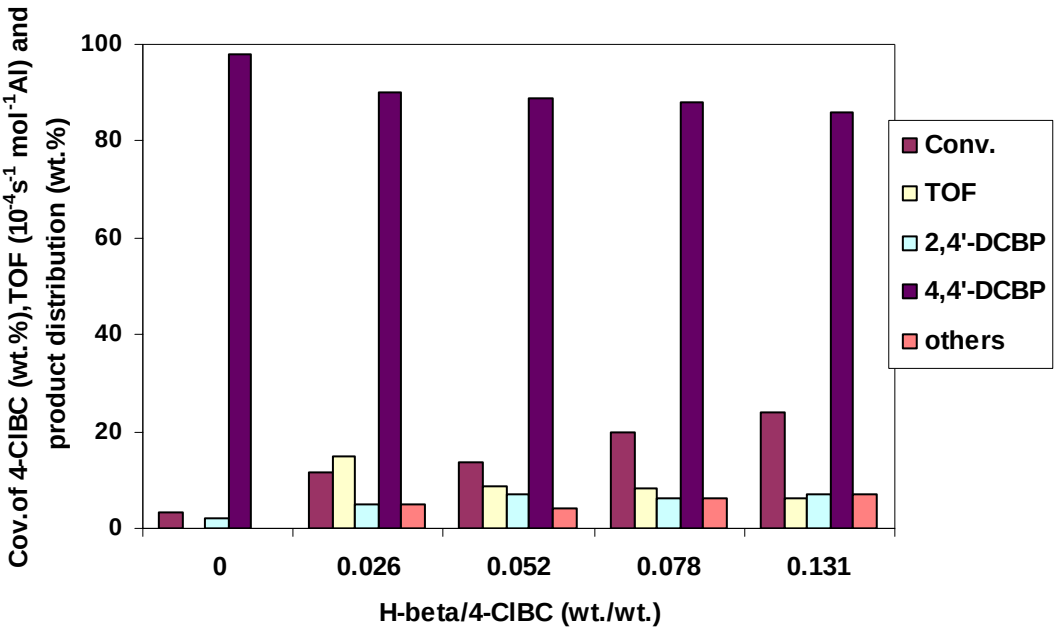

Fig.3.5. Effect of H-beta/4-ClBC ration on the conversion of 4-ClBC, TOF ($10^{-4}s^{-1}mol^{-1}Al$) and product distribution (%). Reaction conditions: catalysts (g) = 0.3; chlorobenzene (mole)=0.044; 4-ClBC (mole)=0.022; reaction temperature (K)=443; reaction time (h)=4.

3.2.3.3 Influence of reaction temperature

Figure 3.6 shows the variation of conversion of 4-ClBC (wt.%), rate of 4-ClBC conversion (10^{-4} $s^{-1}mol^{-1}Al$) and product distribution (wt.%) as a function of reaction temperature A significant increase in the conversion of 4-ClBC and rate of 4-ClBC conversion is achieved with the increase in reaction temperature. The conversion of 4-ClBC

and rate of 4-ClBC conversion increases from 14.1 to 23.1 wt.% and 6.0 to 9.8 (10^{-4} $s^{-1}mol^{-1}Al$), respectively. However, the selectivity for 4,4'-ClBC remains nearly constant in all experiments. One of the reasons for the increased rates at higher temperature may be attributed to an enhancement of the rate of diffusion of 4-ClBC inside the channel of the H-beta; however, reaction rates are usually more temperature dependent than rate of diffusion [43, 44]. The apparent activation energy of 4-ClBC conversion over H-beta estimated to be 40.4 kJ / mol in the temperature range 433-453 K.

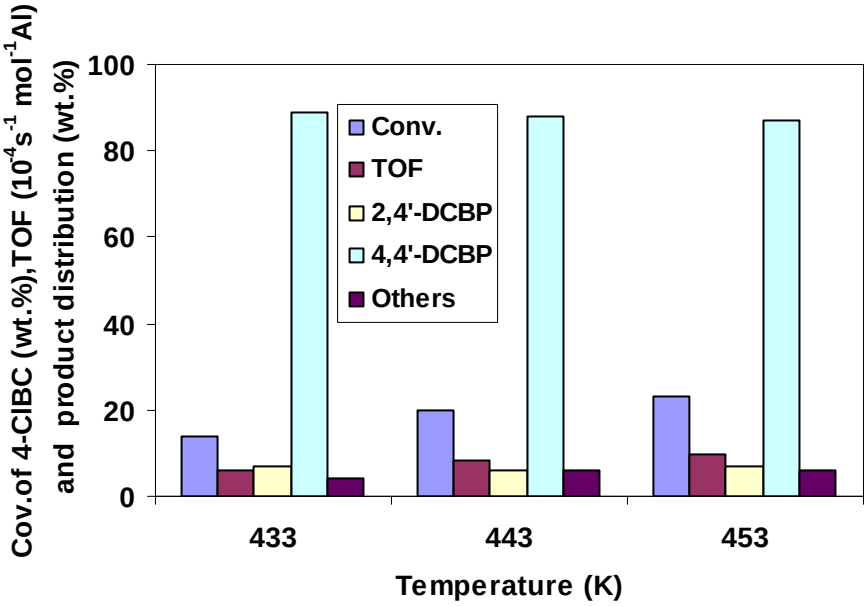

Fig. 3.6. Effect of reaction temperature on conversion of 4-ClBC, TOF ($10^{-4}s^{-1}mol^{-1}Al$) and product distribution (%). Reaction conditions: catalyst / 4-ClBC (wt./wt.) = 0.078; chlorobenzene (mole)=0.044; 4-ClBC (mole)=0.022; reaction time (h)=4.

3.2.3.4 Influence of CB / 4-ClBC molar ratio

Keeping the amount of CB constant changed the CB/4-ClBC ratios. The increase in CB/4-ClBC ratio up to 3 gave a linear rise in the conversion of 4-ClBC and rate of 4-ClBC conversion (Fig. 3.7). The conversion of 4-ClBC and rate of 4-ClBC conversion increased from12.6 to 28.3 wt. % and 5.3 to 12.0 (10^{-4} $s^{-1}mol^{-1}Al$), respectively, as the CB / 4-ClBC

molar ratio increased from 1 to 3.The selectivity for the products was not influenced by the change in molar ratios (Fig. 3.7). The increase in CB/4-ClBC ratio causes decrease in the concentration of 4-ClBC in the reaction mixture, which is effectively solvated in presence of higher concentration of CB. Thus adsorption of 4-ClBC over the acid sites takes place effectively at lower concentration level of 4-ClBC and hence higher conversion of 4-ClBC resulted. At CB/4-ClBC ratio of 3, higher conversion of 4-ClBC was achieved.

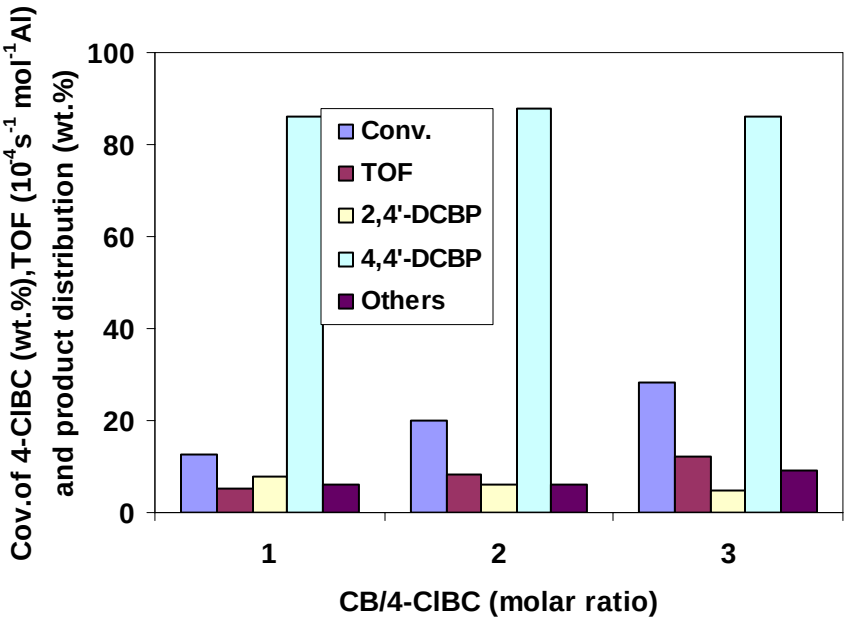

Fig. 3.7. Effect of CB/4-ClBC molar ratio on conversion of 4-ClBC, TOF ($10^{-4}s^{-1}mol^{-1}Al$) and product distribution (%). Reaction conditions: catalyst (g) =0.3; reaction temperature (K): 443; reaction time (h)=4.

3.2.3.5 Effect on catalyst recycling

H-beta sample used in the benzoylation of CB was recycled three times (fresh and two cycles) in order to check the activity and stability of the catalyst. After reaction of each cycle, the catalyst was filtered off, washed with acetone and calcined at 773 K in the presence of air for 16 h. Figure 3.8 lists the results of these experiments. H-beta shows an immediate but little decrease in the activity after each cycle. The conversion of 4-ClBC decreased from 19.8

to 17.0 wt. % when catalyst was recycled from fresh to 2nd cycle, respectively. However, the selectivity for the products remained unaffected. In order to check the structure of the catalyst after each reaction, X-ray diffraction pattern were recorded. XRD measurements indicated that the catalyst retains the H-beta structure. Chemical analysis of the reaction mixture as well as zeolite H-beta after each cycle revealed that minor amount of the aluminum leached out from the zeolite by the HCl (formed during the reaction). The SiO_2/Al_2O_3 molar ratio of the zeolite H-beta increases from 26 to 28.9 after fresh to 2nd cycle, respectively, due to the leaching of minor amount of aluminum from the structure of the H-beta and hence a linear decrease in the activity of the catalyst is observed. The present study indicates that the catalyst can be recycled a number of times without loosing its activity to a greater extent.

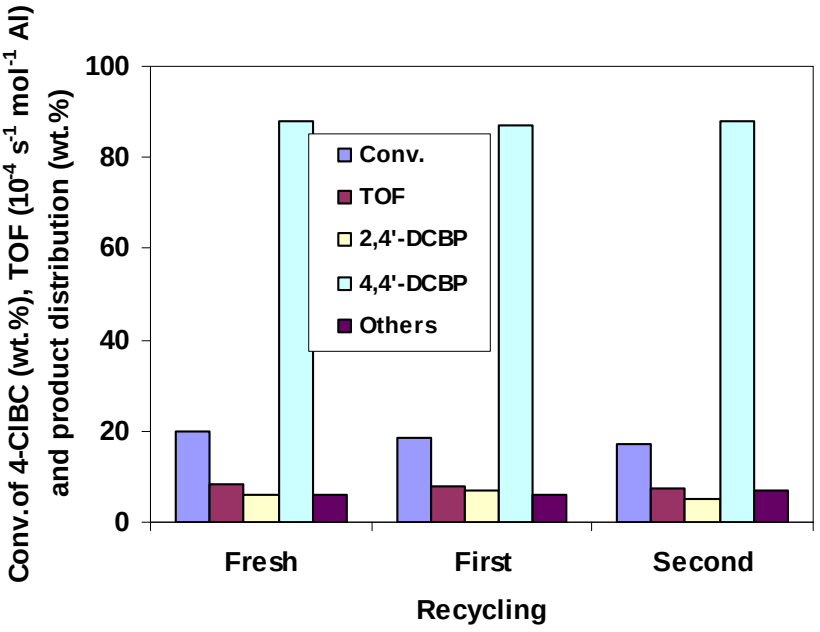

Fig. 3.8. Effect of CB/4-ClBC molar ratio on conversion of 4-ClBC, TOF ($10^{-4}s^{-1}mol^{-1}Al$) and product distribution (%). Reaction conditions: catalyst (g) =0.3; reaction temperature (K): 443; reaction time (h)=4.

3.2.4. Conclusions

It is demonstrated for the first time that zeolite H-beta catalyzes the benzoylation of chlorobenzene with 4-ClBC efficiently, which leads to the formation of 4,4'-DCBP in high

selectivity. At identical reaction conditions the activity (conversion of 4-ClBC) trend after 4 h reaction time is AlCl3> H-beta > Del. H-Y > H.mordenite ≈ RE-Y. H-mordenite and RE-Y are less active due to their weaker acid sites. It is concluded that that the presence of strong Bronsted acid sites in the zeolite catalysts appears to be very important for the polarization of ClC_6H_5COCl (4-ClBC) into an electrophile ($ClC_6H_5CO^+$), which then attacks the chlorobenzene ring resulting in the formation of dichlorobenzophenones. The higher yield of the products can be achieved by increasing the values of the catalyst concentration, reaction temperature and CB/ 4-ClBC molar ratio. Recycling of the catalyst progressively decreases the 4-ClBC conversions to a little extent.

3.3. References

1. A.Walczak, J. Rzasa, S. Labus, Pol PL 170632 (1997).
2. F.J. Hughes, US Pat. 5869662 (1999).
3. J.I.Kroschwitz, M. Howe-Grant (Eds.), Kirk-Othmer, Encyclopedia of Chemical Technology, 4th ed., Wiley, New York, 1995, p.454.
4. G. A. Olah, Friedel-Crafts and Related Reactions, Vol. III (Part I), Interscience Publishers , Wiley, New York, 1964, p.62.
5. G.I.Tsukervanik, Deposited Doc., SPSTL 316 Khp-D82, 4pp (1982).
6. Adam, Ann.Chim. **6** (1888) 224.
7. M.S. Newman, W.T. Booth, J. Am. Chem. Soc. **67** (1945) 154.
8. E. Campaigne, W. B. Reid, J. Am. Chem. Soc. **68** (1946) 1663.
9. S.L. Silver, A. Lowy, J. Am. Chem. Soc. **56** (1934) 2429.
10. L.M. Long, H.R. Henze, J. Am. Chem. Soc. **63** (1941) 1941.
11. M. Crochemore, Eur. Pat. Appl. EP 199661 (1986).
12. P. B.Venuto, Microporous Mater. **2** (1994) 297
13. A. Corma, Chem. Rev. **95** (1995) 559.
14. B.Chiche, A.Finiels, C.Gauthier, P.Geneste, J. Org.Chem. **51** (1986) 2128.
15. A. Corma, M.J. Climent, H. Garcia, P. Primo, Appl. Catal. A: General **49** (1989) 109.
16. I. Neves, F. Jayat, P. Magnoux, G. Perot, F. R. Ribeiro, M. Gubelman, M. Guisnet, J. Chem. Soc. Chem. Commun. (1994) 717.
17. F. Richard, H. Carreyre, G. Perot, J. Catal. **159** (1996) 427.
18. R. Fang, H. W. Kouwenhoven, R. Prins, Stud. Surf. Sci. Catal. **83** (1994) 1441.
19. H. Van Bekkum, A. J. Hoefnagel, M.A.Vankoten, E.A. Gunnewegh, A.H.G.Vog, H.W. Kouwenhoven, Stud. Surf. Sci. Catal. **83** (1994) 379.
20. E.A. Gunnewegh, S.S. Gopie, H. Van Bekkum, J. Mol. Catal. A: Chem. **106** (1996) 5.
21. A.P.Singh, D.Bhattacharya, S.Sharma, J. Mol. Catal. A: Chem. **102** (1995) 139.
22. A.P. Singh, D. Bhattacharya, Catal. Lett. **32** (1995) 327.
23. A.K. Pandey, A.P.Singh, Catal. Lett. **44** (1997) 129.
24. A.P. Singh, A.K. Pandey, J. Mol. Catal. **123** (1997) 141.
25. A.P. Singh, D. Bhattacharya, S. Sharma, Appl. Catal. A: General **150** (1997) 53.
26. B. Jacob, S. Sugunan, A.P.Singh, J. Mol. Catal. A: Chem. **139** (1999) 43.
27. M. Guisnet, D. B. Lukyanov, F. Jayat, P. Magnoux, I. Neves, Ind. Eng. Chem. Res. **34**

(1995) 1624.

28. I. Neves, F. Jayat, P. Magnoux, G. Perot, F.R. Ribeiro, M. Gubelmann, M.Guisnet, J. Mol. Catal.A: Chem. **93** (1994) 169.
29. Y.V.Subba Rao, S.J. Kulkarni, M. Subrahmanyam, A.V. Rama Rao, Appl. Catal. A: General **33** (1995) L1.
30. G.A. Olah, R. Malhotra, S.C. Narang, J.A. Olah, Synthesis (1978) 672.
31. A. Corma, M. J. Climent, H. Garcia, J. Primo, Appl. Catal. **49** (1989) 109.
32. K. Arata, M. Hino, Appl. Catal. **59** (1990) 197.
33. T. Jaimol, P. Moreau, A. Finiels, A.V. Ramaswamy, A.P. Singh, Appl. Catal. A: General **214** (2001) 1.
34. U.Beck, in Ullmann's Encyclopaedia of Industrial Chemistry, Eds. W. Gerhartz, Y.Y.Stephen, F.T.Campbell, R.Pfefferkorn, J.F.Rounsaville, VCH, Weinheim, 1986, vol. A15, p. 91.
35. V.A.Ustinov, G.S.Mironov, V.V.Kopejkim, L.Sineva, USSR SU 654603 (1979)
36. V.A.Ustinov, V.V.Kopeikis, G.S.Mironov and V.I.Mil'to, Zh. Org. Khim., 16 (1) (1980) 233.
37. H. Stephen, J. Chem.Soc. **117** (1920) 510.
38. G.A.Olah, Friedel-Crafts and Related Reactions*,* Vol IV, Wiley Interscience, New York, 1964, p. 246.
39. K. Arata, K.Yabe, I.Toyoshima, J.Catal. **44** (1995) 409.
40. I. Hachiya, M. Mariwaki,, S. Kobayashi, Tetrahedron Lett. **36** (1995) 409.
41. G.A.Olah, S.Kobayashi, J. Am.Chem. Soc. **93**(1971) 6964.
42. Y. Zumi, M. Ogawa, W. Nohara , Kurabe, Chem. Lett. (1992) 1987.
43. S. Gointer, A. Tuel, Appl.Catal.A: General **118** (1994) 173.
44. J.S. Reddy, S. Sivasanker, P. Ratnasamy, Zeolites **12** (1992) 135.

4.1. Isopropylation of isobutylbenzene

4.1.1.Introduction

The alkylation of aromatics through Friedel-Crafts reaction is of substantial industrial and pharmaceutical significance [1]. Alkylation of aromatic nucleus has been traditionally carried out with well-known Lewis acids or organometallic reagents using alkyl halides as the alkylating agents. Isopropylation of benzene and toluene with isopropyl bromide as an alkylating agent and $AlCl_3$ as a catalyst had been studied in detail by Olah [2]. Alkylation with varieties of alkylating agents and Friedel-Crafts catalysts had provided insight into the trends in which activity and selectivity were mostly considered. Alcohols and alkenes can also serve as sources of electrophiles in Friedel-Crafts reactions in the presence of strong acids. Until recently, solid phosphoric acid and Friedel-Crafts catalysts like $AlCl_3$ and BF_3 were used in the synthesis of many fine chemicals and pharmaceutical intermediate [3]. In many cases, more than stoichiometric amount of $AlCl_3$ is used for the reaction, giving poor selectivity because of degradation, polymerization and isomerization. Solid acid catalysis is one of the most important areas of research as varieties of industrially important reactions are being carried out using solid acids [3-5]. The use of a variety of solid acids like zeolitic materials is well defined in the production of aromatics and petrochemicals such as xylenes, ethylbenzene, cumene and linear alkyl benzenes [6-9]. A recent Mobil patent claimed cumene production over MCM-56 and MCM-22 [10]. Acidic zeolites, having Bronsted or Lewis acid centers uniformly distributed throughout the micro pores, have substantial acid strengths and are capable of replacing homogenous bulk Lewis acids. Here we studied liquid phase isopropylation of isobutyl benzene to 3-isobutylcumene and 4-isobutylcumene (Scheme 1) using 2-propanol as alkylating agents (in the presence of nitrobenzene as solvent) over zeolites and H-Al-MCM-41. The products 3-isobutylcumene and 4-isobutylcumene serve as

precursors for making 3-hydroxy benzyl alcohol and 4-hydroxy benzyl alcohol, respectively, which are the intermediates for making bisphenol-F. The results concerning the optimization of the reaction conditions with zeolite, H-beta is presented here.

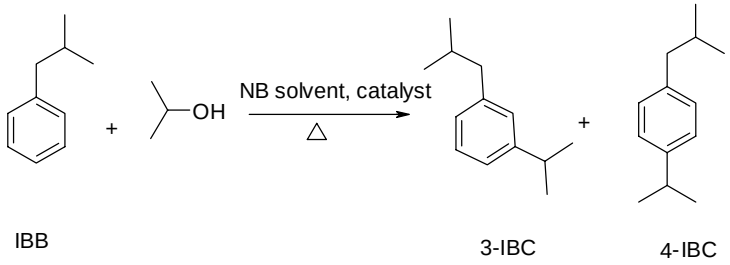

Scheme 4.1

4.1.2. Experimental

The alkylation of isobutylbenzene with 2-propanol was carried out in a 250 ml stainless steel Parr autoclave equipped with a stirrer and a temperature controller. In a typical run freshly activated catalyst (0.5 g) was added to the isobutyl benzene (25 mmol), 2-propanol (25 mmol) and nitrobenzene (20 ml) mixture in the stainless steel autoclave and flushed with nitrogen before heating to the required temperature.

4.1.3. Results and Discussions

4.1.3.1 Effect of different catalysts

Zeolite H-beta was found to be the active catalyst in the isopropylation of IBB to 3-isobutylcumene and 4-isobutylcumene with 2-propanol. Among the three isomers, meta-isomer was found to form in a significant amount followed by para- isomer due to its lower strain energy compared with ortho-isomer. The strain energies for ortho-, meta- and para-isomers were calculated to be -312470.0835, -312474.1799 and -312474.2110 kcal/mol, respectively. The calculated strain energy differences of ortho-isomer with respect to meta-

and para- isomers were 4.0964 and 4.1275 kcal/mol, respectively. The mesoporous H-Al-MCM-41 catalyst having SiO_2/Al_2O_3 ratio of 50 showed higher TOF (10^{-2} h^{-1} mol^{-1} Al) for isobutyl benzene conversion than the other zeolites except H-beta (Table 4.1). Medium pore size and strong acid sites promote the catalytic activity of isopropylation of IBB to *para*- and meta alkylated products and hence H-beta is found to be the active catalyst in the isopropylation of IBB while H-Y, RE-Y showed lower activities due to their weaker acid sites. H-mordenite, having unidimensional pores, showed lower activity than H-Y, RE-Y and H-beta. Small pore openings of zeolite H-ZSM-5 (5.4 x 5.6 and 5.1 x 5.5 Å) made this catalyst inactive for the reaction (< 1 wt.% conversion of IBB). The conventional homogeneous catalyst $AlCl_3$ showed higher activity but poor selectivity for 3-IBC or 4-IBC. The conversion of IBB and 4-IBC/3-IBC ratios over $AlCl_3$ were 79 wt. % and 0.45, respectively.

Table. 4.1 Isopropylation of isobutylbenzene

Catalyst [a]	Conv. of IBB (wt.%)[b]	TOF (10^{-2} h^{-1} mol^{-1} Al)[c]	Product distribution (wt.%)[d]			4-IBC/3-IBC ratio
			3-IBC	4-IBC	Others	
H-beta (26)	17	59.0	44	52	4	1.18
H-Y (4)	3.4	2.5	43	51	6	1.19
RE-Y (4)	4.6	3.3	41	47	12	1.15
H-Mordenite (22)	1.8	5.4	40	60	0	1.5
H-ZSM-5 (41)	0.8	5.2	42	53	5	1.26
H-Al-MCM-41(50)	2.0	14.4	60	40	0	0.67
$AlCl_3$[e]	79	22.0	42	19	39	0.45

[a] SiO_2/Al_2O_3 molar ratio is given in bracket
[b] Reaction conditions : Catalyst (g) = 0.5 ; IBB (mol) = 0.025 ; IPA (mol) = 0.025 ; nitrobenzene (ml)= 25; reaction temperature (K) = 453; reaction time (h) = 12.
[c] (TOF, turn over frequency, moles of IBB converted per mole of aluminum per hour).
[d] 3-IBC = 3-isobutylcumene ; 4-IBC = 4-isobutylcumenee ; Others= disubstituted and higher molecular weight products; [e] Reaction temperature (K)=323.

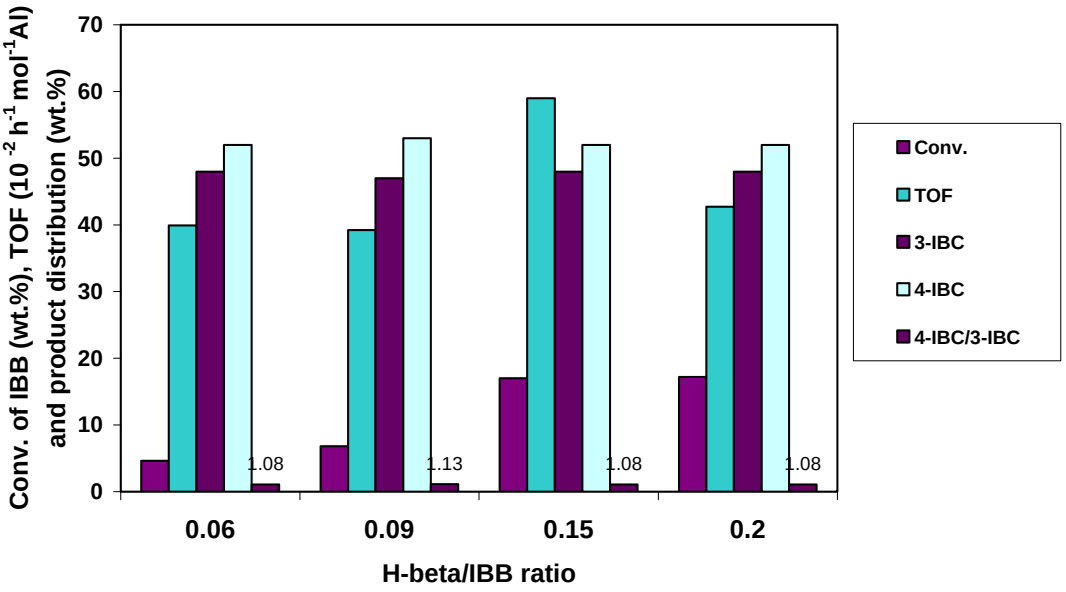

Fig. 4.1. Effect of H-beta/IBB ratio on the conversion of IBB, TOF ($10^{-2}h^{-1}mol^{-1}Al$) and product distribution (wt.%); Reaction conditions; IBB (mol) = 0.025; IPA (mol)=0.025; nitrobenzene (ml)= 25; reaction temperature (K) = 453; reaction time (h) = 12.

4.1.3.2 Effect of catalyst/IBB

Fig. 1 represents the conversion of IBB, rate of IBB conversion (TOF) and product distribution as a function of catalyst loading. The different H-beta/IBB (wt./wt.) ratios were obtained by varying the amount of catalyst loading corresponding to IBB. Without catalyst the conversion of IBB was less than 0.5 wt.%. Addition of small amount of catalyst (H-beta/IBB=0.06 ratio) accelerates the reaction to proceed with higher rate than before. Conversion of IBB increases from 0.5 to 4.6 wt.% when the H-beta/IBB ratio is increased from 0 to 0.06. A sharp increase in conversion and rate of IBB conversion, 17.0 wt.% and 59.0 $x10^{-2}$ h^{-1} mol^{-1} Al, respectively, were observed when 0.15 ratio of H-beta/IBB is used.

Further increase in the ratio did not affect the conversion of IBB significantly whereas selectivity to 3-IBC and 4-IBC was found to be nearly similar in all cases. Increase in the catalyst loading provides higher surface area with higher acid sites concentration for reactant molecules to adsorb on it.

4.1.3.3 Effect of IBB/i-PrOH molar ratio

The effect of molar ratios of reactants on the conversion of IBB, rate of IBB conversion and selectivity to 4-IBC and 3-IBC was studied by changing the alkylating agent (i-PrOH) concentration and keeping IBB concentration constant. Four different combinations of molar ratio of IBB/i-PrOH (1,2,3 and 5) were studied (Fig. 4.2). As the molar ratio of IBB/i-PrOH increases, the i-PrOH concentration decreases and hence the competitive adsorption of i-PrOH on the surface of the catalytic sites increases to react with the substrate molecule.

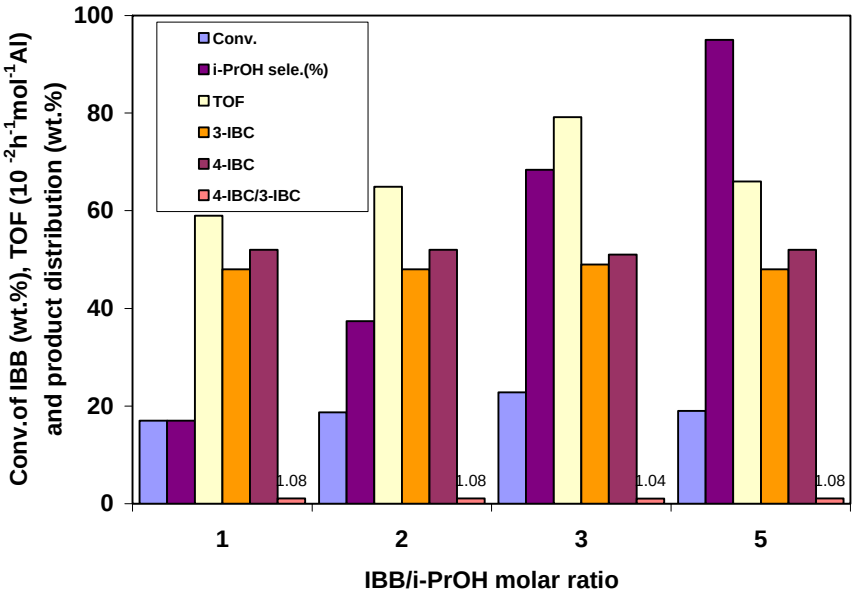

Fig. 4.2 Effect of IBB/i-PrOH molar ratio on the conversion of IBB, TOF ($10^{-2}h^{-1}mol^{-1}Al$) and product distribution (wt.%); Reaction conditions; Catalyst (g) = 0.5 ; IBB (mol) = 0.025 ; nitrobenzene (ml)= 25; reaction temperature (K) = 453; reaction time (h) = 12.

4.1.3.6 Effect of Reaction temperature

The influence of temperature on the isopropylation of IBB with H-beta at constant catalyst/IBB ratio, 0.15, was studied with different temperature ranges. The variation of conversion of IBB, rate of IBB conversion and product distribution as a function of reaction temperature is given in Fig. 4.3. An increase in the conversion of IBB is achieved with the increase in reaction temperature. The conversion of IBB, TOF and 4-IBC/3-IBC ratio increased from 9.0 to 16.1 wt.%, 31.3 to 55.9 x $10^{-2}h^{-1}mol^{-1}Al$ and 1.00 to 1.08, respectively, when the temperature is increased from 413 K to 433 K. Further increase in the reaction temperature, >433 K, gave a marginal increase in the IBB conversion, rate of IBB conversion (TOF) and 4-IBC/3-IBC ratio. The apparent activation energy calculated for the isopropylation of IBB is 18.5 kJ/mol.

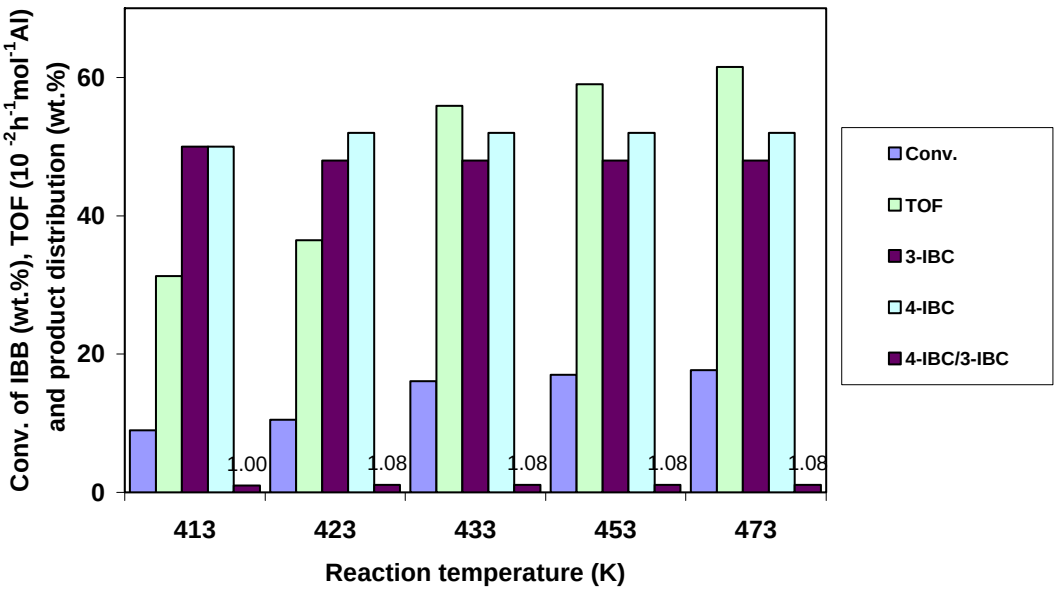

Fig. 4.3. Influence of reaction temperature on the conversion of IBB, TOF ($10^{-2}h^{-1}mol^{-1}Al$) and product distribution (wt.%); Reaction conditions: Catalyst (g) = 0.5; IBB (mol)= 0.025; IPA (mol) = 0.025; nitrobenzene (ml)= 25; reaction time (h) = 12.

4.1.3.6 Effect of recycling

In order to check the stability and catalytic activity of zeolite H-beta in the isopropylation of IBB, three cycles (fresh and two cycles) were carried out using the same catalyst. The results are presented in Table 4.2. After workup of the reaction mixture, the zeolite H-beta was separated by filtration washed with acetone and calcined for 16 h at 773 K in the presence of air. Thus, the recovered zeolite after each reaction was characterized for its chemical composition by EDX and crystallinity by X-ray diffraction (XRD). It was found that there is slight decrease in the content of aluminum and crystallinity of H-beta after each cycle. The activity of H-beta decreases progressively but marginally on each recycle and the conversion of IBB decreases from 17.0 to 16.1 % when H-beta was recycled from fresh to second cycle, respectively, in the isopropylation of IBB. The loss of aluminum and a little decrease in crystallinity of zeolite H-beta may be attributed for the decrease in catalytic activity after each cycle.

Table 4.2. Effect of recycling of H-beta catalyst in the isopropylation of IBB

Catalyst	SiO_2/ Al_2O_3 ratio[a]	Conv.of IBB (wt.%)[b]	TOF ($10^{-2}h^{-1}$ $mol^{-1}Al$)[c]	Product distribution (wt.%)[d]			4-IBC/3-IBC	Crystallinity (%)[e]
				3-IBC	4-IBC	Others		
Fresh	26	17.0	59.0	44	52	4	1.18	100
1st recycle	26.8	16.7	58.0	47	50	3	1.06	98
2nd recycle	27.0	16.1	56.0	46	49	5	1.07	97

[a] Determined by EDX.
[b,c ,d] see foot notes of [c,d,e], respectively , to Table 4.1.
[e] By X-ray diffraction.

4.1.4. Conclusions

Zeolite H-beta catalyzes the isopropylation of IBB efficiently with 2-propanol as the alkylating agent and is found to be superior to other zeolite catalysts. The conventional homogeneous catalyst, $AlCl_3$, does not possess shape-selectivity and favors the formation of large amount of high molecular weight products. Among the isomers, meta-isomer was found to form in a significant amount followed by para isomer as the ortho isomer has relatively high strain energy compared to the other two isomers. Selectivity of the order of 52 % for 4-IBC and 44 % 3-IBC is achieved at 17.0 wt.% conversion level of IBB over H-beta, whereas $AlCl_3$ gave 19 % 4-IBC and 42 % 3-IBC under similar reaction conditions. A higher strength of acid sites of H-beta is responsible for the conversion of IBB. The conversion of IBB increased significantly with increase in catalyst concentration (H-beta), reaction temperature and IBB/ i-PrOH molar ratio. At higher IBB/i-PrOH molar ratio, i.e. 5, the consumption of 2-propanol is comparatively higher (95 %) compared to the equimolar ratio, (2-propanol consumption is 17.0 %). Recycling of the catalyst has not affected the activity of the catalyst significantly.

4.2. Monomethylation of phenylacetonitrile

4.2.1. Introduction

Monomethylated arylacetonitriles are important precursors of 2-arylpropionic acids, the well-known anti-inflammatory drugs [11]. Alkylation of PAN under environmentally benign conditions with non-toxic alkylating agents is of interest for the industries. Base promoted monomethylation of methylene active compounds is not an easy process for industries as substantial quantity of dimethyl derivatives also obtained with the usual methylating agents [12, 13]. The direct monomethylation of PAN was less selective even with

phase transfer catalysts [14, 15]. Tundo et al. observed very high selectivity for the monomethylation of PAN with DMC as methylating agent over gas-liquid phase-transfer catalysts [16, 17]. Basic zeolites were also studied for the alkylation of PAN with methanol under vapor phase conditions, but higher yields of 2-PPN were not achieved [18]. Alkali metal carbonates and organic bases have been studied in detail in the monomethylation of arylacetonitriles and methyl aryl acetates under batch conditions [19]. Solid base catalysts allow easier separation from the product as well as possible regeneration and reuse. Solid bases also have the added advantages of being noncorrosive and environmentally friendly, which allow easier disposal [20].

Mesoporous MCM-41 type silica represents an ideal inorganic support due to higher surface area and sharply distributed pore dimensions, 2-20 nm [21, 22]. Recent researches in the area of organic functionalized and alkali metal ion exchanged mesoporous materials with high surface area suggest that these materials could be developed as basic catalysts, especially for the reactions of large molecules [23-25]. Organic functionalization of the internal mesopores of MCM-41 can be achieved, either by covalently grafting of various organic species onto the surface, or by incorporating functionalities directly during the synthesis. The attachment of functional groups to the mesoporous silica walls can be achieved by the direct reaction of surface hydroxyl groups with reactive silylating agents. The organosilane having ligands such as amine is directly grafted to the silica surface by an in-situ silylation procedure [26-28]. Among the organo functionalized mesoporous materials, aminopropyltriethoxysilylated mesoporous silica has been studied extensively as an organic-inorganic hybrid solid for various applications [29-33].

4.2.2. Experimental

Monomethylation of phenylacetonitrile with dimethyl carbonate was carried out in a 250 ml stainless steel Parr autoclave equipped with a stirrer and a temperature controller between 443 and 473 K and at autogeneous pressure with solid base catalysts (Scheme 4.2). In a typical run, freshly activated (at 423 K in case of NH_2-Na-Al-MCM-41 and NH_2-Si-MCM-41, and 573 K for all other catalysts, 3 h) catalyst (0.5 g) was added to the PAN (1.5 x 10^{-2} mol) and DMC (0.3 x 10^{-1} mol) mixture and heated to attain required temperature. The products were analyzed by gas chromatograph (HP 6890N) equipped with FID detector and capillary column (HP-5, 50 m x 0.2 mm) of 5 % methyl silicone gum and identified by GC-MS and H^1-NMR of the samples.

^{1}H NMR for 2-PPN (200 MHz) ($CDCl_3$) (δ): 1.63-1.67(3H, d); 3.9-3.93(1H, q); 7.38 (5H, aromatic).

The conversion (%) is defined as the percentage of moles of PAN transformed into 2-PPN. The rate of PAN conversion or turn over frequency (TOF) is calculated as the moles of PAN converted per hour and per gram of the catalyst. The selectivity (%) for a product is expressed as the amount of the particular product divided by the total amount of products and multiplied by 100.

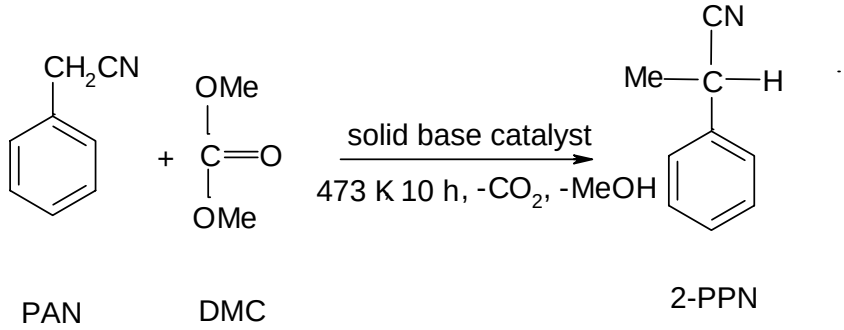

Scheme 4.2

4.2.3. Results And Discussion

4.2.3.1. Effect of different catalysts

Table 4.3 depicts the activities of different catalysts in the monomethylation of PAN. A steady increase in the conversion of PAN to 2-PPN over faujasites catalysts was observed in the order: Na-X, Na-Y < K-X, K-Y < Cs-X, Cs-Y. The conversion of PAN (%), rate of PAN conversion ($10^{-4}h^{-1}g^{-1}$) and selectivity to 2-PPN (%) over Na-X, K-X and Cs-X are 11.1, 3.3, 21, and 17.9, 5.3, 34 and 29.5, 8.8, 50, respectively. Almost similar trend of conversion and selectivity was found in case of Na-Y, K-Y, and Cs-Y. These results suggest that monomethylation of PAN to 2-PPN, is mainly enhanced by the increase in size electropositive character of the alkali metals. Zeolite K-beta gave 12.6 % conversion of PAN with 27 % selectivity to 2-PPN at the rate of 3.8 x $10^{-4}h^{-1}g^{-1}$ while K-L shows 55.5 % conversion of PAN with 53 % selectivity for 2-PPN. The higher conversion of PAN over K-L indicates the presence of stronger basic sites over the K-X, K-Y, K-beta, Cs-X and Cs-Y catalysts.

The activity for the conversion of PAN is found to increase when Na-Al-MCM-41 is exchanged with KNO_3 solution. Conversion of PAN, rate of PAN conversion ($10^{-4}\ h^{-1}g^{-1}$) and selectivity to 2-PPN over Na-Al-MCM-41, and K-Na-Al-MCM-41 are 11.1, 3.3, 31 and 56.2, 16.8, 70, respectively. The exchange of Na^+ by K^+ in Na-Al-MCM-41 could cause formation of bulk potassium silicate and potassium aluminate with some residual K_2O species. Under identical reaction conditions, conventional catalyst, K_2CO_3 gave 80 % selectivity to 2-PPN at 100 % conversion of PAN.

As seen from Table 4.3, at similar conversion level of PAN over the catalysts NH_2-Si-MCM-41 (7.5), and Na-Al-MCM-41 (10.2 and 11.1 %, respectively), selectivity to 2-PPN over the former is found higher (72 %) than over the latter (31%). The higher selectivity over APTES

functionalized catalyst indicates the higher basic strength of amine function, which could convert the intermediates into required product at similar reaction conditions. When both the functionalities (Na^+ and $–NH_2$) were mixed, the catalyst, NH_2-Na-Al-MCM-41 (7.5), exhibited activity three times higher than that of Na-Al-MCM-41 or NH_2-Si-MCM-41 (7.5). The possible reason might be understood that the quality and distribution of the functional

Table 4.3. **Physico-chemical properties of different catalysts used in the monomethylation of PAN**

Catalyst	SiO_2/Al_2O_3 (mole ratio)	Surface area (m^2/g)	Conv. of PAN (%)[a]	TOF (10^{-4} h^{-1} g^{-1})	Product selectivity (%)[b]	
					2-PPN	Others
Na-X	2.4	620	11.1	3.3	21	79
K-X	2.4	615	17.9	5.3	34	66
Cs-X	2.4	605	29.5	8.8	50	50
Na-Y	4.1	612	13.0	3.9	19	81
K-Y	4.1	606	15.1	4.5	32	68
Cs-Y	4.1	598	24.7	7.4	53	47
K-L	6.8	215	55.5	16.6	53	47
K-beta	26.0	743	12.6	3.8	27	73
Na-Al-MCM-41	33	1243	11.1	3.3	31	69
K-Na-Al-MCM-41	14	540	56.2	16.8	70	30
NH_2-Si-MCM-41(7.5)[c]	-	889	10.2	3.0	72	28
NH_2-Na-Al-MCM-41(7.5)[c]	33	658	34.6	3.8	83	17
K_2CO_3	-	-	100	30.0	80	20

[a] Reaction conditions: PAN : 0.015 mol; DMC : 0.3 mol; catalyst : 0.5 g; reaction temperature: 473 K; reaction time :10 h; [b] 2-PPN= 2-phenylpropionitrile; others = intermediates, dimethylated and ring alkylated products; [c]APTES loading =7.5 wt.%.

monolayers on the mesoporous materials is greatly influenced by the population of silanol groups, adsorbed water molecules [34], and resultant charge of the surface. The charge compensating alkali ion (Na^+) in aluminosilicates gels directs the organo-silane to assemble and anchor into coupling agents, TEOS, at regular interval between one molecule to another. APTES moieties arrange spatially within the mesopores and hence result uniform distribution of active sites. As a result, nucleophilicity of confined APTES moiety inside the mesopores is sufficient enough for the transformation of PAN to 2-PPN effectively. Much attention was given for the exploitation of heterogeneous basic catalyst, NH_2-Na-Al-MCM-41, to bring forth a best catalytic system for the selective conversion of PAN to 2-PPN through optimizing both the reaction and catalyst parameter.

4.2.3.2. Effect of APTES loading

Effect of APTES concentration in the monomethylation of PAN was studied over NH_2-Na-Al-MCM-41 catalysts with different concentration of APTES, i.e., NH_2-Na-Al-MCM-41 (7.5), NH_2-Na-Al-MCM-41 (16), NH_2-Na-Al-MCM-41 (30) and NH_2-Na-Al-MCM-41 (42) containing 0.34, 0.74, 1.13, and 1.89 mmol/g, respectively, (Fig. 4.4). It is seen that NH_2-Na-Al-MCM-41 (7.5) gave about 83 % of 2-PPN at 34.6 % conversion level of PAN. A quick as well as sharp increase in conversion (34.6 to 66.4 %) was observed when NH_2-Na-Al-MCM-41 (16) is used. The rate of PAN conversion exactly doubled when the concentration of APTES molecules in the catalyst is doubled which confirms the fact of active sites concentration dependent conversion of PAN. Further increase in the loading (1.13 mmol/g) increases the activity of the catalyst and thereafter it levels off and no appreciable change in rate of PAN conversion was observed. It is believed that 1.13 mmol/g must be the optimum loading and further increase in loading does not show any appreciable conversion of PAN and selectivity to 2-PPN and moreover higher loading of APTES makes the structure of

MCM-41 much less order which is evident from the broad signal in XRD (Fig 2.5). The selectivity for 2-PPN was found to be in the range of 83 to 91% when APTES loading was increased from 0.34 to 1.13 mmol/g, respectively. Increase in the loading of APTES groups on mesoporous walls increase the distribution of basic amine-groups up to the optimum level. Above that level, only degradation of long-range order was observed. NH_2-Na-Al-MCM-41 (30) catalyst has been chosen for further optimization studies.

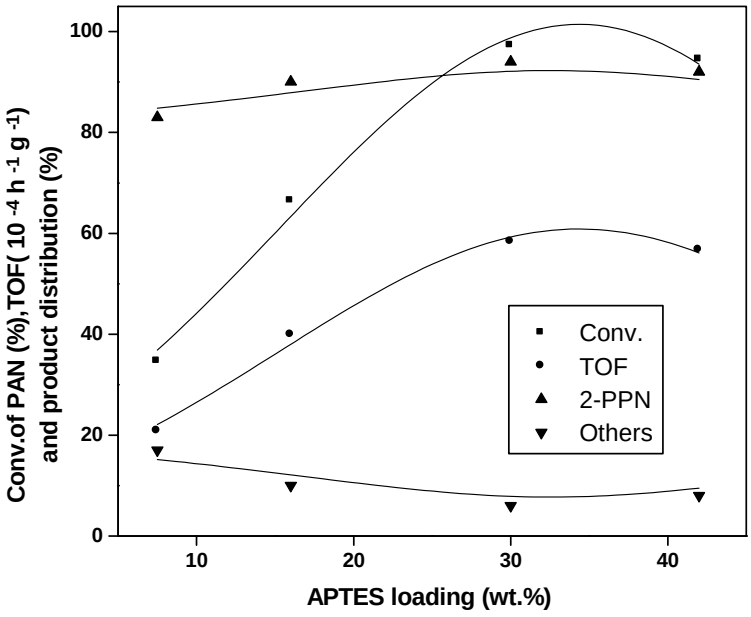

Fig. 4.4. Effect of APTES group loading on the conversion of PAN (%), TOF (10^{-4} $h^{-1}g^{-1}$) and product distribution (%); Reaction conditions: PAN: 0.03 mol; DMC: 0.3 mol; catalyst: 0.5 g; reaction temperature: 473 K; reaction time: 10 h.

4.2.3.3. Duration of run

The effect of reaction time on the conversion of PAN, rate of PAN conversion and selectivity to 2-PPN was studied over NH_2-Na-Al-MCM-41 (30) at 473 K and at autogeneous pressure (Fig. 4.5).

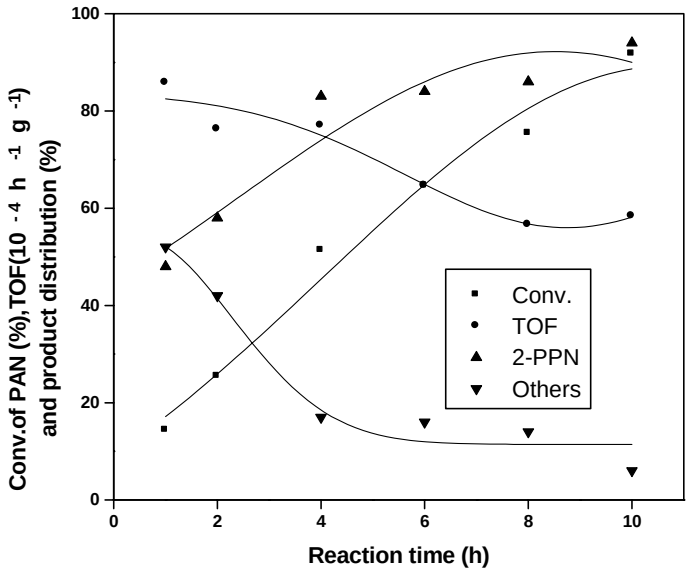

Fig. 4.5. Conversion of PAN (%), TOF ($10^{-4}h^{-1}g^{-1}$) and product distribution (%) vs. reaction time (h) over catalyst NH_2-Na-Al-MCM-41 (30); Reaction conditions: PAN: 0.03 mol; DMC: 0.3 mol;catalyst: 0.5 g; reaction temperature: 473 K.

To collect sample at regular interval of time, reaction was stopped and the reactor was allowed to cool down to room temperature. The conversion of PAN and selectivity to 2-PPN increase linearly with the reaction time up to 10 h. At initial hours of reaction, higher rate of PAN conversion with lower selectivity to 2-PPN suggests that formation of intermediates, PAN anion, $ArCH(COOCH_3)CN$ and $ArC^{-}(COOCH_3)CN$ takes place consecutively in the initial hours of reaction (Scheme-1). These intermediates transform into 2-PPN in the course of reaction time and hence conversion of PAN as well as selectivity to 2-PPN increase linearly with reaction time. The maximum conversion of PAN (>91.7 %) with the rate of PAN conversion, 58.3 x 10^{-4} $h^{-1}g^{-1}$, and higher selectivity to 2-PPN (>94 %) were obtained at 10 h of reaction time. Selectivity to 2-PPN in the initial hour of reaction was found lower but steadily increased with reaction time. The decrease in rate in later hours of reaction may be attributed to shifting of the equilibrium between intermediates and PAN towards 2-PPN and intermediates. The rate of formation of intermediates by the reaction of PAN with DMC is highly facilitated by the active sites (nucleophilic centre) in the catalyst.

4.2.3.4. Effect of catalyst/PAN (wt./wt.) ratio

Figure 4.6 shows the effect of catalyst loading, i.e., NH_2-Na-Al-MCM-41 (30) / PAN (wt./wt.) ratio on the conversion of PAN, TOF, and 2-PPN selectivity in the methylation of PAN at 453 K and 10 h of reaction time. When there was a lower loading of catalyst against higher concentration of PAN, conversion of PAN to 2-PPN was less. Lower conversion is due to the lesser concentration of active sites than the threshold concentration. Threshold concentration can be understood as concentration of a catalyst at which active sites are equally spaced and exposed to the reactant molecules without allowing much crowd of reactant molecules near the active sites. Since the monomethylation of PAN proceeds via intermediates, all the steps in the mechanistic path require to be activated by the active sites. Hence threshold concentration of active sites is required for the conversion of PAN into 2-PPN at any given time. When the catalyst/PAN (w/w) ratio increased from 0.06 to 0.09, increase in the conversion of PAN from 16.5 to 48.2 %, rate of PAN conversion (TOF x 10^{-4} $h^{-1}g^{-1}$) from 24.8 to 48.2 and selectivity for 2-PPN from 35 to 80 % were observed, which reflects the above fact. This sharp increase in the conversion of PAN due to the slight increase in the catalyst concentration is due to crowding of reactant molecule over the active sites is minimized significantly. When the catalyst/PAN (w/w) ratio increased from 0.09 to 0.11, still higher conversion of PAN (91.7 %) with maximum selectivity of 2-PPN (94 %) is resulted. There was little increase in conversion of PAN and nearly similar selectivity to 2-PPN observed when the catalyst/PAN (w/w) ratio is increased above 0.11. These results confirm that higher efficiency of active sites can be exploited only at the optimum catalyst concentration with respect to reactant concentration. The optimum loading of catalyst is found to be 11.4 % with respect to PAN.

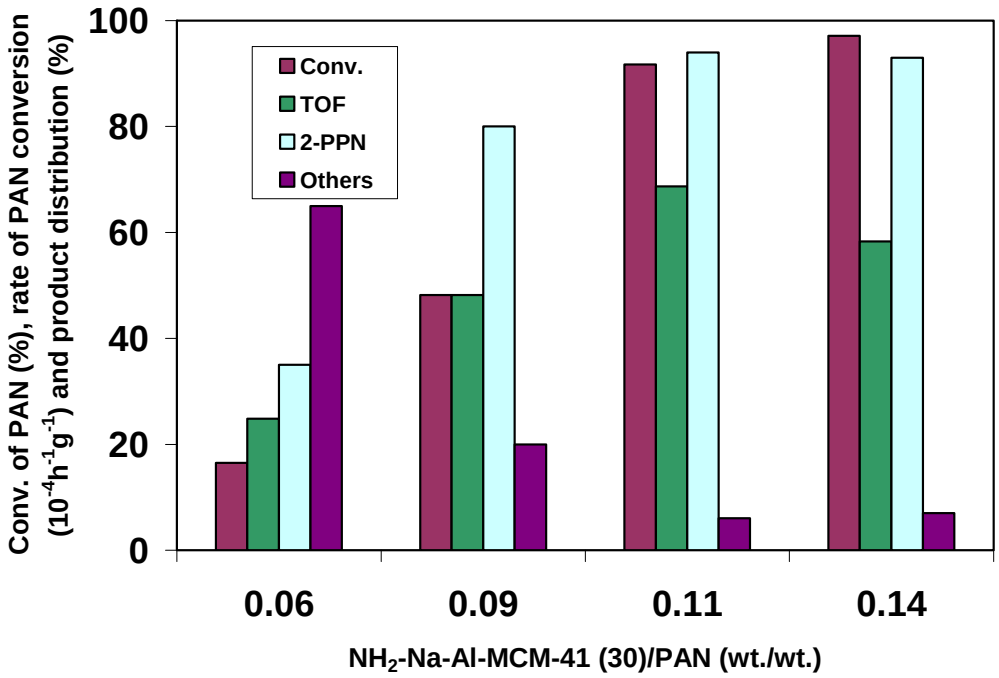

Fig. 4.6. Effect of NH_2-Na-Al-MCM-41 (30)/PAN (wt./wt.) ratio on the conversion of PAN (%), TOF (10^{-4} $h^{-1}g^{-1}$) and product distribution (%); Reaction conditions: PAN: 0.03mol; DMC: 0.3 mol; reaction temperature: 473 K.

4.2.3.5. Effect of DMC/PAN molar ratio

Effect of PAN concentration in the monomethylation reaction of PAN was studied and depicted in Table 4.4. By keeping DMC concentration constant and change in the PAN concentration of the reaction mixture were done to get various molar ratio of DMC/PAN. At lower DMC/PAN molar ratio, conversion of PAN was found lower but the rate of PAN conversion was higher. The rate of PAN conversion at 10 h reaction time increases with decrease in DMC/PAN molar ratio mainly due to the increase of PAN concentration. But in the initial hours of reaction, the rate of PAN conversion over all the ratios are more or less similar. At DMC/PAN ratio of 3, the conversion of PAN, rate of PAN conversion (TOF x 10^{-4} $g^{-1}min^{-1}$) and selectivity to 2-PPN after 10 h reaction time were found to be 63.5 %, 2.1 and 91 %, respectively, where as at DMC/PAN molar ratio of 20, the conversion of PAN, rate of

PAN conversion (TOF) and selectivity to 2-PPN were found to be 97.5 %, 0.48 and 92 %, respectively.

Table 4.4 Effect of PAN concentrations in the monomethylation of PAN[a]

Parameters	PAN (moles)			
	0.015	**0.03**	**0.05**	**0.1**
Conv. of PAN				
30 min	42.3	13.8	12.0	5.6
60 min	65.0	24.6	22.3	13.3
120 min	68.5	46.4	49.2	25.4
600 min	97.5	97.1	84.6	63.5
Selectivity to 2-PPN				
30 min	22	34	42	46
60 min	49	64	61	59
120 min	57	78	74	76
600 min	92	93	94	91
Rate (10^{-4} $min^{-1}g^{-1}$)				
30 min	4.3	2.7	4.0	3.7
60 min	3.2	2.4	3.7	4.4
120 min	1.7	2.3	4.1	4.2
600 min	0.48	0.97	1.4	2.1

[a] Reaction conditions: DMC= 0.3 mol; reaction temperature= 453 K; NH_2-Na-Al-MCM-41 catalyst =0.5 g.

Higher concentration of PAN in the reaction mixture will enhance the PAN adsorption over the active sites and formation of PAN anion intermediate. In the initial hours of reaction,

selectivity for 2-PPN increases as the DMC/PAN molar ratio decreases. These results suggest a phenomenon that, adsorption of intermediates predominates over PAN at lower DMC/PAN molar ratio and hence higher possibility of formation of 2-PPN. DMC works more as a solvent at higher DMC/PAN molar ratio and helps the intermediates relaxation through solvation. During this relaxation period of intermediates, PAN molecules get adsorbed over the active sites, rather than intermediates and hence lower selectivity for 2-PPN.

4.2.3.6. Effect of reaction temperature

The influence of reaction temperature (between 423 and 473 K) on the selective mono methylation of PAN with constant NH_2-Na-Al-MCM-41 (30) /PAN ratio (wt./wt.) of 0.14, and DMC/PAN ratio of 20, was studied (Table 4.5). As an alternate pathway provided by a catalyst helps the reactant molecules to cross the energy barrier for attaining thermodynamically stable product. The rate of PAN conversion is enhanced with increase in temperature. Since the monomethylation of PAN proceeds through formation of intermediates, which are to be catalytically activated, elevation of reaction temperature favors the rate of PAN conversion. The conversion of PAN, rate of PAN conversion (TOF x 10^{-4} $h^{-1}g^{-1}$) and selectivity to 2-PPN increase from 11.8 to 34.2 % and 7.0 to 20.5 and 29 to 67 %, respectively, when the temperature is increased from 423 to 433 K at 10 h reaction time. A linear increase in the conversion of PAN, rate of PAN conversion and selectivity to 2-PPN were observed when the temperature is increased up to 453 K. Beyond 453 K, the conversion of PAN, rate of PAN conversion and selectivity to 2-PPN level off. At lower temperature ranges (<453 K) and at 4 h of reaction time, it was observed that conversions of PAN as well as 2-PPN yields were lower (Table 4.4). It is also seen that rate of PAN conversion is lower at lower reaction temperature (<453 K) at 4 h of reaction time compared to the rates at 10 h reaction time.

Table 4.5. **Effect of temperature and reaction time on methylation of PAN**

Reaction temperature (K)	Reaction time (h)	Conversion (%)[a]	TOF (10^{-4} h^{-1} g^{-1}) [b]	Product selectivity (%)	
				2-PPN	Others
423	4	2.6	3.9	30	70
423	10	11.8	7.0	29	71
433	4	6.3	9.4	37	63
433	10	34.2	20.5	67	33
443	4	12.2	18.3	44	56
443	10	77.4	46.4	88	12
453	4	22.9	34.3	68	32
453	10	82.2	49.3	90	10
473	4	51.3	76.8	83	17
473	10	90.2	54.1	91	9

[a]Reaction conditions: PAN : 0.015 mol; DMC : 0.3 mol; NH_2-Na-Al-MCM-41: 0.25 g.
[b] Rate of PAN conversion= number of moles of PAN converted per hour of reaction time per gram of catalyst.

But when the temperature increased to 473 K, the rate of PAN conversion at 4 h of reaction time is higher than at 10 h of reaction time. This result evident the formation of intermediates with higher rate in the initial hours of reaction favors at higher reaction temperature. At higher temperatures there is an enhancement in the polarization of PAN into a PAN-anion, which activates the DMC molecule at carbonyl carbon position results in forming an intermediate A (Scheme 4.3). Intermediate A is activated by the basic sites to produce intermediate B (Scheme 4.3) with higher nucleophilic in character which attacks methyl group of DMC and rearranges to form 2-PPN and dimethylcarbonate. These all transformations are highly facilitated by higher reaction temperatures. The apparent activation

energy calculated for the methylation of PAN at lower conversion level is 114.0 kJ/mol (Fig. 4.7).

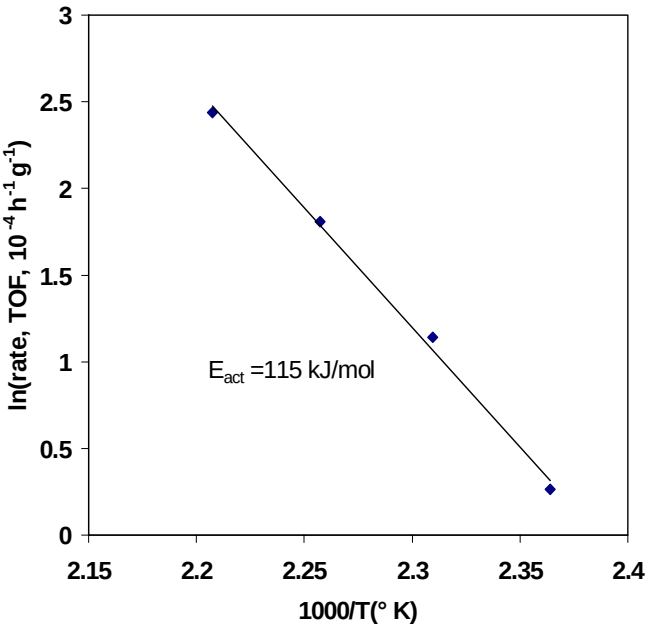

Fig. 4.8. Arrhenius plot for the rate of reaction (TOF, 10^{-4} h^{-1} g^{-1}) with different temperatures.

4.2.3.7. Recycling

To study the deactivation of basic sites, the catalyst was reused without any further treatment. After the reaction completed, the reaction mixture was decanted and a fresh reaction mixture was charged and continued the reaction. Fig. 9 shows the results of conversion of PAN, rate of PAN conversion (TOF) and selectivity for 2-PPN over fresh, first and second reused NH_2-Na-Al-MCM-41 (30) catalyst. A decrease in the PAN conversion is seen immediately in the first reuse, but selectivity to 2-PPN remains nearly ~ 90 %. Second reused catalyst shows a drastic decrease in activity (PAN conversion 52.2 %) as well as selectivity to 2-PPN (79 %). The decrease in activity may be due to either the formation of carbonaceous material inside pores of the catalyst, which block the active sites or formation of quaternary ammonium salts. The C, H, N elemental analysis confirms that there is an increase in carbon content in the

recycled catalyst compared to the fresh catalyst whereas nitrogen content remains almost the same in both fresh and recycled catalyst. Formation of large amount of "others" in case of second reuse can be accounted to the increase in carbon content (either as undesorbed products or formation of quaternary ammonium salts), which lowers the nucleophilic character of the amines. To confirm that, triethoxysilyl propyltriemthylammonium salt was prepared by the reaction of 3-APTES molecules with DMC and used as a catalyst. Almost full conversion of PAN with 85 % selectivity to 2-PPN could be achieved when neat 3-APTES was used as a catalyst where as only 50 % conversion of PAN with 65 % selectivity to 2-PPN was obtained when triethoxysilyl propyltriemthylammonium salt was used as a catalyst (Table 4.6).

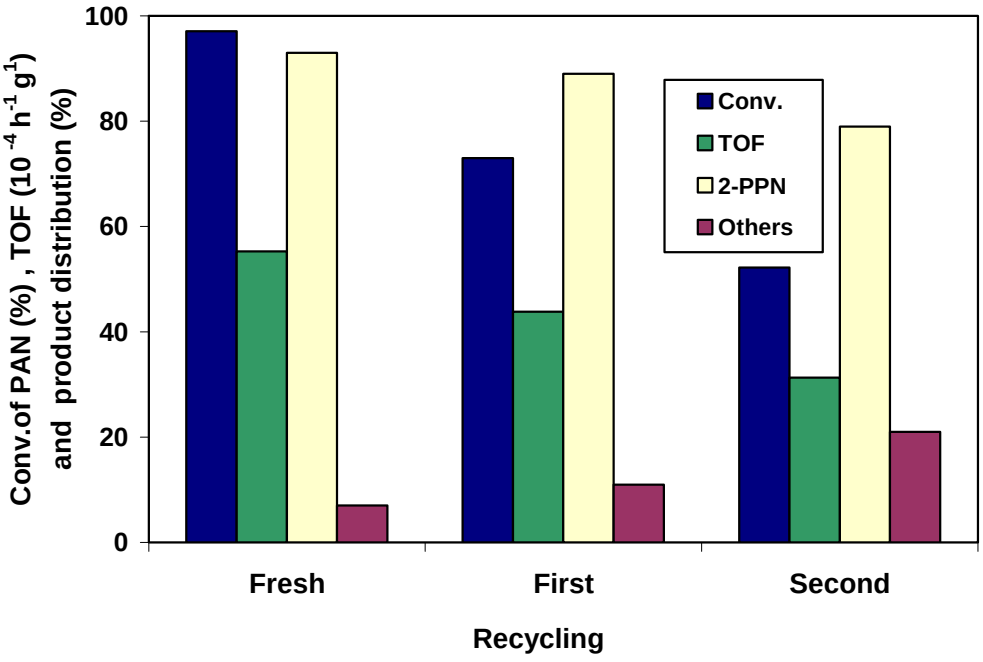

Fig. 4.8. Effect of recycling on the conversion of PAN (%), TOF (10^{-4} h^{-1} g^{-1}) and product distribution (%); Reaction conditions: PAN: 0.03 mol; DMC: 0.3 mol; catalyst: 0.5 g; reaction temperature: 473 K.

These results reveal that quaternary ammonium salt is less active than 3-APTES for the conversion of PAN and selectivity to 2-PPN under similar reaction conditions. Hence,

formation of quaternary ammonium salt in case of recycling catalysts are responsible for less activity of the catalyst for the conversion of PAN to 2-PPN.

Table 4.6 Effect of recycling of catalysts over the conversion of PAN.

Catalyst	Surface area (m^2/g)	Elemental analysis (%)			Conv. of PAN (%)[a]	Product distribution (%)	
		C	H	N		2-PPN	Others
Fresh	550	6.93	1.90	1.58	77.7	93	7
Recycle-1	308	7.62	2.32	1.51	75.6	89	11

[a] Reaction conditions: NH_2-Na-Al-MCM-41 /PAN (wt./wt.) : 0.07; DMC : 0.2 mol; reaction temperature: 453 K; reaction time :10 h.

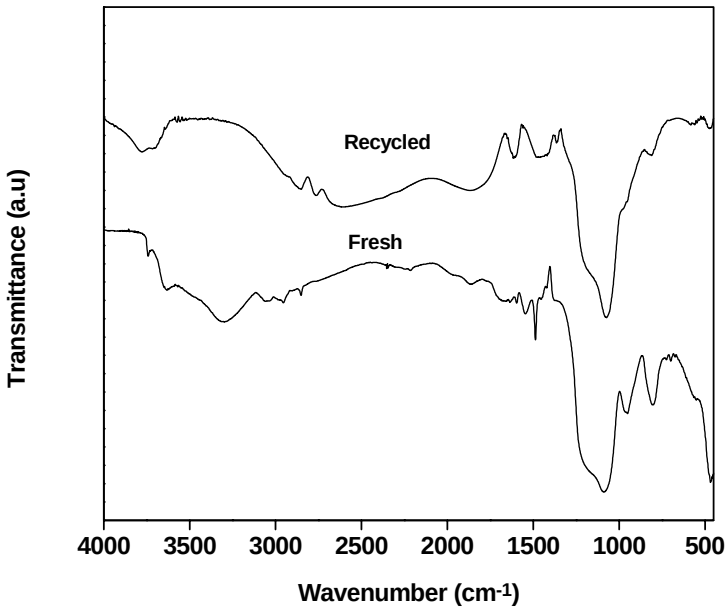

Fig.4.9. FT-IR spectrum of NH_2-Na-Al-MCM-41 (30); a: Fresh catalyst; b: recycled

FT-IR spectrum of used NH_2-Na-Al-MCM-41 (30) catalyst shows little decrease in intensity of the peaks compared to the fresh catalyst, corresponding to the stretching

frequency of amine functions and additionally some new, but weak bands also formed which may be correlated to carbonaceous materials formed over catalytic sites and stick over on it (Fig 4.9).

The stretching band of NH_2 and CH_2 groups found to be shifted to higher energy side in case of used catalyst (3619, 3298, 3026, 2940, 2877 and 1817 cm^{-1} to 3634, 3306, 3056,2955, 2851 and 1857 cm^{-1}, respectively). Fig. 4.10 shows the XRD pattern of the fresh and used NH_2-Na-Al-MCM-41 (30) catalysts. There is a decrease in intensity of the peak (*hkl* 100) but at the same time pore structure remain without collapse. This fact was also confirmed by decrease in surface area of the samples.

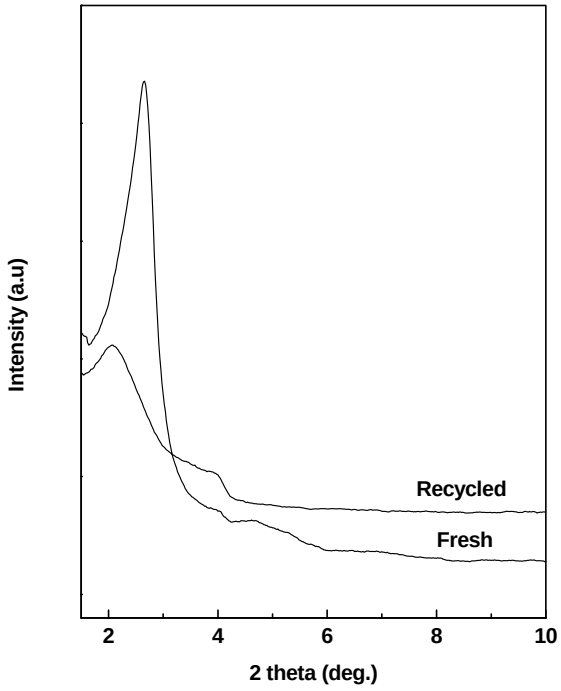

Fig. 4.10. X-ray diffractograms of NH_2-Na-Al-MCM-41 (30); (a) Fresh (b) recycled.

4.2.3.8. Mechanism of the reaction

Scheme 4.3 explains the possible mechanism for the conversion of PAN into 2-PPN over NH_2-Na-Al-MCM-41. 3-Aminopropylsilyl groups anchored on the walls of mesoporous silica

are the source of basic sites (Scheme 4.3, eqn.1). PAN anion is generated by the activation of PAN over basic sites (Scheme 4.3, eqn.2).

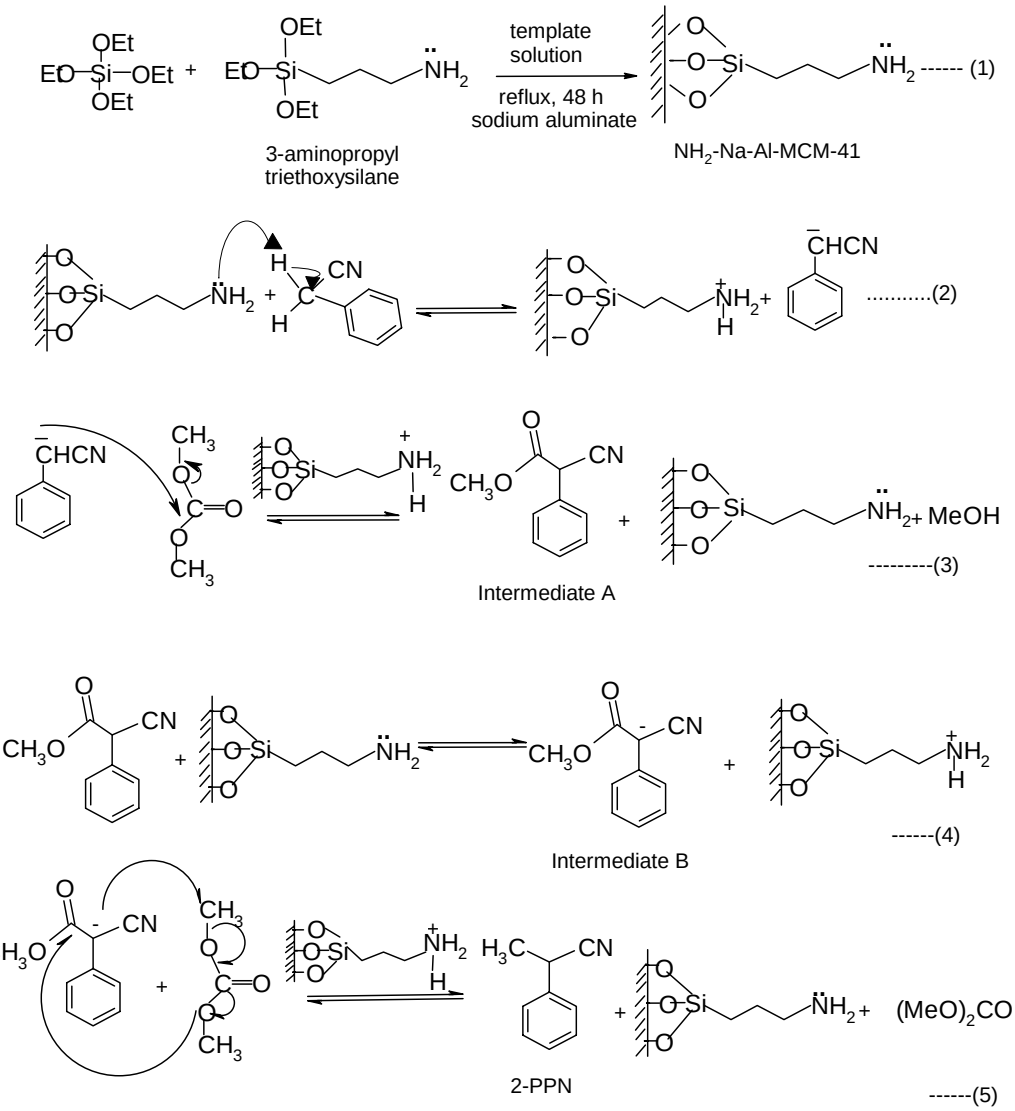

Scheme 4.3

DMC has double selectivity, i.e., both as methoxycarbonylating agent according to a $B_{Ac}2$ mechanism and as a methylating agent according to a $B_{A1}2$ mechanism [19]. Both reaction pathways are highly selective. PAN anion attacks carbonyl carbon of the DMC and hence the

formation of an intermediate A takes place (Scheme 4.3, eqn.3), which is highly acidic and reacts with the base immediately to form anion of the intermediate B (Scheme 4.3, eqn.4). DMC as a solvent has been shown to provide a suitable polar and aprotic environment for selectively orienting the reactivity of methoxycarbonylation and methylation reactions, respectively, in consecutive steps. Intermediate B, which is highly nucleophilic attacks CH_3 group of DMC and possibly converts into 2-PPN and gives back DMC (Scheme 4.3, eqn.5). In the course of reaction, basic sites of the catalysts are regenerated and methanol also formed as bi-product. The DMC is regenerated back and continuously utilized in the reaction.

4. 2. 4.Conclusions

NH_2-Na-Al-MCM-41 catalysts prepared by co-condensation of APTES, TEOS and sodium aluminate, are showing higher conversion of PAN and selectivity to 2-PPN compared to the microporous zeolites, alkali ion exchanged Na-Al-MCM-41, and conventional K_2CO_3 catalysts. Catalyst optimization study reveals that 30 wt % loading of APTES group over mesoporous aliminosilica exhibits maximum conversion of PAN and selectivity to 2-PPN. Reaction parameter study reveals that higher efficiency of active sites can be exploited only at the optimum catalyst concentration corresponds to reactant concentration, optimum molar ratio of DMC/PAN and higher reaction temperature. The optimum loading of catalyst was found to be 11.4 %. Higher concentration of DMC at DMC/PAN molar ratio (>10) facilitates the formation of 2-PPN by effective solvation and maximum random distribution of the intermediates, to access the catalytic sites effectively. Increase in reaction temperature enhances the activity of PAN conversion selectively towards 2-PPN. Recycling studies show that formation of quaternary ammonium salt in case of recycling catalysts is responsible for less activity of the catalyst for the conversion of PAN to 2-PPN.

4.2.5. References

1. G.A. Olah and S.J. Kuhn, Friedel-Crafts and Related Reactions Vol. II, G.A. Olah (Ed), Interscience, New York, 1964.
2. G.A.Olah, S.H. Flood, S.J. Kuhn, M.E. Moffatt, N.A. Overchuck, J. Am. Chem. Soc. **86** (1964) 1046.
3. G.A. Olah, S. Kobayashi, M. Tashiro, J. Am. Chem.Soc. **94** (1972) 7448.
4. A.V. Ramaswamy, in Petrotech-99, Third Int. Petrol. Conf. New Delhi, **Vol. III** (1999) 1.
5. C. Flego, G. Pazzuconi, E. Bencini, C.Perego, Stud. Surf. Sci. Catal. **126** (1999) 461.
6. S. Nojima, A. Yasutake, Y. Tanaka, JP 10298117, 1998.
7. A.K. Ghosh, US 5907073, 1999.
8. R. A. Grigoresa, I. Cojocaru, P. Obloja, C. Papuzu, G. Pop, R. Boeru, G. Ignatescu, S. Ichim, G. Ivanus, T. Stan, RO 11093, 1996.
9. H. Ming-Yuan, L. Zhoghui, M. Enze, Catalysis Today **2** (1988) 321.
10. J.C. Cheng et al., US Pat. 5453554, 1995.
11. J-P. Rieu, A. Boucherle, H. Cousse, G. Mouzin, Tetrahedron **42** (1986) 4095.
12. A. Bomben, C.A. Marques, M. Selva, P.Tundo, Tetrahedron **51** (1995) 11573.
13. W.G. Kenyon, E.M. Karser, C.R. Hauser, J. Org. Chem. **30** (1965) 4135.
14. C.M. Starks, C. Liotta, Phase Transfer Catalysis, Academic Press Inc. New York, 1976, 170.
15. E.V. Dehmlov, S.S. Dehmlov, Phase Transfer Catalysis, Verlag Chemie, Weinheim, 1983, 123.
16. P. Tundo, F. Trotta, G. Molagho, J.Chem.Soc. Perkins Trans. I (1989) 1070.
17. P. Tundo, G. Molagho, F. Trotta, Ind.Eng. Chem.Res. **28** (1989) 881.
18. Z. -H. Fu, Y. Ono, J. Catal. **145** (1994) 166.
19. M. Selva, C.A. Marques, P.Tundo, J.Chem.Soc. Perkins Trans. I (1994) 1323.
20. H. Hattori, Chem.Rev. **95** (1995) 537.
21. C.T. Kresge, M.E. Leonowicz, W.J. Roth, J.C. Vartuli and J.S. Beck, Nature **359** (1992) 710.
22. S. Biz, M.L. Occelli, Catal. Rev. Sci. Eng. **40** (1998) 329.
23. A. Corma, V. Fornes, R. M. Martin-Aranda, H. Garcia, J. Primo, Appl. Catal. A. Gen. **59** (1990) 237; A.Corma, D. Kumar, Stud. Surf. Sci. Catal.**117** (1998) 201.

24. K. R. Kloetstra, H. van Bekkum, J. Chem. Soc. Chem. Commun. (1995) 1005; H. van Bekkum, K. R. Kloetstra, Stud. Surf. Sci. Catal.**117** (1998) 171.
25. C. Noda Perez, E. Moreno, C.A. Henriques, S. Valanga, Z. Gabelica, L.F. Monteiro, Microporous Mesoporous Mater. **41** (2000) 137.
26. K. Moller, T. Bein, Chem. Mater. **10** (1998) 2950.
27. A. P. Wight, M. E. Davis, Chem. Rev. **102** (2002) 3589.
28. J. H. Clark, D. J. Macquarrie, J. Chem. Soc. Chem. Commun. (1998) 853.
29. D. Brunel, Micropor. Mesopor. Mater. **27** (1999) 329.
30. H.Y. Huang, R. T. Yang, Ind. Eng. Chem. Res. **42** (2003) 2427.
31. D. J. Macquarrie, D.B. Jackson, J. Chem. Soc. Chem. Commun. (1997) 1781.
32. E. Angeletti, C. Canepa, G. Martinetti, P. Venturello, Tetrahedron Lett. **29** *(*1988) 2261.
33. G. Demicheli, R. Maggi, A. Mazzacani, P. Righi, G. Sartori, F. Bigi, Tetrahedron. Lett. **42** (2001) 2401.
34. W. Gao, L. Raven, Langmuir **11** (1995) 1860.

5.1. Introduction

Dypnone is a useful intermediate for the production of a large range of compounds. It has been used as a softening agent, plastisizer and perfumery base. Dypnone has been prepared conventionally by the action of sodium ethoxide, aluminum bromide, phosphorous pentachloride, aluminum triphenyl, zinc diethyl, calcium hydroxide, anhydrous hydrogen chloride, anhydrous hydrogen bromide, aluminum chloride, aluminum *tert*-butoxide or hydrogen fluoride on acetophenone as described in the earlier literature [1-4]. In addition, it has been obtained by the action of aniline hydrochloride on acetophenone, followed by treatment with hydrochloric acid. Unfortunately, its synthesis is not always an easy task and Lewis acid catalysts have several disadvantages if applied to industrial processes such as wasting large amounts of catalysts, corrosion of reactor, water pollution by acidic wastewater, and difficulty of catalyst recovery. In addition, $AlCl_3$ being a strong Lewis acid also catalyzes other undesirable side reactions such as polycondensation of ACP to a mixture of other products. In view of the above, it was of interest to develop a new solid catalyst for the selective synthesis of dypnone. Modified zeolites are known to catalyze selectively aldol condensation of ACP to dypnone [5-8]. The objective of the present work is to replace the conventional Lewis acids catalyst with environmentally friendly solid acid catalysts such as sulfated zirconia (SZ) sulfated titania (ST) which are open structure and H-beta zeolite is closed three dimensional porous structure. We have chosen the later among other zeolites because it has been synthesized and characterized in our lab shows a good activity towards a variety of acylation reactions [9-11] and halogenation reactions [12]. It has also been reported that a comparative study of SZ with H-beta zeolite for alkylation of isobutene [13]. Another objective is to enhance the selectivity for dypnone and to minimize the formation of consecutive products in the condensation of ACP using solid acid catalysts. This paper

presents the results of a study comparing the performance of sulfated metal oxides with H-beta catalyst in the condensation of ACP (scheme 1). The condensation of ACP to dypnone has not been reported yet using such catalysts. The influence of catalyst concentration and reaction temperature is also reported using SZ as catalyst.

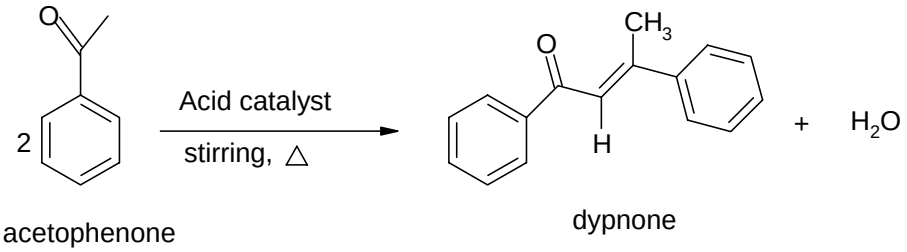

Scheme 5.1

5.2. Experimental

Acidity of the catalysts was evaluated by the temperature programmed desorption of ammonia from 303 K to 873 K (in several steps) using the method described in the literature [14]. The physico-chemical properties of the samples are given in Table 5.1. Before reaction, the catalysts were dehydrated at 573 K for 3 h.

Table 5.1: Physico-chemical properties of catalysts

Catalyst	Sulfur content (wt%) [a]	Surface area (m^2/g) [b]	NH_3 desorbed (mmol/g) at (K)						NH_3 chemisorbed at 303 K ($mmolg^{-1}$)
			303-353	353-433	433-513	513-653	653-773	773-873	
SO_4^{2-}/ZrO_2	3.08	100.6	0.16	0.07	0.17	0.29	0.15	0.61	1.45
SO_4^{2-}/TiO_2	3.04	145	0.01	0.14	0.01	0.03	0.01	0.17	0.37
H-beta[c]	-	745	0.08	0.1	0.15	0.43	0.36	0.07	1.19

[a] measured by SEM JEOL(JSM-5200); [b] measured by N_2 adsorption (NOVA).
[c] SiO_2/Al_2O_3 molar ratio=26; degree of H^+-exchange= >98.7%.

5.2.1. Catalytic reaction

Reactions were performed in the liquid phase under batch conditions. In a typical reaction, the activated catalyst (0.5 g) was added to ACP (0.042 mol) and the resulting suspension was magnetically stirred at 433 K. The course of the reaction was followed by analyzing the reaction mixture periodically using a gas-chromatograph (HP 6890) equipped with a flame ionization detector (FID) and a capillary column (HP 5% silicone gum). The products were also identified by GC/MS (Shimadzu, QP 2000 A) analysis. The isolation of pure products was accomplished by silica gel (60-120-mesh) column chromatography with 5 % ethyl acetate in petroleum ether as eluting solvent. TLC and GC confirmed the formation of pure compound. The major products obtained in this study are in agreement with the spectroscopic data of the pure compound.

Spectroscopic data of dypnone: ^{1}H NMR (200 MHz) ($CDCl_3$) (δ): 2.48(s, 3H); 7.05(m, 1H); 7.05-7.87(m, 10H). GC-FT-IR (vapor phase): 1610 cm^{-1} (-C=C-); 1675 cm^{-1} (-C=O).

The conversion is defined as the percentage of ACP transformed. The rate of ACP conversion is given as the amount of ACP (mmol) converted per gram of the catalyst per hour during the initial period. The selectivity (wt.%) for a product is expressed as the amount of the product divided by the amount of total products and multiplied by 100.

5.3. Results and discussion

5.3.1 Effect of various catalysts

The catalytic activity, rate of ACP conversion and selectivity to dypnone formation with different catalysts, under similar reaction conditions, are given in Table 5.2. The results with $AlCl_3$ are also included for comparison. As seen from Table 5.2, trans and cis dypnone together with ketene are formed in the condensation of ACP. The aldol condensation of ACP

produces dypnone as a major and primary product while ketene is a secondary product. As can be seen from Table 2, SZ and zeolite H-beta exhibit similar and higher activity compared to the ST. However, the selectivity for dypnone over all catalysts remains nearly constant. The conversion of ACP, rate of ACP conversion and selectivity for dypnone over SZ, ST and H-beta are found to be 40.1, 28.5, 40.8 wt.%, 6.7, 4.8, 6.8 mmol g^{-1} h^{-1} and 86, 86 and 85 wt. %, respectively. $AlCl_3$ catalyst is found to be more active (180.5 mmol g^{-1} h^{-1}) with comparable selectivity (84 wt.%) to dypnone. The higher conversion of ACP over SZ and H-beta seems to be due to the fact that these catalysts exhibit stronger acid sites (Table 5.1).

Table 5.2. Condensation of acetophenone with various catalysts

Catalyst	Conversion of ACP (wt.%)[a]	Rate of ACP conv. ($mmolg^{-1}h^{-1}$)[b]	Product distribution (wt. %)	
			Dypnone	Others[c]
SO_4^{2-}/ZrO_2	40.1	6.7	86	14
SO_4^{2-}/TiO_2	28.5	4.8	86	14
H-beta	40.8	6.8	85	15
$AlCl_3$[c]	36.1	180.5	84	16

[a] Reaction conditions: catalyst(g)=0.5; acetophenone(mol) = 0.042; reaction temperature (K) = 433; reaction time(h) = 5
[b] Rate of ACP conversion($mmolg^{-1}h^{-1}$) is expressed as the ACP converted per hour per g ram of the catalyst
[c] Others = cis form of dypnone and ketenes
[d] Reaction time (h) = 0.16

As can be seen from Table 5.2, SZ and zeolite H-beta exhibit similar and higher activity compared to the ST. However, the selectivity for dypnone over all catalysts remains nearly constant. The conversion of ACP, rate of ACP conversion and selectivity for dypnone over SZ, ST and H-beta are found to be 40.1, 28.5, 40.8 wt.%, 6.7, 4.8, 6.8 mmol g^{-1} h^{-1} and 86, 86 and 85 wt. %, respectively. $AlCl_3$ catalyst is found to be more active (180.5 mmol $g^{-1}h^{-}$

[1]) with comparable selectivity (84 wt.%) to dypnone. The higher conversion of ACP over SZ and H-beta seems to be due to the fact that these catalysts exhibit stronger acid sites (Table 5.1). These results indicate that strong acid sites are the most important factor to enhance both the protonation and the dehydration and consequently to force the aldol condensation of ACP to dypnone. Optimization of the reaction condition was done with catalyst SZ and other catalysts were compared under optimized conditions.

5.3.2. Duration of the run

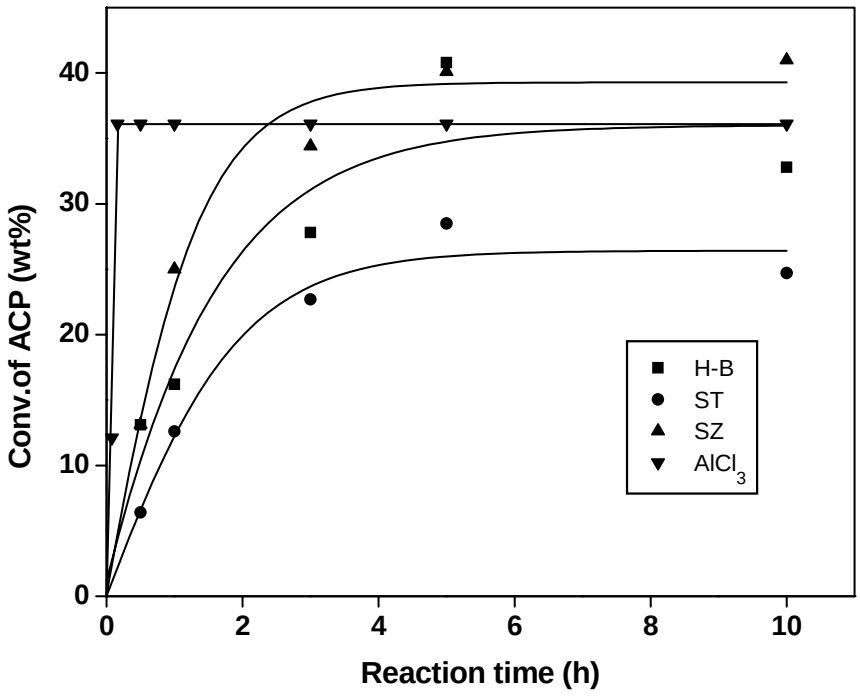

Fig. 5.1. Effect of different catalysts on conversion of ACP (wt.%); Reaction conditions: catalyst (g)=0.5; acetophenone (mol) = 0.042; reaction temperature (K) = 433; reaction time(h) = 5.

Fig. 5.1 shows the time dependence of the conversion of ACP (wt.%) over SZ, ST, H-beta and $AlCl_3$ under similar conditions. H-beta showed a lower initial activity compared to SZ and $AlCl_3$, because of diffusional resistance in H-beta. However, after 2 h of reaction time H-beta performed better than $AlCl_3$. The lower activity of $AlCl_3$ after 2 h may be attributed to the amount of $AlCl_3$ (in relation to ACP) used in the reaction, which was less than the stoichiometric amount normally required. The ST catalyst was considerably less active than SZ and $AlCl_3$, because of diffusional resistance in H-beta.

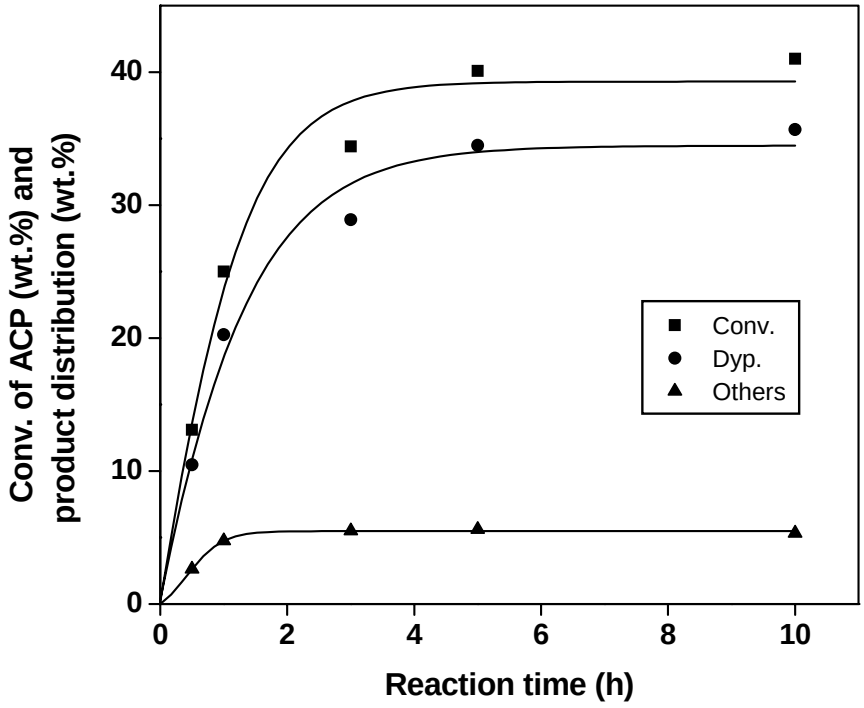

Fig. 5.2. Effect of reaction time on conversion (wt.%) of ACP and dypnone selectivity (%) over SZ catalyst; Reaction conditions: catalyst (g)=0.5; acetophenone (mol) = 0.042; reaction temperature (K) = 433.

However, after 2 h of reaction time H-beta performed better than $AlCl_3$. The lower activity of $AlCl_3$ after 2 h may be attributed to the amount of $AlCl_3$ (in relation to ACP) used in the reaction, which was less than the stoichiometric amount normally required. The ST catalyst was considerably less active than H-beta and SZ due to its lower acidity and weaker acid sites

(Table 5.1). Based on this conversion of ACP after 1 h of reaction time, positive trend in activities for the catalyst SZ was studied varying other reaction parameters. Fig. 5.2 shows the conversion of ACP and product distribution over SZ with the increase in reaction time up to 10 h. Reaction conditions were detailed in Table 5.2. It can also be seen from the results that there is a steady increase in the conversion of ACP and the yield of dypnone, which level off after 3 h of reaction time. The result shows that the reaction time influenced the conversion of ACP and product yields in the condensation of ACP.

5.3.3. Influence of catalyst/ACP ratio on ACP conv. Vs reaction time

Fig. 5.3 compares the conversion of ACP as a function of reaction time using different concentrations of catalyst under similar conditions as those depicted in Table 5.2. The conversion of ACP is found to increase markedly up to 2 h of reaction time with the increase in SZ/ACP ratio from 0.05 to 0.15. However, for longer reaction time (5 h) the conversion of

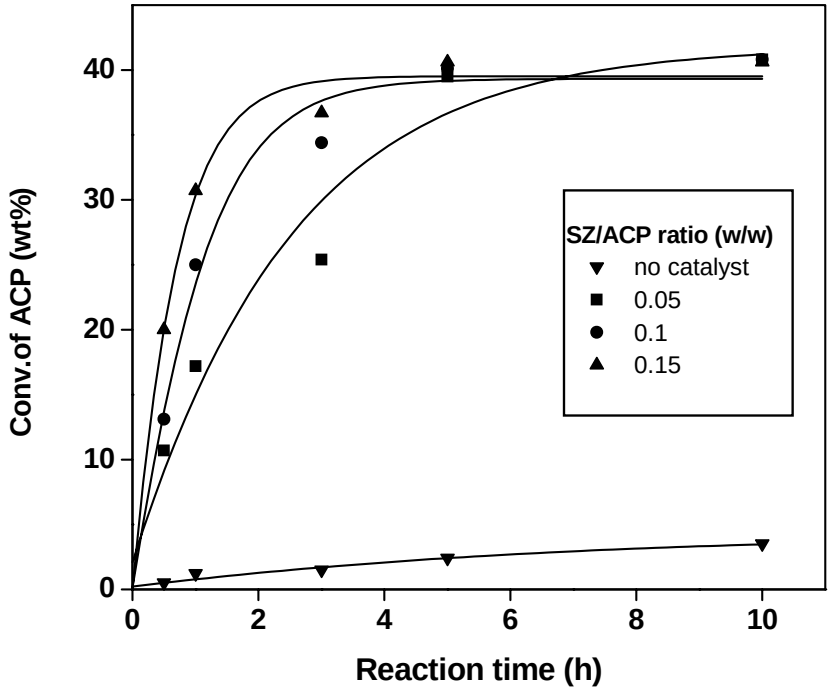

Fig. 5.3. Effect of catalyst/ACP ration on conversion of ACP (wt.%); Reaction conditions: acetophenone (mol) = 0.042; catalyst (g)=0.5; reaction temperature (K) = 433.

ACP is similar at all catalyst concentrations. A negligible, lower conversion of ACP (wt.%) is observed in the absence of catalyst. Fig. 5.4 shows the effect of SZ (catalyst)/ ACP ratio (wt./wt.) on the conversion of ACP, rate of ACP conversion and product distribution. The catalyst/ACP ratio was varied from 0.05 to 0.15 by keeping the concentration of ACP constant. The total surface area available for the reaction depends on the catalyst loading. It was found that with an increase in catalyst/ACP ratio the conversion of ACP increases linearly from 17.2 to 30.7 wt. % for the reaction time of 1 h. The reason is due to the increase in the total number of acid sites available for the reaction.

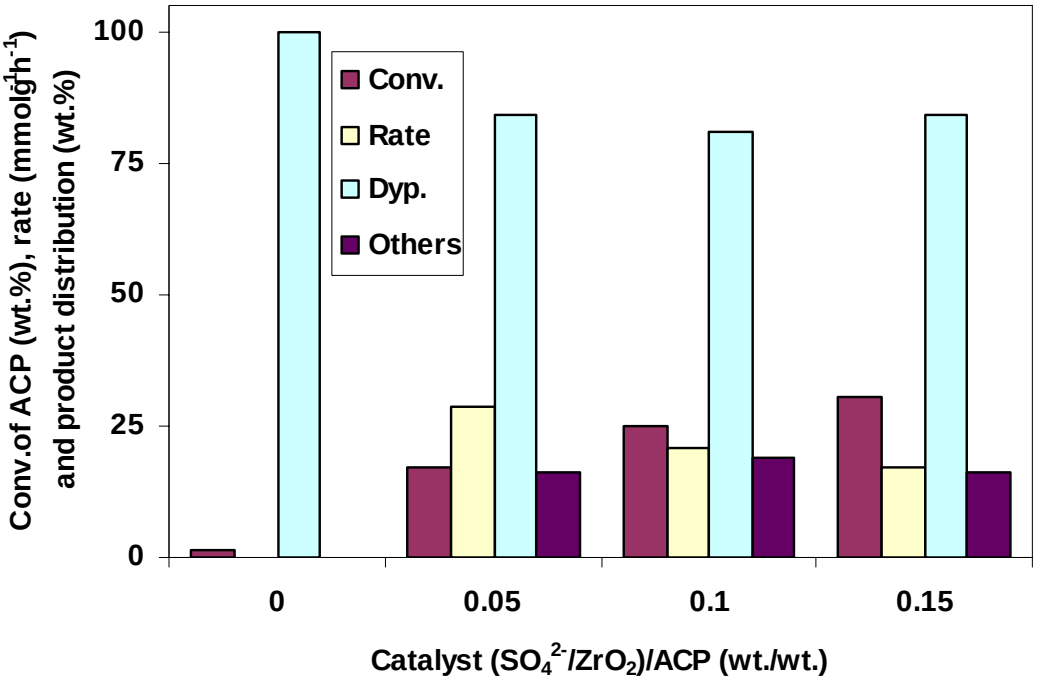

Fig. 5.4. Effect of catalyst/ACP ration on conversion of ACP (wt.%), rate and product distribution (wt.%); Reaction conditions: acetophenone (mol) = 0.042; reaction temperature (K) = 433; reaction time (h) = 5.

The corresponding rate decreases from 28.7 to 17.1 $mmolg^{-1}h^{-1}$ respectively. No change in the dypnone selectivity is observed with the change in catalyst/ACP ratio. These results indicate

the need of a catalyst for decreasing the activation energy barrier in the condensation of ACP to dypnone.

5.3.4. Influence of reaction temp. on ACP conv. Vs reaction time

Fig. 5.5 shows the effect of the reaction temperature on the conversion of ACP Vs reaction time during the condensation of ACP. The reaction temperature was varied between 403 K and 433 K. Increasing the reaction temperature increases the catalytic activity sharply up to 3 h of reaction time and the conversion of ACP levels off with reaction time at all reaction temperature studied. The effect of reaction temperature on the conversion of ACP, rate of ACP conversion and product distribution is investigated in the range of 403-443 K

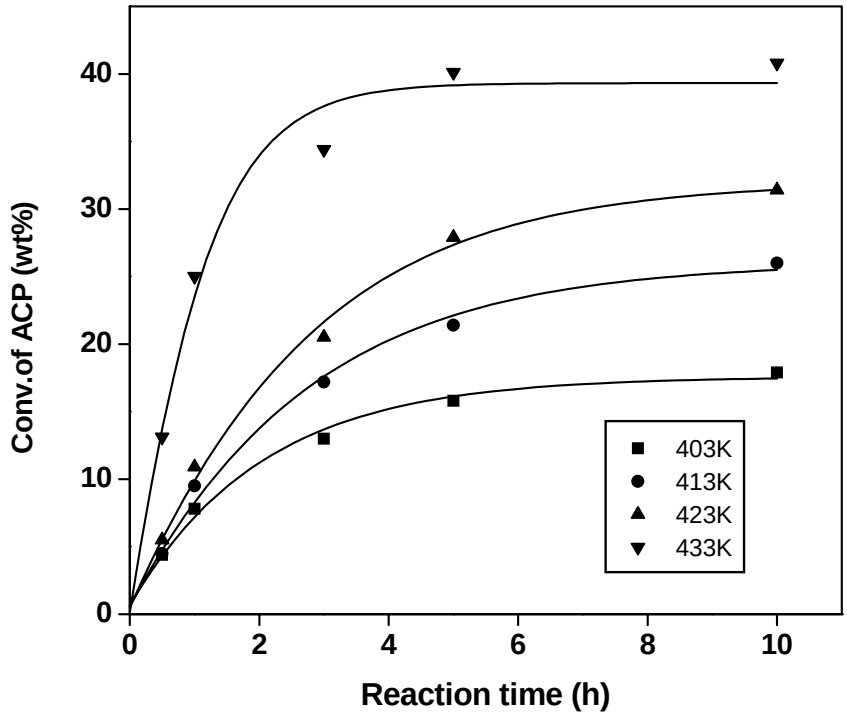

Fig. 5.5 Influence of reaction temperature (K) on the conversion of ACP (wt.%) over SZ catalyst with reaction time (h) ; Reaction conditions: catalyst(g)=0.5; acetophenone(mol) = 0.042.

using the SZ as catalyst (Fig. 5.6). The conversion of ACP and rate of ACP conversion increases from 17.1 to 40.1 wt.% and 2.8 to 6.7 $mmolg^{-1}h^{-1}$ respectively, when the temperature is raised from 403 to 433 K. However, the selectivity for dypnone remains nearly constant as shown in Fig. 5.6. A maximum in dypnone selectivity (87 wt.%) over this catalyst is observed at 403 K. The apparent activation energy for the condensation reaction over SZ is estimated to be 40.8 kJ mol^{-1}.

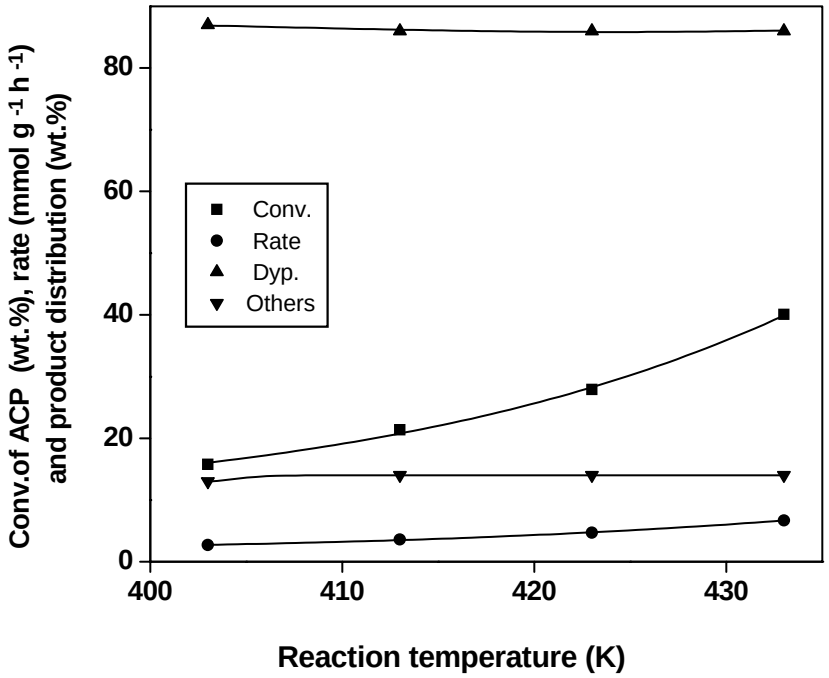

Fig. 5.6. Effect of reaction temperature (K) on the conversion of ACP (wt.%), rate of ACP conversion (mmol g^{-1} h^{-1}) and product distribution, over SZ catalyst; Reaction conditions: catalyst (g)=0.5; acetophenone (mol) = 0.042; reaction time (h) = 5.

5.3.5 Catalyst recycling

SZ sample used in the condensation of ACP was recycled two times (Fresh+ two cycles). Fig. 5.7 presents the results of these experiments. The catalyst shows a marginal decrease of the activity after the use of fresh catalyst. However, after first recycle of the

catalyst, a minor decrease in the catalytic activity was noticed without loosing its selectivity for dypnone. The present study indicates that the catalyst can be recycled a number of times without loosing its activity to a greater extent.

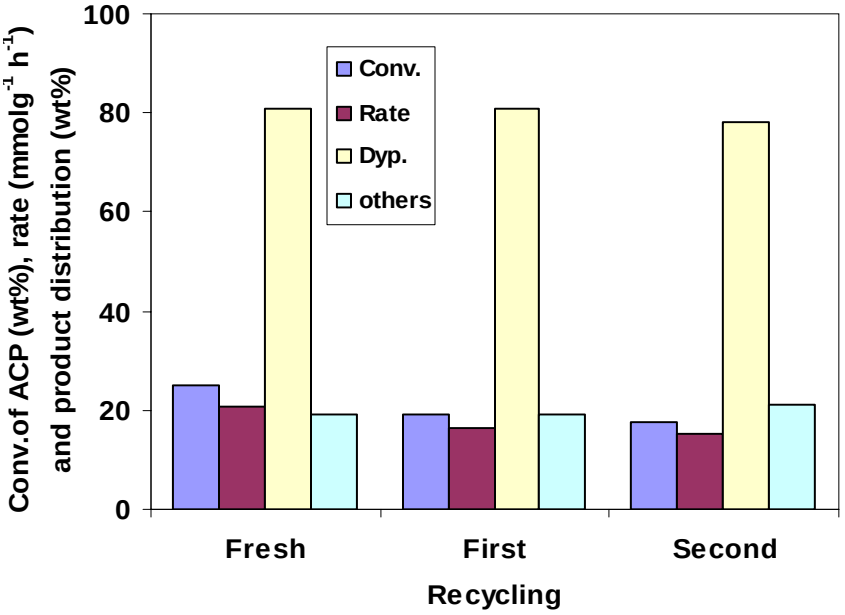

Fig. 5.7. Effect of recycling of catalyst (SZ); Reaction conditions: catalyst (g)=0.5; acetophenone (mol) = 0.042; reaction time (h) = 5.

5.3.6. Mechanism

The formation of dypnone takes place when one of acetophenone molecule gets protonated and forms its conjugate acid (Scheme 5.2, eq.1). The electrophilic addition of the carbonium ion (conjugate acid) to the enol form of another molecule produces aldol (Scheme 5.2, eq.2). Further protonation of the alcoholic OH of the aldol and elimination of water molecule forms a carbonium ion intermediate (Scheme 5.2, eq.3). Loss of H^+ from the α-C atom results in the formation of α, β-unsaturated ketone (dypnone) (Scheme 5.2, eq.4).

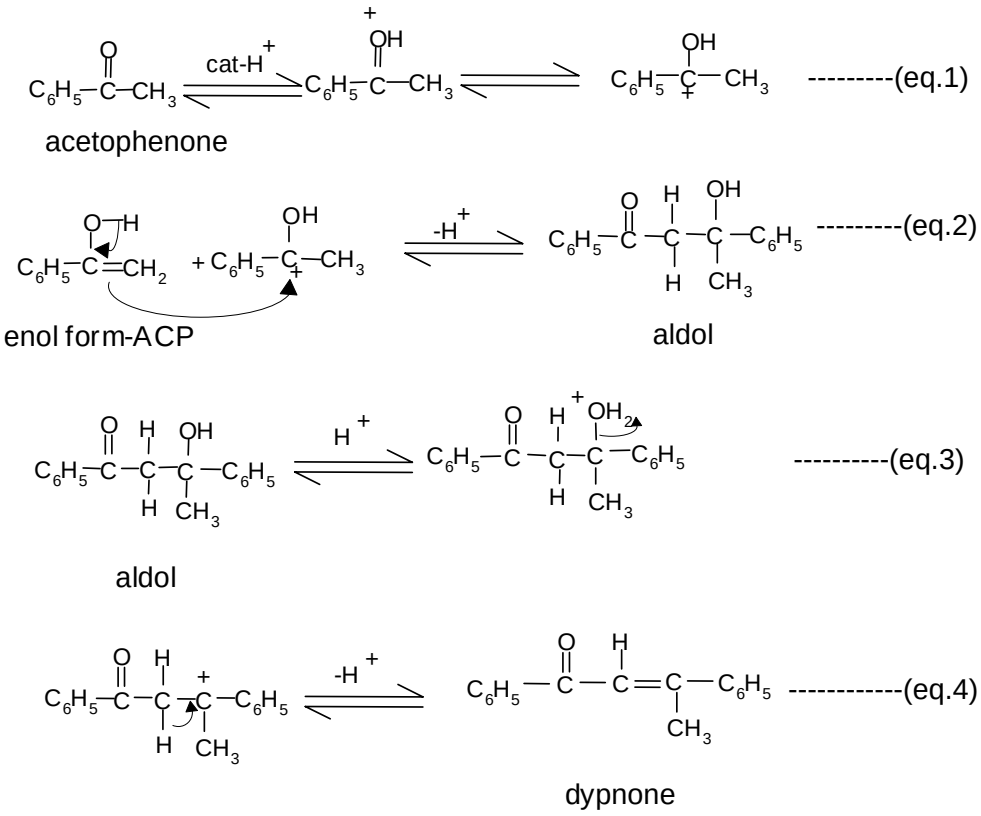

Scheme 5.2

5.4 Conclusions

It is found that SZ and H-beta exhibit similar activity (rate of ACP conversion), which is higher than that of sulfated titania. From the TPD of NH_3 it is seen that both sulfated zirconia and H-beta are highly acidic and possess strong acid sites, as seen from NH_3 desorption in the temperature range of 513 K to 873 K, which are responsible for the reaction. The conversion of ACP increases with reaction time, the catalyst concentration and reaction temperature. The SZ is recycled two times to show that there is only a marginal decrease in activity on recycled catalyst with no loss in the selectivity for dypnone.

5.5. References

1. W. Taylor, J. Chem. Soc. (1937) 304.
2. N. O. Calloway and L. D. Green, J. Am. Chem. Soc. **59** (1937) 809.
3. H. Adkins and F. W. Cox, J. Am. Chem. Soc. **60** (1938) 1151.
4. J. H. Simons and E. O. Ramler, J. Am. Chem. Soc. **65** (1943) 1390
5. H. Garcia, J. C. Maria, A. Corma, S. Iborra and J. Primo, Appl. Catal. A: General **130** (1995) 5.
6. H. P. Hagen, U.S. Patent 4 433 174 (1984).
7. P.B. Venuto, Microporous Mater. **2** (1994) 297.
8. P.B. Venuto and P.S. Landis, J. Catal. **6** (1966) 237.
9. T. Jaimol, P. Moreau, A. Finiels, A.V. Ramaswamy and A.P. Singh, Appl. Catal. A: General **214** (2001) 1.
10. V.D. Chaube, P. Moreau, A. Finiels, A.V. Ramaswamy and A.P. Singh, J. Mol. Catal. A: Chemical **174** (2001) 355.
11. C. Venkatesan, T. Jaimol, P. Moreau, A. Finiels, A.V. Ramaswamy and A.P. Singh, Catal. Lett. **75** (2001) 119.
12. A.P. Singh, S.P. Mirajkar, S. Sharma, J. Mol. Catal. A. **150** (1999) 241.
13. A. Corma, M.I. Juan-Rajadell, J.M. Lopez-Nieto, A.Martinez, and C. Martinez, Appl. Catal. A: General **111** (1994) 175.
14. A. P. Singh, D. Bhattacharya, and S. Sharma, J. Mol. Catal. A: Chemical **102** (1995) 139.

6.1. Introduction

Transition metal-catalyzed reactions have gained a steadily increasing importance in recent research and developments. Fine tuning of reaction parameters of known or newly discovered metal catalyzed transformations along with the catalyst development had a good impact on the synthesis of natural and non-natural biological active compounds (valuable intermediates in the pharmaceutical and agrochemical industries) as well as theoretically interesting molecules. Among the process, palladium catalyzed transformations have played a leading role in developing and understanding totally new reaction types and peculiar path ways of transformations. Two of the most general and widely used palladium catalyzed processes are the arylation and alkenylation of alkenes, generally known as Heck reactions and the nucleophilic substitution of allylic substrates.

Carbon-carbon bond forming reactions represent the potential applications of palladium catalysts [1]. Among pool of palladium catalysts, carbometallated Pd (II) compounds, especially palladacycles, have emerged as very promising catalysts for C-C bond forming reactions [2-5]. Cyclopalladated phosphines, phosphinite, chelating diphosphines, carbene ligands and dimethylglycine have also been reported [6-9], however, a desired option for commercial realization stays back as the catalysts either require hazardous phosphate ligands for the stabilization of Pd in its zero valence state or tedious synthesis and activation procedures. A recent trend in catalysis related with environmental and economic concerns is the transformation of a homogeneous catalytic system into a heterogeneous system in which the active centers are supported on a solid, making the catalyst easily recoverable from the reaction mixture with the possibility of reuse and waste minimization [10-12]. For this reason, the activity of Pd and its metallic complexes supported over variety of solid supports,

particularly active charcoal, silica, and inorganic oxides have been studied for C-C coupling reactions [13-18]. Pd modified zeolites have been studied in the Heck reaction [19-20], but the smaller pore dimension limit their applications for larger molecules. Moreover Pd-zeolites catalysts need to be activated for getting the active metallic Pd in zero state.

The discovery of mesoporous molecular sieves has simulated a renewed interest in developing adsorbent, sensors and the design of catalysts due to their high surface areas with narrow pore size distributions (2-20 nm) [21, 22]. Kosslick et al. have studied the anchoring of alkylsilylsulfonic acid into the walls of Al-MCM-41 to stabilize the catalytic active palladium complex that was formed during the course of reaction [23]. Silica supported palladacycle catalysts have been studied for C-C coupling reactions [24, 25]. Corma et al. have reported an oxime-carbapalladacycle complex covalently anchored to silica as an active and reusable heterogeneous catalyst for Suzuki cross-coupling in water [26]. Various attempts towards the immobilization of organometallic complexes have been made previously, such as attachment to supporting materials by chemisorption, immobilization by steric hindrance in zeolite micropores (ship-in-a-bottle concept), or supported liquid phase catalysts [27].

Ortho-palladation with the weakest of palladation agents (Li_2PdCl_4) under very mild conditions, due to steric promotion of an aromatic C-H bond activation was studied by Dunia et al [28]. In this study, carbometallation was used to immobilize the palladium catalysts on MCM-41 support. Carbometallation of anchored ligands with palladium metal centre enhanced by steric constraint of mesopores have been exploited to get heterogeneous palladium catalyst.

Recently, we have reported for the first time that aliphatic C-metallated palladacycle synthesized in the pores of 3-hydroxypropyl triethoxysilane functionalized MCM-41 was found as an active and stable catalyst for Heck alkenylation of bromobenzne [29]. Here we report the synthesis and characterization of palladacycle-MCM-41 materials along with the

catalysts textural properties. The influence of synthesis conditions on the catalytic performance of the catalysts has been studied in the Heck alkenylation of bromobenzene. The heterogeneity of the catalyst has also been examined.

6.2. Experimental

Synthesis of palladacycle has been detailed in chapter 2. Here the complete characterizations of the sample and optimization studies are presented. Scheme 6.1 shows the synthesis procedure for obtaining palladacycle immobilized on solid materials.

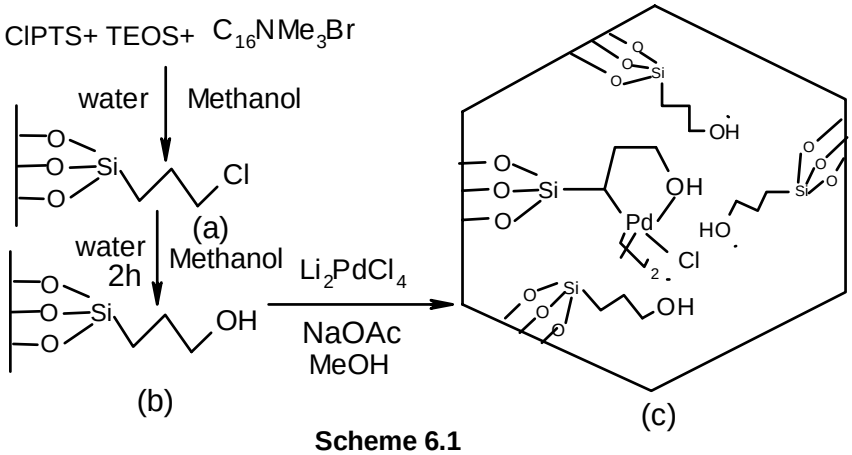

Scheme 6.1

6.2. 1. Heck alkenylation reactions

Heck alkenylation reactions were carried out in a 25 ml glass reactor. In a typical experiment 0.03 g catalyst and 2.4 x 10^{-3} mol potassium carbonate were added into a solution of 2 x 10^{-3} mol bromobenzene and 3 x 10^{-3} mol of styrene in 5.0 ml N-methyl-2-pyrrolidone solvent (Scheme 6.2). The reaction mixture was heated under stirring for specified time. At regular intervals samples were collected and analysed by GC (HP 6890 N series) equipped with FID detector and HP-5 capillary column. Peak positions of reaction products were

compared and matched with the retention times of authentic samples. Identity of the products was also confirmed by GC-MS and ^{1}H-NMR analysis.

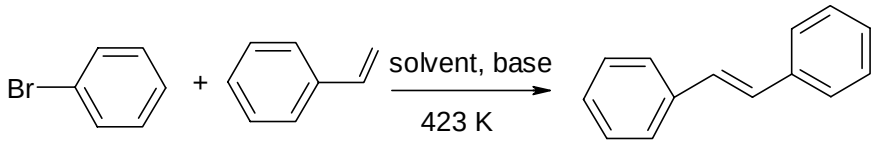

bromobenzene styrene *trans*-stilbene

scheme 6.2

6.2. 2. Homoaryl coupling reactions

Homoaryl coupling reactions were carried out in a 25 ml glass reactor. In a typical experiment 0.05 g catalyst and 2.4 x 10^{-3} mol potassium carbonate were added into a solution of 1 x 10^{-2} mol halobenzene in 5.0 ml dimethylformamide (DMF) solvent (Scheme 6.3). The reaction mixture was heated under stirring for specified time. At regular intervals samples were collected and analysed by GC (HP 6890 N series) equipped with FID detector and HP-5 capillary column. Peak positions of reaction products were compared and matched with the retention times of authentic samples. Identity of the products was also confirmed by GC-MS and ^{1}H-NMR analysis.

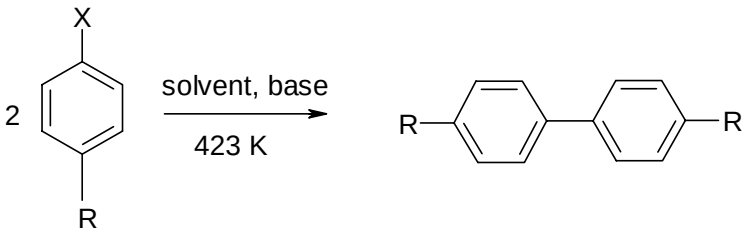

halobenzene biphenyls

(x=Cl,Br; R= -OH,-NO_2)

Scheme 6.3

6.3. Results and discussions

6. 3.1. Synthesis of catalysts

In order to immobilize the homogeneous catalyst on a heterogeneous solid surface, an organic linker group is needed. Organic functionalization of the internal surfaces of MCM-41 can be achieved, either by covalently grafting of various organic species onto the surface, or by incorporating of functionalities directly during the preparation. The organosilane having ligands such as chlorine or amine is directly grafted to the silica surface by an in-situ silylation procedure. The chlorine functional group gets hydrolyzed into hydroxyl group either at synthesis condition or at post-synthesis hydrolysis treatment. These types of ligands permit formation of complexes through coordination bond with metal centers [31, 32]. There are three types of ≡ SiOH groups over siliceous MCM-41 surface [33], e.g. isolated single, hydrogen bonded and geminal ≡ SiOH groups, of which only the single and geminal ≡ SiOH groups are responsible for active silylation. The Hydrolysis of required composition of ClPTS and TEOS (0.05-0.3 and 0.095-0.7, respectively) in the presence of TMAOH enriches the mother liquor with single and geminal ≡ SiOH monomer silica species. Co-condensation of symmetrical $Si(OH)_4$ and unsymmetrical $RSi(OH)_3$ species results to the formation of uniformly distributed organo functionalized silica.

Six different molar ratios of TEOS to ClPTS in the synthesis mixture have been taken while synthesis to obtain materials with a range of different concentration of ClPTS functional groups over MCM-41. Six different samples are designated as Cl-M1, Cl-M2, Cl-M3, Cl-M4, Cl-M5 and Cl-M6 and the respective hydrolyzed samples are designated as OH-M1, OH-M2, OH-M3, OH-M4, OH-M5 and OH-M6. The fraction of functionalized silicon atoms in the synthesis gel (x) was set in the range of 0.025 to 0.3 as it was reported that material prepared with fraction of silicon atom in that range is more stable and hydrophobic in nature because of

hydrophobisation of all the silanol groups. The higher fraction of functionalized silicon atoms obtained in the synthesized material was 0.2 (Table 6.1). From C, H elemental analysis it was observed that effective loading of ClPTS groups into the coupling agent, TEOS was about 60 wt % with respect to the amount of ClPTS taken in the synthesis gel.

Table 6. 1 Molar composition of silylating agent and coupling agents in the synthesis of mesoporous materials with the molar composition: (1-x) TEOS: x ClPTS: 0.25 C_{16}TAB: 0.3 TMAOH: 90H_2O: 10 MeOH

Catalysts	TEOS (mol)	ClPTS (mol)	x		ClPTS (mmol/g)		% of Loading	Surface area (m^2/g)
			In put	Out put[a]	In put	Out put[a]		
Cl-M0	0.1	0	0	0	-	-	-	1050
Cl-M1	0.12	0.003	0.024	0.016	0.42	0.27	64	760
Cl-M2	0.107	0.007	0.061	0.036	1.08	0.6	56	735
Cl-M3	0.093	0.01	0.097	0.059	1.78	0.99	56	855
Cl-M4	0.08	0.013	0.14	0.1	2.7	1.67	62	614
Cl-M5	0.067	0.017	0.202	0.159	4.21	2.65	63	726
Cl-M6	0.05	0.02	0.286	0.196	6.66	3.26	49	715

[a] Calculated from the data obtained from C, H analysis

Table. 6. 2 Physical characteristics of the catalysts (OH-M)

Catalysts	2θ	d_{100} (Å)	Unit-cell parameter, a_0 (Å)	BET surface area (m^2/g)
OH-M1	2.57	34.36	39.68	547
OH-M2	2.49	35.47	40.96	578
OH-M3	2.47	35.75	41.29	862
OH-M4	2.48	35.61	41.12	624
OH-M5	2.34	37.74	43.58	732
OH-M6	2.4	35.9	41.46	712

The physical properties of OH-M samples are given in Table 6.2. Palladation was carried out over OH-M1, OH-M2, OH-M3, OH-M4, OH-M5, and OH-M6 samples under similar reaction conditions to obtain Pd-OMS1, Pd-OMS2, Pd-OMS3, Pd-OMS4, Pd-OMS5 and Pd-OMS6, respectively. All the palladation reactions were carried out at 335 K in methanol and with sodium acetate (Table 6.3). Dunia et al. have achieved best results when ortho-palladation of a sterically crowded primary benzylamine, α-phenylneopentylamine, was performed with Li_2PdCl_4 and excess sodium acetate in methanol [28]. Polar solvents have some advantages over non-polar solvents in the palladation reactions due to their strong solvating effect that assists in the generation of three- coordinate intermediate of the $[L_2PdX_2(solv)]$- type required for subsequent C-H bond activation [34]. Here the same steric effect due to the organofunctionalized mesoporous structure has been utilized for the activation of aliphatic C-H activation. Formation of a quasi-immobilized palladium complex inside the mesopores when the anchored 3-hydroxypropyltriethoxy silane is treated with palladium source creates a steric constraint which might be expected to cause aliphatic C-H bond activation and hence

carbometallation occurs with weakest of palladation reagents and weak ligands under mild conditions. In the case of porous catalysts incorporating with organic functionalities, not only

Table 6.3. Physico-chemical characteristics of the catalysts (Pd-OMS)

Catalysts	2θ	d_{100} (Å)	Unit-cell parameter, a_0 (Å)	BET surface area (m^2/g)	Pd cont. (%)	Conv. of bromoben. (wt.%)[g]	Yield *tran*-stilbene	TON[h]
Pd-OMS1[a]	2.62	33.71	38.93	351	0.44	5.8	100	93
Pd-OMS2[b]	2.76	32.0	36.95	384	0.88	27.3	95	205
Pd-OMS3[c]	2.77	31.88	36.82	632	0.94	33.8	90	213
Pd-OMS4[d]	2.40	36.83	42.53	640	1.12	42.4	89	340
Pd-OMS5[e]	2.49	39.42	40.96	862	1.05	57.8	90	389
Pd-OMS6[f]	2.4	35.9	41.46	722	0.97	38.5	92	280

[a-f] OH-M1, OH-M2, OH-M3, OH-M4, OH-M5, OH-M6, and OH-SiO_2 respectively =1 g; Li_2PdCl_4=1.4 x10^{-4}mol (1.5% Pd); NaOAc= 50 mg; methanol= 20mL; reaction temperature=335 K; reaction time= 24 h.
[g] BB=2 mmol; styrene=3 mmol; K_2CO_3= 2.4 mmol; NMP=5.0 ml; temp.=423 K ;catalyst=30 mg; reaction time=5 h.
[h]TON (Turn over number)= moles of BB converted per mole of Pd.

the constraint of the surface, but also of the pore itself has to be considered potentially resulting in an even larger constraint [35]. The spatial confinement induced by the pore walls forces the propyl group to cyclise in presence of electrophilic metal centre. Two main possible factors determine the easier aliphatic carbometallation with weakest palladation reagents: (i) a large effective volume of the ligand (3-hydroxypropyltriethoxysilane) incorporated into MCM-41 pore walls must increase an internal energy of the intermediate bi-nuclear coordination compounds due to a set of unfavorable non-bonding interaction [36], thus stimulating an intermediate dissociation to form reactive three coordinate species; (ii) the same steric effect must result in a weakening of Pd-O bond in the coordination intermediate, to make the palladium (II) centre more electrophilic. Both effects essentially facilitate the C-H

bond activation [37]. The palladation results obtained with the week palladation reagents, Li_2PdCl_4, in methanol in the presence of sodium acetate at room temperature may be considered as the most convincing evidence for the mesoporous structure promoted aliphatic C-H bond activation.

Table 6.4. Effect of different synthesis conditions

Catalysts	2θ	d_{100} (Å)	Unit-cell parameter, a_0 (Å)	BET surface area (m^2/g)	Pd cont. (%)	Conv. of bromoben. (wt.%)[i]	Yield *tran*-stilbene	TON[j]
Pd-OMS51[a]	2.32	38.07	43.96	590	0.32	71.1	90.0	1570
Pd-OMS52[b]	2.36	37.42	43.21	605	0.35	86.6	90.0	1748
Pd-OMS53[c]	2.34	37.74	43.58	723	0.26	76.6	90.0	2082
Pd-OMS54[d]	2.38	37.1	42.85	894	0.38	53.6	90.0	997
Pd-OMS55[e]	2.44	36.2	41.8	802	0.71	74.0	91	736
Pd-Si-MCM-41[f]	2.86	30.9	35.66	1020	0.14	No reaction	-	-
SiO_2-Pd[g]	-	-	-	255	0.26	5.6	100	152
Am-PdMS	2.56	34.5	39.85	261	1.26	85.5	91	477

[a] OH-M5=1.0 g; Li_2PdCl_4=1.4 x 10^{-4}mol; NaOAc=0.05 g; methanol= 20 cc; reaction temperature=303 K; reaction time =24 h.
[b] OH-M5=1.0 g; Li_2PdCl_4=1.4 x 10^{-4}mol; methanol= 20 cc; reaction temperature=335 K; reaction time =24 h.
[c] OH-M5=1.0 g; Li_2PdCl_4=1.4 x 10^{-4}mol; acetone= 20 cc; reaction temperature=335 K; reaction time =24 h;
[d] OH-M5=1.0 g; $Pd(Oac)_2$ =1.4 x 10^{-4}mol; chloroform= 20 cc; reaction temperature=335 K; reaction time =24 h.
[e] OH-M5=1.0 g; $Pd(Oac)_2$ =1.4 x 10^{-4}mol; NaOAc=0.05 g; chloroform = 20 cc; reaction temperature=335 K; reaction time =24 h.
[f ,g] Si-MCM-41/OH-SiO_2 =1.0 g; Li_2PdCl_4=1.4 x 10^{-4}mol; NaOAc=0.05 g; methanol= 20 cc; reaction temperature=335 K; reaction time =24 h.
[h] Am-MCM-41= 1g; $Pd(Oac)_2$ =1.4 x 10^{-4}mol; chloroform= 20 cc; reaction temperature=335 K; reaction time =24 h.
[i] BB=2 mmol; styrene=3 mmol; K_2CO_3= 2.4 mmol; NMP=5.0 ml; temp.=423 K ;catalyst=30 mg; reaction time=5 h; [j] TON (Turn over number)= moles of BB converted per mole of Pd.

Few samples were prepared with or without addition of base and at room temperature to study the effect of base and synthesis temperature. Chloroform or acetone has also been used instead of methanol but found that Li_2PdCl_4 was not dissolving in chloroform. Palladium acetate was taken as palladium source in chloroform solvent. The different conditions in the preparation of different palladacycle catalysts are also given in Table 4. For comparison, 3-aminopropylated MCM-41 (Am-MCM-41) have been palladated with $Pd(OAc)_2$ under similar reaction conditions to get Am-PdMS catalyst and the characterization data are compared with Pd-OMS catalysts. Liquid phase palladation of 3-aminopropyltriethoxysilane with $Pd(OAc)_2$ in $CDCl_3$ has been done and analysed by liquid phase ^{13}C- NMR spectra and diffuse reflectance UV-vis spectra. The results are compared with the solid sample prepared with Am-MCM-41.

6.3.2. X-ray diffraction (XRD)

The XRD pattern of the as-made samples shows an intense peak due to d_{100} reflection, at 2θ between 2.0 and 2.5 accompanied by weaker reflections at 2θ between 4.0° and 6.5°, corresponding to the d_{110}, d_{200} and d_{210} spacing (hexagonal symmetry p6mm) which are characteristic peaks of MCM-41 [21]. The XRD peak intensity of template extracted and hydrolyzed OH-M1 and OH-M2 decreased significantly as compared to the peak intensity of Cl-M1 and Cl-M2, respectively. Likewise the peak intensity of Pd-OMS1 and Pd-OMS2 catalysts decreased further when compared to the peak intensity of OH-M1 and OH-M2, respectively (Fig 6.1). As can be seen from the Table 6.1 that the fraction of organo functionalized atom over Cl-M1 and Cl-M2 is lower and hence might have left more silanol groups free. While treating the catalysts with acidic solvents in case of template extraction and basic solvents in case of palladation reaction, the active Si-O bond in ≡ SiOH hydrolyzed easily and hence the long-range order of the structure collapsed as reflected in the XRD

pattern (Fig. 6.1). On the other hand, OH-M3, OH-M4, OH-M5 and respective palladated materials Pd-OMS3, Pd-OMS4, and Pd-OMS5 retain their long-range order after palladation as seen in X-ray diffraction (Fig 6.2). As the concentration of organo-functional group increases the surface of the silica walls become more passive due to the silylation, which help in retaining the long-range order during reaction with acidic or basic solvents. The unit cell parameter ($a_0=2d_{100}/\sqrt{3}$) of the palladated materials is close to 40Å (Table 6.3).

The XRD pattern of palladium metal has major diffraction peaks at 2θ=40.0°(111) and 46.5°(200), which are found in case of Pd-OMS catalysts prepared with Li_2PdCl_4, NaOAc in methanol at 335 K, confirming the presence of bulk Pd on the surface apart from metallated palladium (Fig. 6.3). Fig. 6.4 shows the XRD pattern of OH-M-5, which is palladated with different amount of Pd under similar reaction conditions (Pd-OMS5 series). It was observed that when the loading of Pd is lower, there was no diffraction pattern of metallic Pd observed.

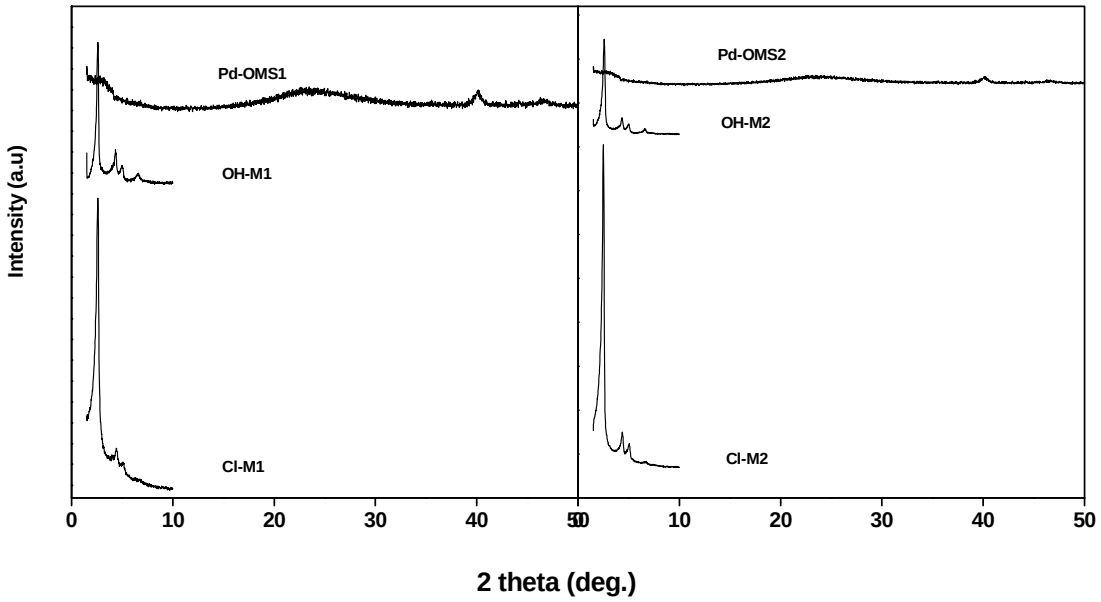

Fig. 6.1 X-ray diffraction patterns of Cl-M, OH-M and Pd-OMS

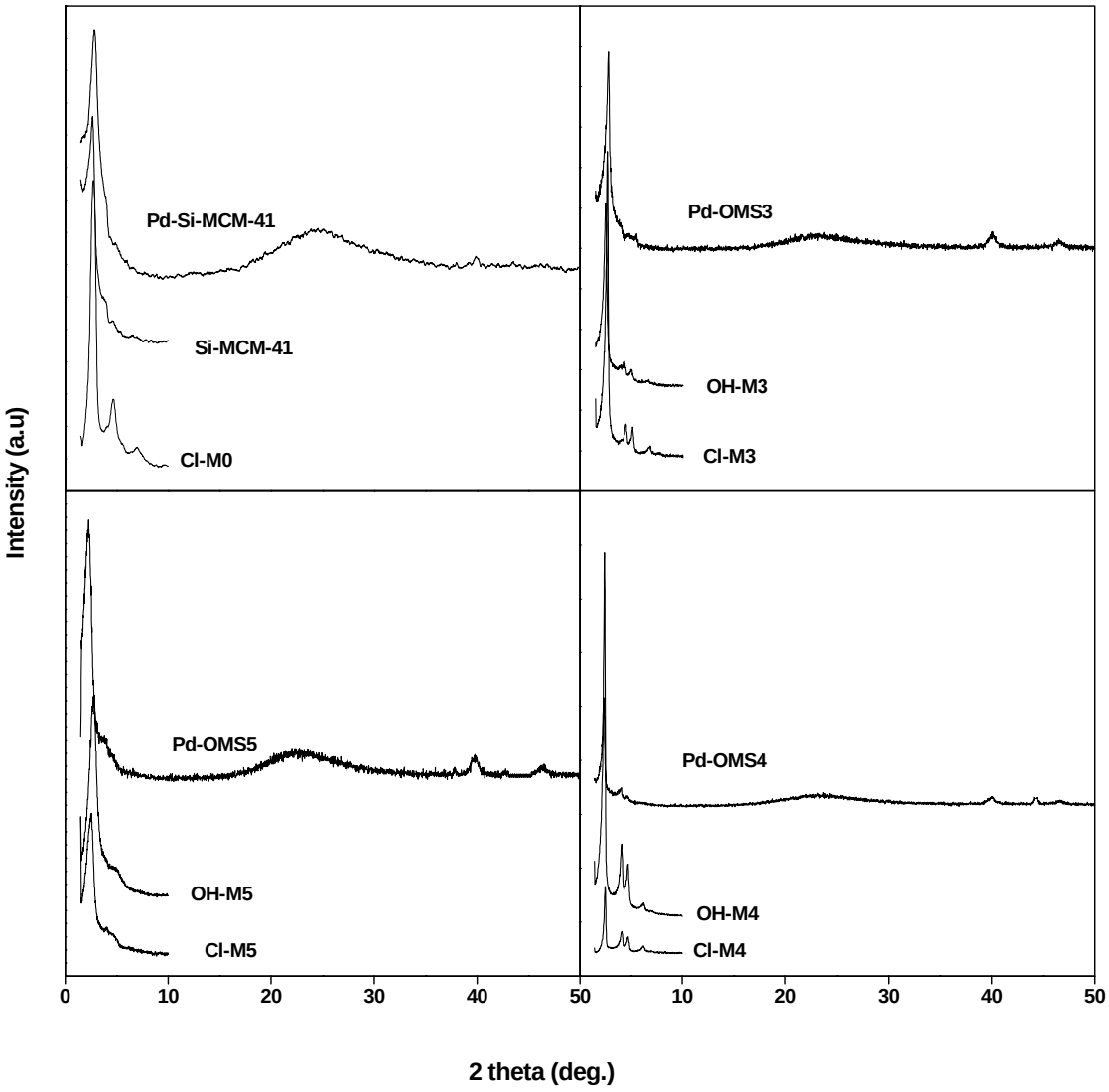

Fig. 6. 2 X-ray diffraction patterns of Cl-M, OH-M, Si-MCM-41, Pd-OMS and Pd-Si-MCM-41

As the loading increases the diffraction pattern corresponding to the Pd arises. At higher loading of Pd (Pd-OMS5 (1.4), Pd-OMS5 (1.68)) the peak intensity corresponding to Pd is higher. This shows that as the concentration of Pd increases while loading the chance for depositing bulk Pd at the surface also increases.

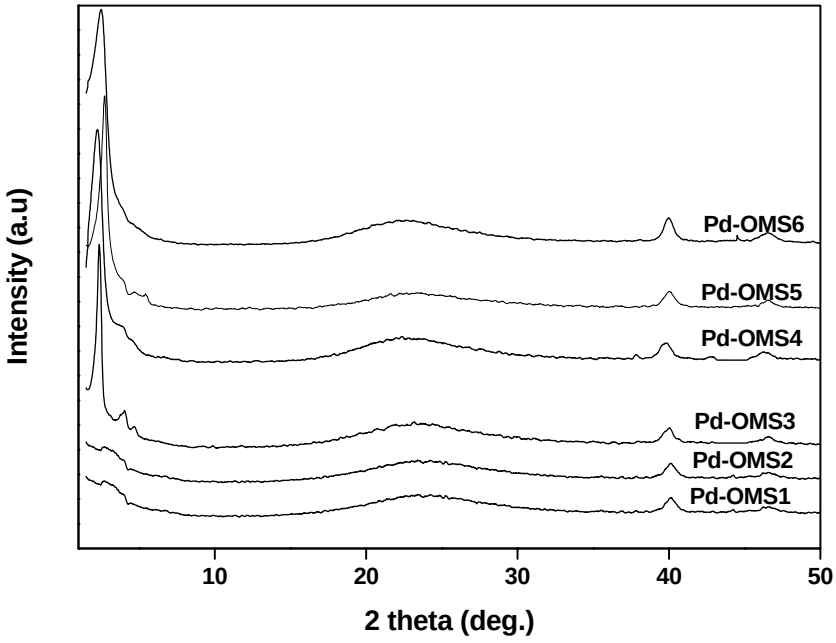

Fig. 6.3 X-ray diffraction patterns Pd-OMS catalysts

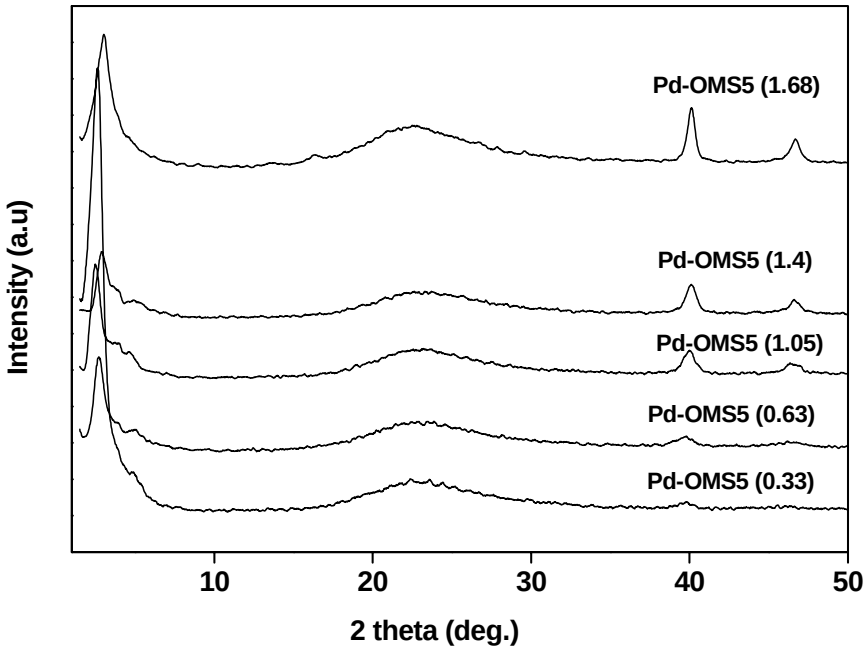

Fig. 6.4. X-ray diffraction patterns of Pd-OMS5 catalysts

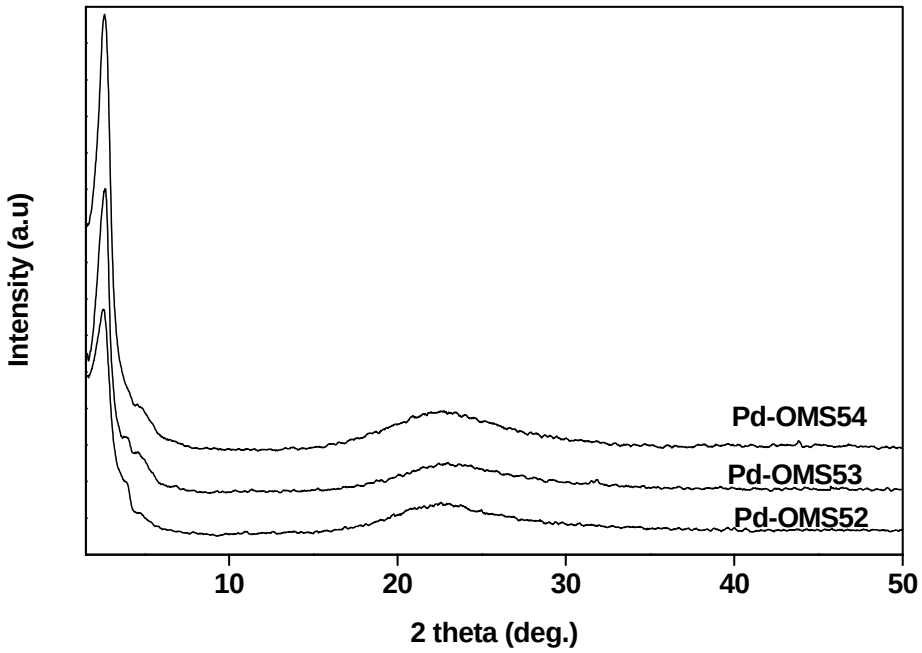

Fig. 6. 5 X-ray diffraction patterns of Pd-OMS52, Pd-OMS53 and Pd-OMS54.

Palladation of OH-M5 with Li_2PdCl_4 and sodium acetate in methanol either at room temperature or at 335 K produces bulk Pd^0 on the surface as evidenced by XRD pattern. Base added during palladation catalyses the formation of palladacycle and also the deposition of Pd as bulk on the surface of silica. Catalysts prepared with different solvents such as methanol (Pd-OMS52), acetone (Pd-OMS53) and chloroform (Pd-OMS54) with Li_2PdCl_4 at 335 K without addition of base showed no characteristic Pd peak (Fig 5). Pd-OMS54, prepared with $Pd(OAc)_2$ in $CHCl_3$ at 335 K shows no Pd^0 peaks but the same when prepared with sodium acetate shows Pd^0 peaks. These results suggest that formation of palladacycle and deposition of bulk Pd on the surface mainly depend on the solvents and base used. It was found that the propyl alcohol acts as a ligand in which the loan pair of electron on oxygen atom coordinate with palladium which in turn coordinate with the carbon atom of propyl chain by cyclisation at very mild conditions without formation of any bulk Pd at the silica surfaces.

6.3.3. ICP-OES and CHN analyses

The palladium content in the materials was determined by ICP-OES analysis. When similar concentration of Pd (1.5% Pd) was treated with OH-M samples with different concentration of ClPTS, the uptake of Pd through coordination of ligands proportionally increases with the concentration of ligands (ClPTS) in the material, which is an evident, that loading of palladium depends on the concentration of the ligand (Table 6.3). Total Pd content in the synthesized materials was achieved in the range of 0.3 to 1.7 % that depended on both the loading of ClPTS groups and Pd concentration used in the reaction solution (Table 6.3). When similar concentration of ligands is exposed to different concentration of Pd, the uptake of Pd increases as the concentration of Pd increases in the solution upto a certain level and then it levels off. The maximum uptake of Pd reaches to 70% in case of catalyst Pd-OMS5 (1.05) then it decreases to 40% when higher concentration of Pd used in the solution. Palladation with organo functionalized silica also shows lower Pd uptake (0.25 %Pd) when compared to Pd-OMS5. The lower Pd uptake can be accounted for the slow palladation process over OH-SiO_2, as there is no spatial confinement as in the case of OH-M5. The spatial confinement induced by the pore walls of OH-M drives the palladation more faster than in OH-SiO_2. Pd content was lower in the materials, which were synthesized either at room temperature or without addition of base or with acetone as a solvent as compared to the material synthesized at 335 K and with addition of base in methanol even though the reaction conditions are the same. Pd-OMS51, which was synthesized under room temperature, showed 0.32% Pd where as Pd-OMS5 (1.05), synthesized at 333 K showed 1.05% Pd (Table 6.4). Similarly Pd-OMS52, which was synthesized without addition of base, showed Pd content only 0.35%. Pd-OMS54, which was synthesized with palladium acetate and $CHCl_3$ as a solvent at 335 K without addition of base, showed Pd content 0.38 but when the same one

was synthesized at 333 K with addition of sodium acetate (Pd-OMS55) showed Pd 0.71%. Pd-OMS53, prepared with acetone as a solvent shows a very low Pd uptake compare to the same one prepared with methanol solvent. The non-polar solvent (acetone, 0.26 %Pd) favors palladation lesser extent than polar solvent (methanol, 1.05 %Pd). From thermal studies, it was confirmed that addition complex formed exclusively when acetone was used as a solvent (exothermic peak around 673 K, Fig 6.10c). This data clearly indicate that palladium complex has been formed at mild reaction conditions irrespective of the solvent and base but at the same time the base and reaction temperature enhances not only the formation of palladacycle but also the reduction of palladium salt into Pd^0. So under the optimum reaction conditions, the formation of palladacycle is enhanced. For comparison un-functionalized Si-MCM-41 was treated with palladation reagents and found much lower Pd uptake (0.14% Pd). This result clearly shows that propyl alcohol plays an important role in stabilizing Pd as Pd (II) in the palladacycle complex. C, H, N analyses of the samples show that there is a linear increase in carbon content as we go from Cl-M1 to Cl-M6 catalysts (Table 6.3).

Table 6. 4. Effect of Pd loading (%)

Catalysts[a]	Surface area (m^2/g)	Pd content (%)[b]		Conv. of BB (wt.%)[c]	Yield *trans*-stilbene (%)	TON
		Input	Out put			
Pd-OMS5 (0.33)	911	0.48	0.33	18.8	100	403
Pd-OMS5 (0.62)	863	0.9	0.62	37.8	91.0	431
Pd-OMS5 (1.05)	862	1.5	1.05	57.8	92.0	389
Pd-OMS5 (1.4)	763	3.0	1.40	90.1	91.0	455
Pd-OMS5 (1.68)	887	6.0	1.68	70.0	100	291

[a] number in bracket denotes the Pd content present in the catalyst.
[b] input is based on the amount of Pd in solution during palladation reaction; out put is based on the ICP-OES analysis.
[c] bromobenzene (BB)=2 mmol; styrene=3 mmol; K_2CO_3= 2.4 mmol; NMP=5.0 ml; temp.=423 K ; catalyst=30 mg; reaction time=5 h.

6.3.4. Adsorption studies

The surface areas of functionalized MCM-41 materials were in the range of 500-900 m^2/g, which are comparable to the previously reported organo functionalized MCM-41 with organosilane functional groups [30]. Surface area of OH-M1 and OH-M2 were 547 and 578 m^2/g, respectively. The lower in surface areas for OH-M1 and OH-M2 compared to Cl-M1 (760 m^2/g) and Cl-M2 (735 m^2/g), respectively, is attributed to their collapsing of long-range order, which is also evident from XRD pattern. OH-M3, OH-M4, OH-M5 and OH-M6 materials do not show much difference in surface area confirming the fact that as the concentration of functionalized silicon atom increases the passive character of the silica walls towards acidic or basic solvent mixture also increases. The respective palladated catalysts show either similar or little higher surface areas. The surface area, average pore diameter as well as pore volume found to increase when the material is palladated. The increase in surface area is attributed to the metal content and cyclisation of propyl group inside the pores of MCM-41. The palladium, which enters into the pore, causes the pores widen than before to sufficiently get accommodated and therefore there was increase in pore diameter as well total pore volume (Fig. 6.6). The BJH (Braunauer-Joyner-Halenda) pore size distribution of Pd-OMS5 illustrates a narrow peak centred at 28.8 Å for the pore diameter and pore volume measured was 0.63 cc/g. In case of pore size distribution of OH-M5, average pore diameter was in the range of 28.4 Å and the pore volume measured was 0.43 cc/g.

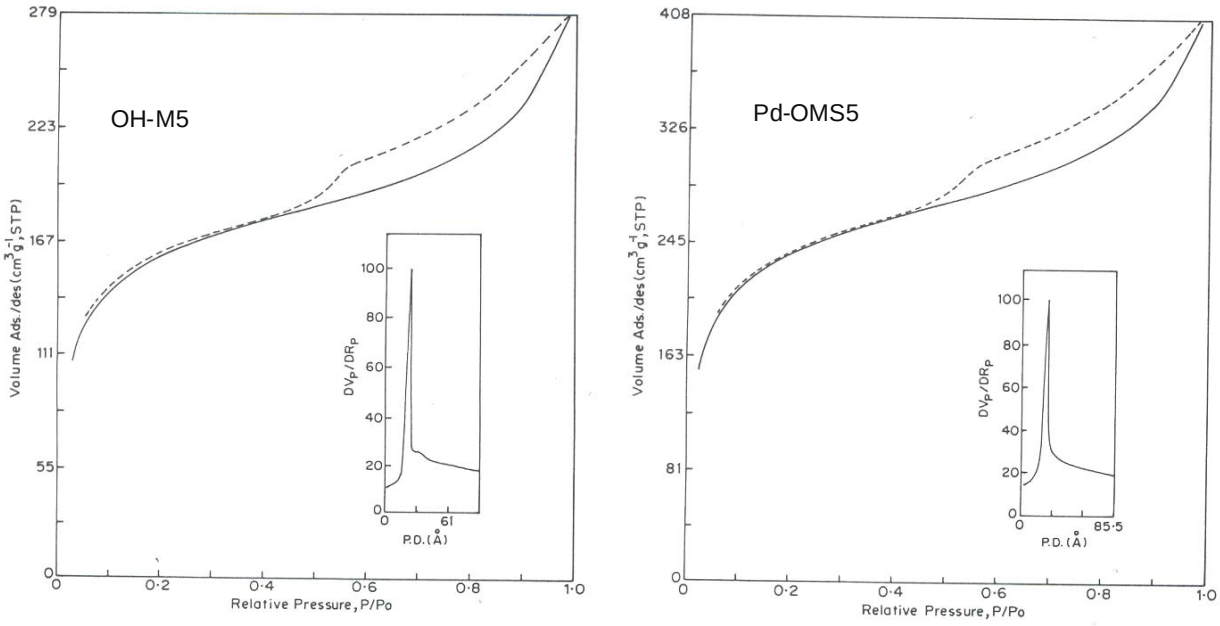

Fig. 6. 6. Nitrogen adsorption-desorption isotherms and pore size distribution (inset) for OH-M5 and Pd-OMS5

6.3.5. Fourier transform infra red spectra (FTIR)

Fig. 6.7 shows the FTIR spectroscopy of the as-synthesized Cl-M5, OH-M5 and Pd-OMS-5 materials. OH-M5 containing propylalcohol group has a strong band in the region between 1300 and 800 cm^{-1}, assigned for the C—O stretching band and intense O—H stretching adsorption in the region of 3600-2500 cm^{-1}. In case of as-synthesized Cl-M5 sample, very strong stretching bands in the region 2950-2850 cm^{-1} and deformation bands in the region 1400-1420 cm^{-1} were observed. In OH-M5 sample, the methylene stretching bands of the propyl chain, in the region 2950-2850 cm^{-1}, and their deformation bands, at 1414, 1440, 1475 cm^{-1} are comparatively weaker (Fig. 6.7).

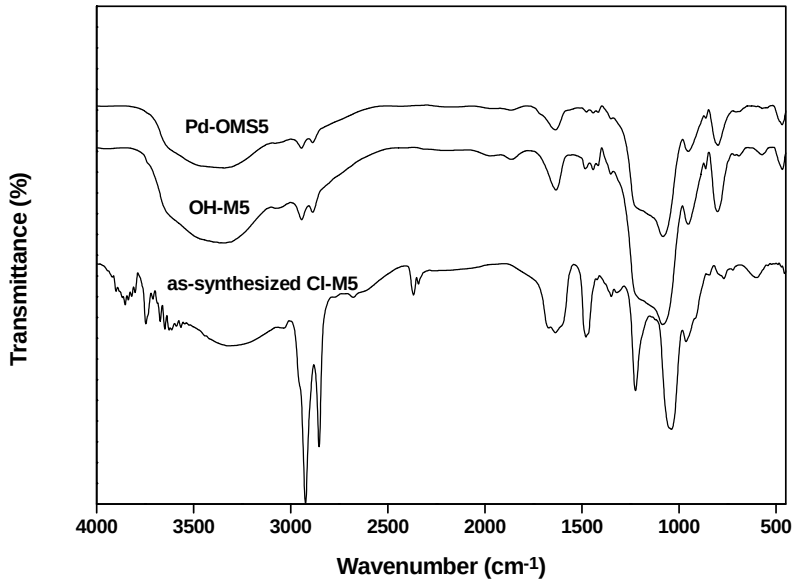

Fig. 6. 7 FT-IR spectra of as-synthesized Cl-M5, OH-M5 and Pd-OMS5.

These bands can be assigned to the symmetric bending ("scissoring") mode of the three distinct methylene groups of the propyl chain. The first one, at 1416 cm^{-1}, is assigned to a methylene directly bonded to silicon [38] is also present in the palladated samples but the intensity is comparatively weak. After the palladation it was found that intensity of the O—H stretching vibration also decreased. The C—H stretching bands also shifted from 2887, 2941 cm^{-1} to 2894, 2951 cm^{-1}, respectively, and one more extra band at 2851 cm^{-1} was also seen in Pd-OMS5. The shift towards higher energy side indicates the change of bonding behaviour of C-H bond. These data provide the supplement evidence of the cyclometallation of propyl alcohol group, which is anchored on the walls of MCM-41 in the presence of palladation reagents.

6.3.6. TGA–DTA analyses

The thermal stability of the palladated catalysts could be measured by TGA-DTA analysis. The weight losses observed for Cl-M5, OH-M5 and Pd-OMS5 (1.68) correspond to the loss

of propylchloride, free propylalcohol and complexed propylalcohol are 30,20 and 18 wt %, respectively (Fig. 6.8). It is clearly seen from the weight loss profile that 30 wt % loss

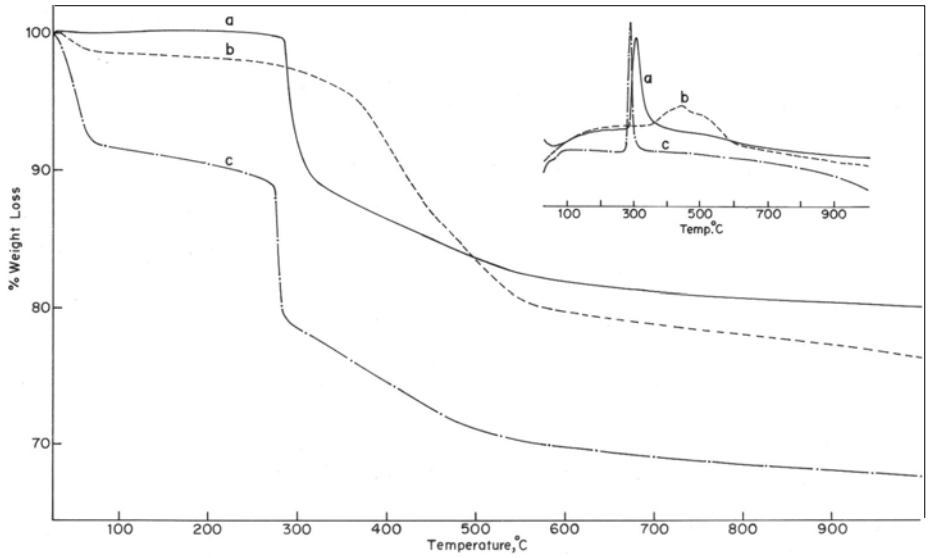

Fig. 6. 8. TGA-DTA curves of (a) Cl-M5 (b) OH-M5 and (c) Pd-OMS5.

corresponds to propylchloride are reduced to 20 wt % due to propyl alcohol as expected. An exothermic peak centered at 280°C in Cl-M5 is shifted to 300°C in OH-M-5. The palladated sample Pd-OMS5 exhibits two broad peaks centered at 450 and 500°C. The two exothermic peaks can be interpreted in such a way that palladium complex formation with the ligands propylalcohol in two different ways. The exothermic peak at 500°C can be assigned to the formation of palladacycle while the exothermic peak at 450°C to the formation of addition complex (PdX_2L_2; L=ligand; X=-Cl or –OAc)[2-4]. When the similar concentration of ligands was treated with different concentration of Pd, it was observed that at lower Pd concentration, palladacycle predominates whereas at higher concentration of Pd, addition complex as well palladacycle formed [Fig. 6.9]. OH-M was treated with Li_2PdCl_4 in methanol either at 335 K

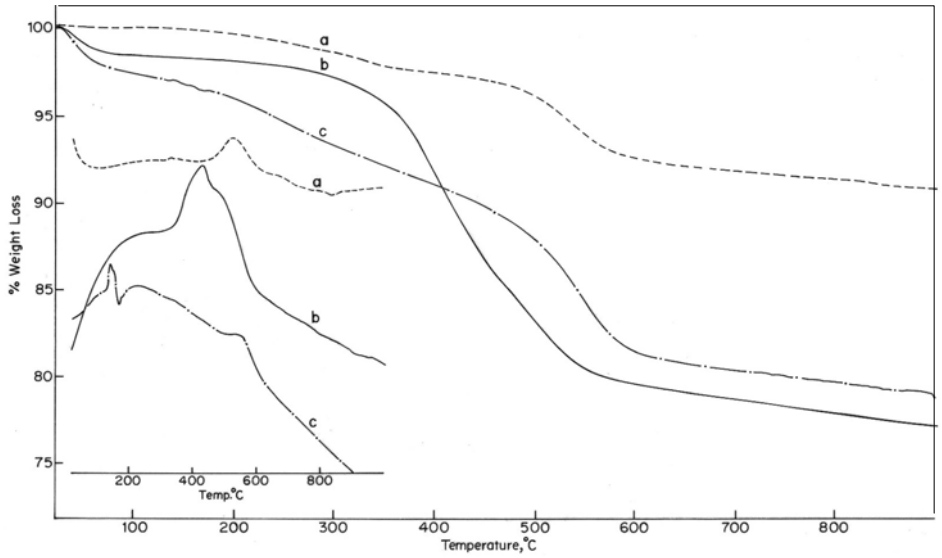

Fig. 6. 9. TGA-DTA curves of (a) Pd-OMS5 (0.33) (b) Pd-OMS (1.68) and (c) Pd-OMS5 (1.05).

or at room temperature, with or without addition of base to know about the formation of palladacycle and stability of the same. It was observed that the exothermic peak centered around 400°C assigned for the addition complex predominates when OH-M was treated without addition of base at 335 K (Fig. 6.10c). Addition of base during synthesis catalyses the formation of palladacycle even at room temperature (Fig 6.10b). Pd-OMS54, prepared using acetone as a solvent shows two exothermic peaks at 410° and 520°C [Fig 6.10]. The uptake of Pd is lower in case of Pd-OMS54 as measured by ICP-OES analysis, and formation of addition complex predominates over palladacycle. These results suggest that palladacycle formation requires optimum reaction conditions and base. Polar solvent, methanol, favors the formation of palladacycle at room temperature.

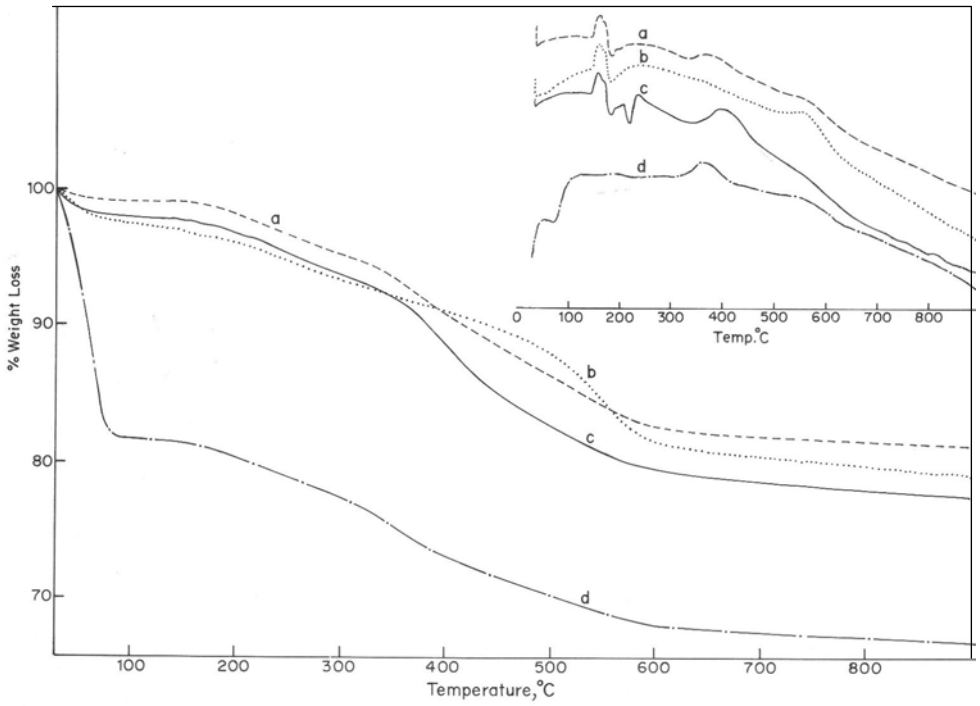

Fig. 6. 10. TGA-DTA curves of (a) Pd-OMS5 (b) Pd-OMS51 (c) Pd-OMS52 and (d) Pd-OMS53.

6.3.7. Electron microscopy

Scanning electron micrographs show the particle morphology of the samples. SEM photographs of OH-M5 and Pd-OMS5 shown in Fig. 6.11 are typical for mesoporous materials. Uniform particles sizes (1-2μm) were present in OH-M5. Pd-OMS5 sample show particles sizes in the range of 1-3 μm. The same material when palladated under different solvent system show different morphologies. Pd-OMS53 prepared in acetone medium shows uniform spherical and cylindrical rod crystals.

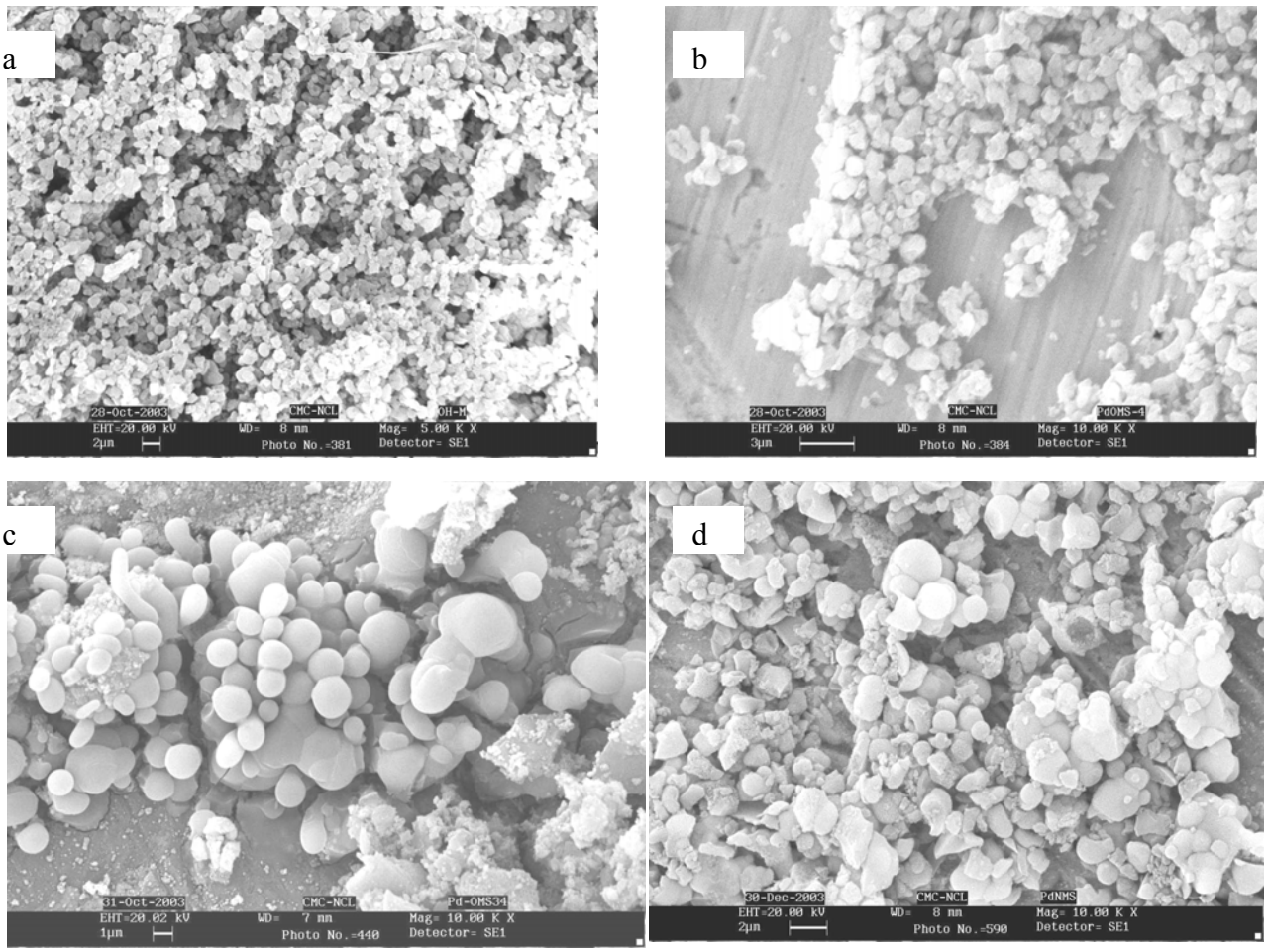

Fig. 6. 11. SEM photographs of (a) OH-M5 (b) Pd-OMS5 (c) Pd-OMS53 (d) Am-PdMS.

6.3.8. NMR Studies

Fig. 6.12 shows the ^{29}Si NMR spectra of Pd-OMS5. The peak at 67.0 ppm is due to the cross-linked silicon atom. The concentration of cross-linked silicon atom is higher and hence the concentration of Q_3 species along with Q_4 species is accountable. In order to confirm the cyclic palladation with aliphatic carbon and oxygen of OH group, 125.76 MHz solid-state ^{13}C CP/MAS spectra of OH-MCM-41 and Pd-OMS have been recorded on a Bruker DRX-500 NMR spectrometer spun at 10 and 8 kHz, respectively, and are shown in Fig. 6.13. Three

main peaks of OH-M5 observed at (δ) 8.67, 25.28, and 63.63 ppm have been shifted to 8.33, 25.368, and 63.65 ppm, respectively, in Pd-OMS5. The shift of methylene carbon next to the silyl silicon towards high field is sufficiently higher, 0.34 ppm, compared to that of the middle carbon and carbon atom neighbor to the OH group in Pd-OMS5. The shift of signal corresponding to methylene carbon next to silyl silicon to high field confirms that the carbon exhibited different environment after palladation while other two carbons are not showing much difference. The shift towards higher field confirms the complexation of the ligand with Pd centre.

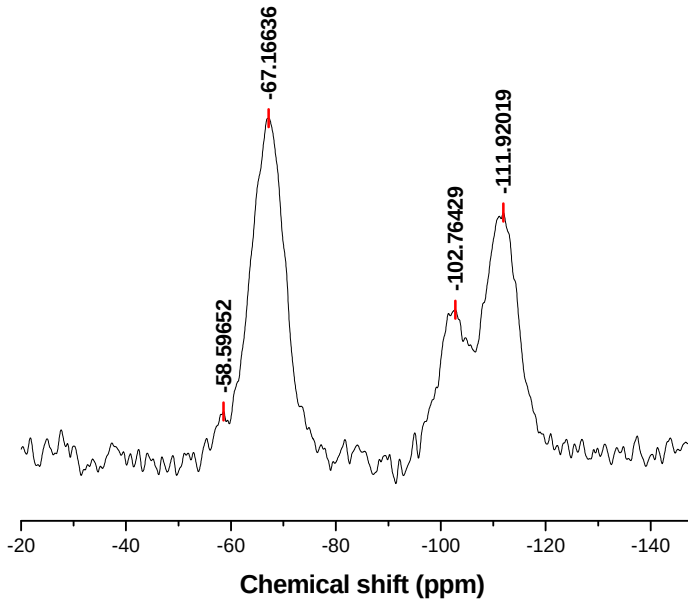

Fig. 6. 12. ^{29}Si NMR spectra of Pd-OMS5 catalyst

Liquid state ^{13}C NMR spectra of 3-aminopopyltriethoxysilane (APTES) in $CDCl_3$ and APTES+$Pd(OAc)_2$ have been recorded on a Bruker 300 MHz instrument to evident the formation of Pd complex (Fig. 14). APTES shows three well distinct peaks (C_1, C_2 and C_3 at 7.16, 26.72 and 44.54 ppm, respectively) corresponding to the three carbons of propyl group.

When the APTES is added with palladium acetate and heated at 333 K for 24 h, it shows broader and almost invisible peaks corresponding to carbons C_1 and C_3 which strongly confirms the formation of palladium complex.

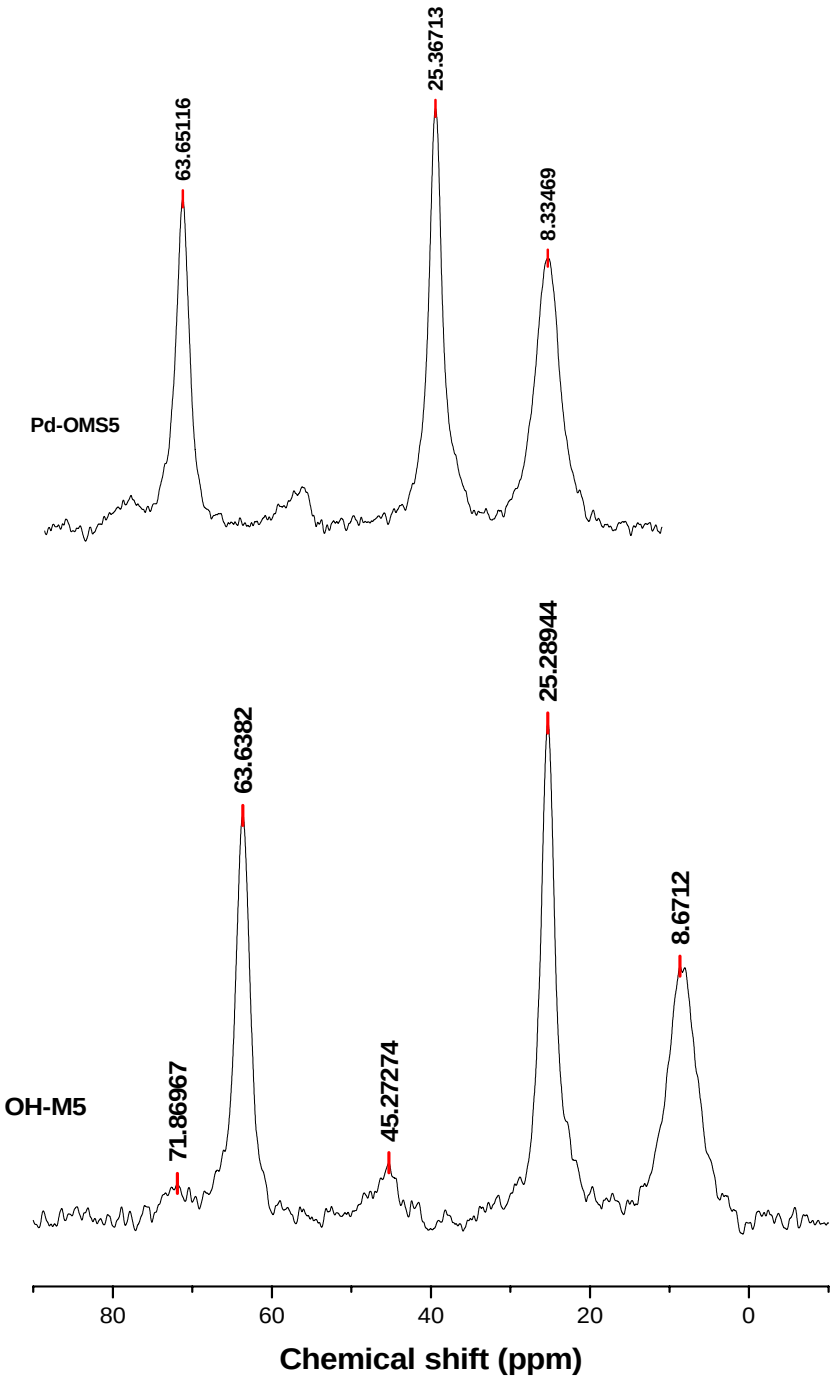

Fig. 6.13. ^{13}C CP MAS NMR spectrum of OH-M5 and Pd-OMS5.

A peak at 26.72 ppm corresponding to C_2 carbon of the propyl group in APTES is found shifted towards higher field (24.7 ppm) after palladation. Though the shift is not much as in case of completely complexed solid, this shift suggests that there is an equilibrium existing between partly complexed and uncomplexed ligand and hence the shift is not much. This analysis confirms the formation of palladacycle complex with 3-aminopropylsilyl ligands anchored onto the walls of MCM-41.

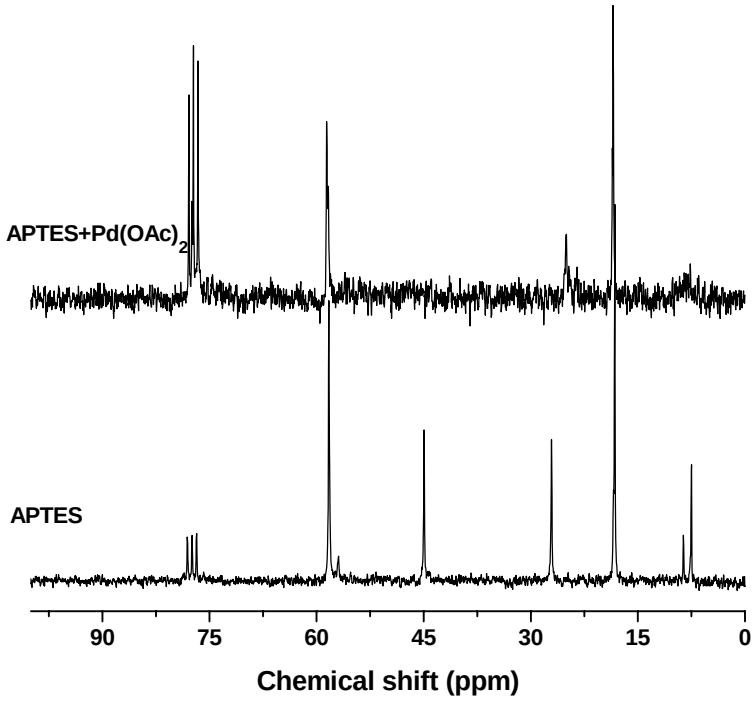

Fig. 6. 14. Liquid state ^{13}C NMR spectra of APTES and $Pd(OAc)_2$+APTES in $CDCl_3$

6.3.9. XPS Studies

Pd (3d) XPS spectra of Pd-OMS5 (1.4), Pd-OMS51, Pd-OMS54 and Am-PdMS support the formation of palladacycle (Fig. 6.15). The binding energy of adventitious C 1*s* core level, which is 284.6 eV [39], was used to correct for the energy shift due to the surface charging. The accuracy of the measured B.E was ± 0.2 eV. The peak maximum of the Pd (II) $3d_{5/2}$ line for all the samples except Am-PdMS is centered around 336 eV. Pd-OMS5 (1.4)

shows a weak Pd (0) $3d_{5/2}$ line at a binding energy of 334.7 eV, which is found to be absent in case of other samples. Palladium present in palladacycle is in Pd (II) form and the binding energy is slightly lower compared to Pd (II) in PdO (335.6 eV). Pd-OMS54 prepared with $Pd(OAc)_2$ shows no shoulder corresponds to Pd (0) on its surface where as Pd-OMS5 (1.4) prepared with Li_2PdCl_4 as Pd source at 333 K with methanol as a solvent and sodium acetate as base shows weaker band at 334.7 eV which is characteristic binding energy of Pd(0).

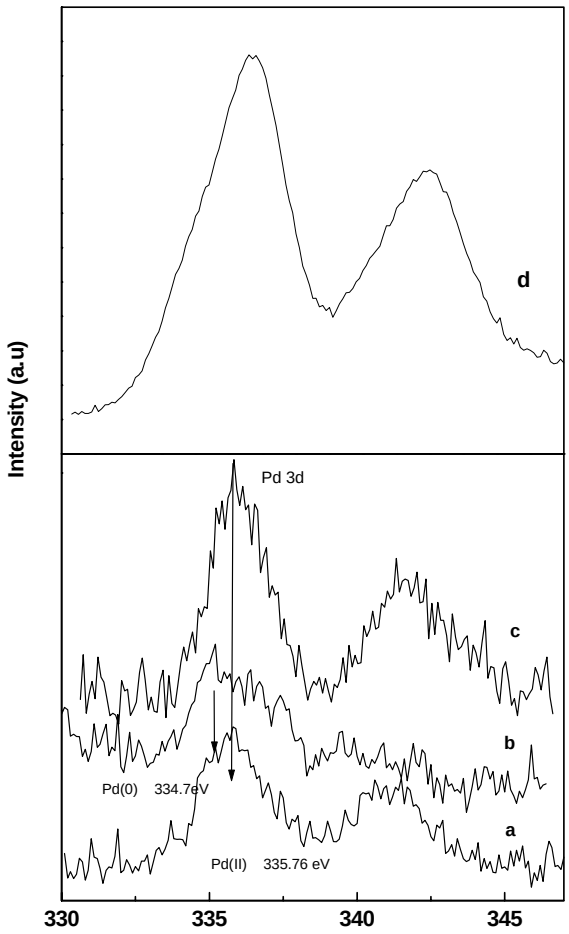

Fig. 6. 15. XPS spectra of (a) Pd-OMS5 (1.4) (b) Pd-OMS53 (c) Pd-OMS51 and (d) Am-PdMS.

Pd-OMS51 prepared at room temperature shows clear peak corresponding to Pd(II) at 336.4 eV(Fig. 6.15c). Similarly Am-PdMS shows clear and sharp peak at 337.6 eV confirms the formation of highly stable palladacycle (Fig. 6.15d).

6.3.10. UV-vis spectral studies

The diffuse reflectance spectra (200-800 nm) of Pd-OMS catalysts display nearly identical features with three absorption bands in the UV region in the range 260 and 450 nm with reference to $BaSO_4$ standard (Fig. 6.16). Pd-OMS5 shows a characteristic absorption band at 284 nm corresponding to metal-ligand charge transfer d-p transition. The shift towards higher energy value was resulted from the metallation (Fig 6.16). When the palladation was carried out at room temperature over OH-M5, an intense absorption band around 281 nm indicates the formation of palladacycle exclusively. A weak shoulder at 346 nm followed by the intense band may be due to the little formation of addition complex (Fig 6.16). The absorption band around 346 nm is getting more visible along with one more broad band at 475 nm when the OH-M5 was palladated without addition of base at 335 K (Fig 6.16). Palladation with acetone as a solvent shows weak but exclusive absorption band corresponding to the rigid palladacycle (Fig. 6.16).

To confirm the above fact, UV-Vis spectra of APTES in $CHCl_3$ solvent was recorded before and after addition of palladium acetate in to APTES to evident the complexation. In the DR-UV-Vis spectrum, it is clearly seen that the absorbance band for the neat palladium acetate in $CHCl_3$ at 400 nm gets shifted to 300 nm when subjected to complexation with APTES ligand (Fig. 6.17). The blue shift of the absorption peak clearly evident the formation of Pd complex. In the DR-UV-Vis spectrum of solid Am-PdMS, the most characteristic absorption bands at 261 and 400 nm indicate the formation of rigid palladium complex and non-rigid addition complex. The blue shift found in case of solid Am-PdMS catalyst (139 nm)

is higher than that of Pd complex in $CHCl_3$ solution (100 nm) as there are higher degrees of freedom in case of liquid than solid. Absorption spectrum of neutral palladium (II) complexes is generally characterized by ligand-metal charge transfer d-p transition. The observed spectral features are consistent with Pd (II) [d^8] diamagnetic species [40]. These results confirm the formation of rigid palladacycle and non-rigid addition complex when OH-M5 or Am-MCM-41 was treated with palladation reagents even at mild reaction conditions

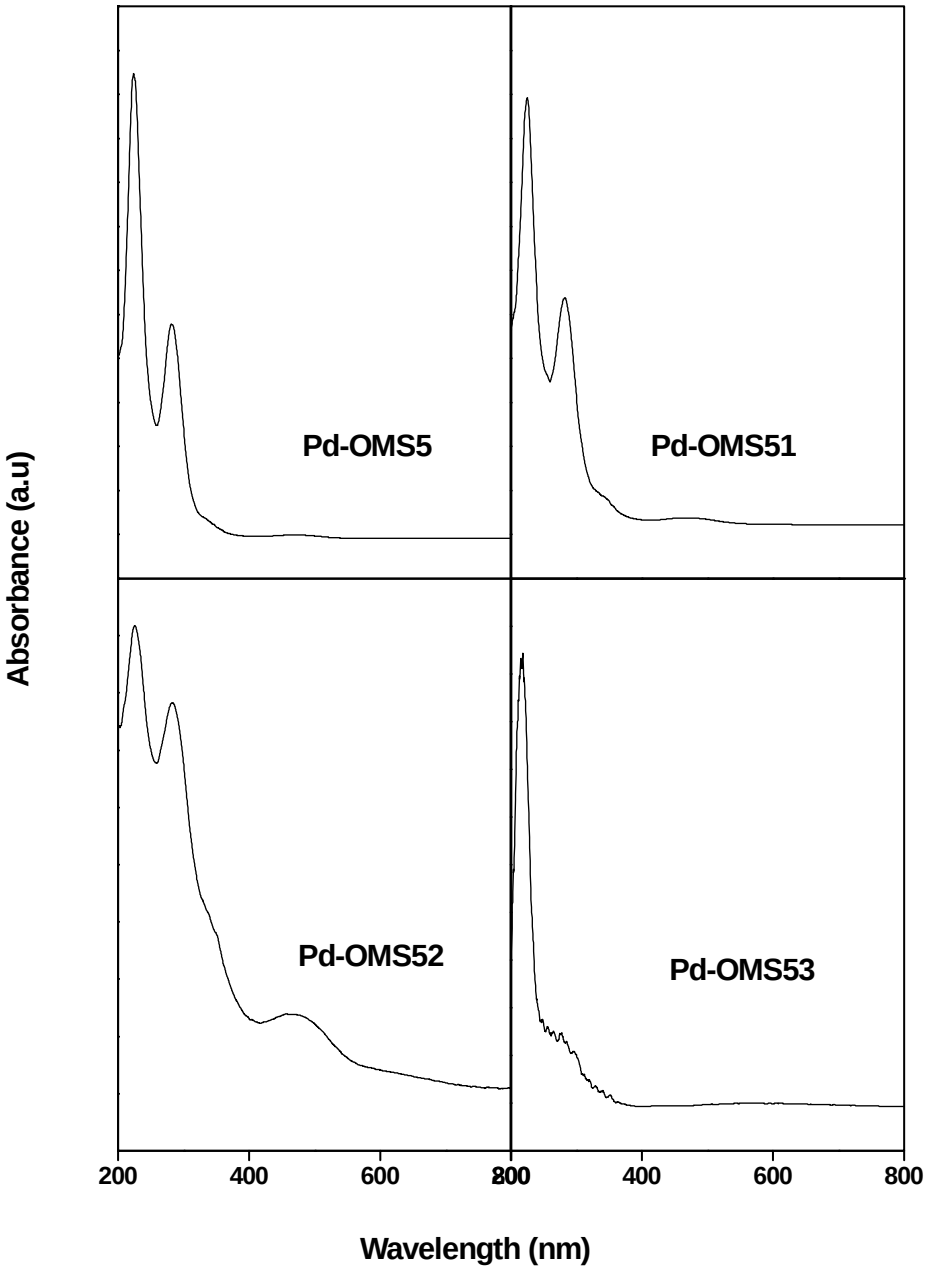

Fig. 6.16. UV-Vis spectra of Pd-OMS catalysts

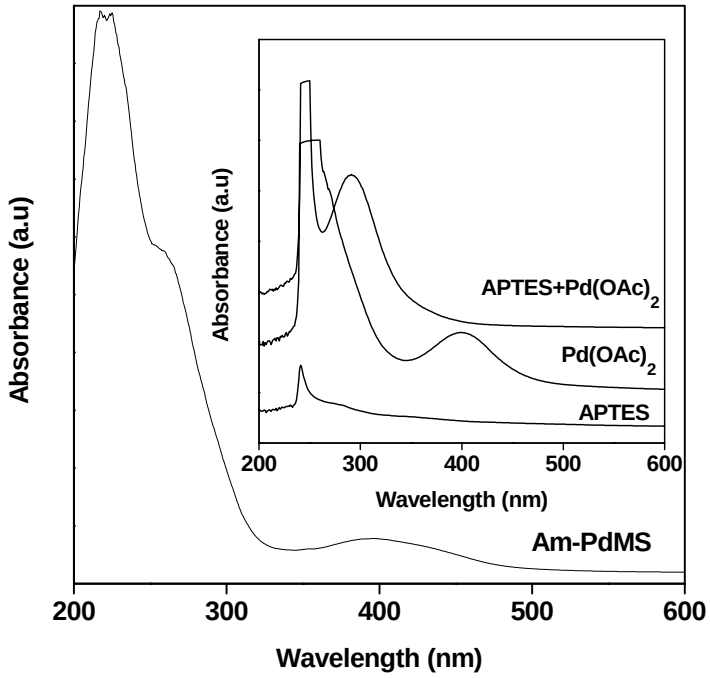

Fig. 6.17. UV-Vis spectrum of APTES, $Pd(OAc)_2$, APTES+ $Pd(OAc)_2$ in $CHCl_3$ and Am-PdMS.

6.3.11. Heck alkenylation

Heck alkenylation of bromobenzene (BB) with styrene has been performed to evaluate the catalysts prepared under different reaction conditions. Palladacycle-SiO_2 shows lower activity for the conversion of BB. The uptake of Pd consequently signified in the Heck alkenylation reaction. Under the similar reaction condition the conversion and TON increases linearly from Pd-OMS1 to Pd-OMS5 and thereafter decreases which implies exceeding the optimum loading of ClPTS groups. As the reaction proceeds at the active Pd metal centre, the TON (with respect to Pd) varies significantly when the Pd content is changed. The Pd uptake increases proportional to the amount of ligand (3-hydroxypropyltriethoxysilane) present in the mesoporous walls of MCM-41 and so the rate of reaction (TON) increases accordingly. As it

can be seen from Table 3, though the Pd content is higher in Pd-OMS2 than in Pd-OMS4 the activity was shown lower which might be attributed to the formation of bulk Pd in Pd-OMS2, which is catalytically inactive for such reaction. The same fact also was observed in Pd-OMS3 where Pd content was higher than those of Pd-OMS4 and Pd-OMS5 but found to be lower active. From these experiment it was clearly seen that whenever there are less number of ligands available for the formation of palladacycle, the excess palladium present in the solution tend to deposit at the surface of silica near to the anchoring point of functional group. To confirm this fact, palladation was performed with Si-MCM-41 (where there is no functional group) under similar reaction conditions and found that uptake of palladium in the form of bulk Pd was substantially low as seen in XRD which is inactive for this reaction. In order to study the effect of base and reaction temperature palladation was performed with and without addition of base either at room temperature or at 333 K. Palladacycle prepared at room temperature shows lower Pd content but moderate activity. Catalytic activity of Pd-OMS54 prepared with palladium acetate with chloroform solvent was found to be lower when compared to the one prepared with base and at 333 K (Pd-OMS55). Table 4 shows effect of Pd (%) loading over OH-M5 in the Heck alkenylation reaction. When OH-M5 was treated with different concentration of Pd containing solution, the uptake of Pd increases upto 70% and then started decreasing. Conversion of bromobenzene increases as the Pd content increases in the catalyst. A maximum of 1.68 % Pd content in the catalyst (Pd-OMS5 (1.68) was achieved but at the same time the catalyst shows less activity in the conversion of bromobenzene than Pd-OMS5 (1.4) containing 1.4 % Pd. This result confirms that activity of Pd will arise only from Pd present as Pd(II) in palladacycle and not from bulk Pd deposited on the surface.

6.3.11.1. Effect of different bases

The effect of different bases in Heck alkenylation of bromobenzene is given in Table 6.5. The reactions were conducted at a fixed bromobenzene concentration of 2 x 10^{-3} mol, styrene concentration of 3 x 10^{-3} mol, base concentration of 2.4 x 10^{-3} mol and Pd concentration of 4.8 x 10^{-6} mol. The reaction was performed at 423 K for 10 h. Organic bases, trimethyl amine and tributyl amine showed less activity in alkenylation of bromobenzene. Sodium acetate showed lower activity than sodium carbonate.

Table 6.5 Effect of different bases on Heck alkenylation of bromobenzene

Base	Conv. Of bromobenzene (wt%)[a]	Sel. to trans-stilbene (%)	TON
Triethyl amine	20.9	91	88
Tributyl amine	26.0	93	109
Sodium acetate	32.0	87	135
Sodium carbonate	56.5	88	238
Potassium carbonate	84.6	90	356

[a] Reaction condition: bromobenzene=2 mmol; styrene=3 mmol; base=2.4 mmol; NMP=5.0 mL; catalyst= 0.2 mol% Pd; temperature=423 K.

Potassium carbonate showed 84.6 wt.% conversion of bromobenzene with 90 % selectivity to trans-stilbene. So all the other parameters have been done with potassium carbonate as base.

6.3.11.2 Effect of reaction temperature and time

Figure 6.18 shows effect of reaction temperature on conversion of bromobenzene and Arrhenius plot of reciprocal of temperature against rate of the reaction. To study the effect of temperature on the conversion the reaction was performed at different temperatures. The Heck alkenylation reactions were conducted by varying the temperature from 403 to 433 K at a fixed bromobenzene concentration of 2 x 10^{-3} mol, styrene concentration of 3 x10^{-3} mol,

potassium concentration of 2.4 x10^{-3} mol and Pd concentration of 4.8 x 10^{-6} mol. It was observed that at 403 K temperature, the conversion was low. At initial hours of reaction, 0.5 h, the conversion of bromobenzene, yield of trans-stilbene and TON are 5.0 wt.%, 90 %, 21 at 403 K; 10.6 wt.%, 89 %, 45 at 413 K; 17.5 wt.%, 92 %, 73 at 423 K and 19.8 wt.%, 91%, 83 at 433 K, respectively. As it can be seen there, the initial reaction rate increases gradually with the reaction temperature. Selectivity to trans-stilbene remains above 90 % in all the cases.

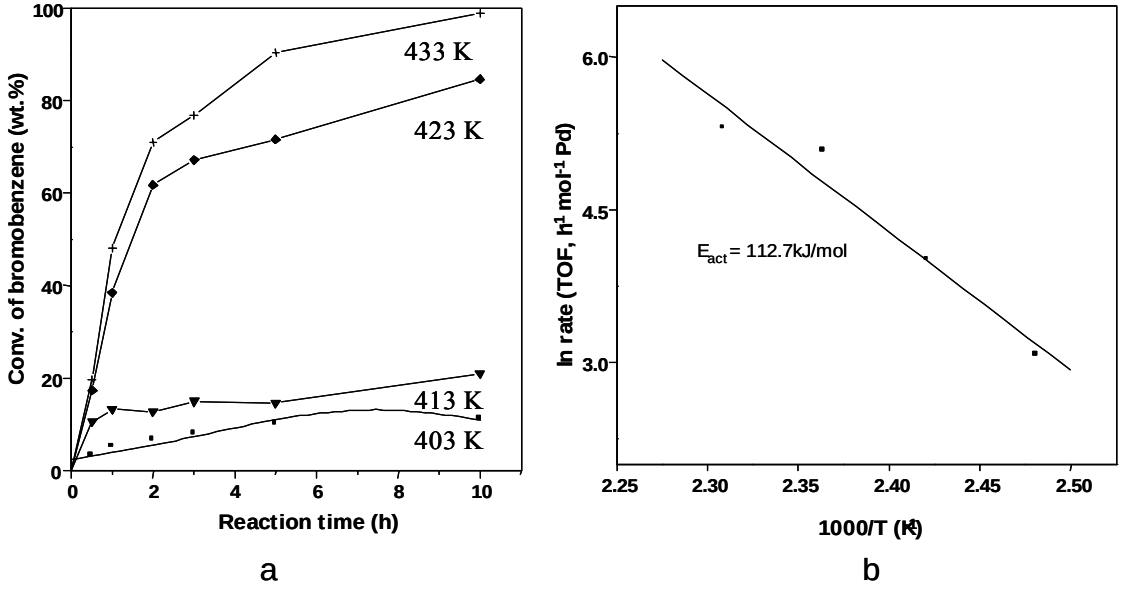

Figure 6.18 a) Effect of reaction temperature and reaction time on conversion of BB
b) Arrhenius plot

The conversion of BB, yield of *trans*-stilbene, and TON after 10 h of reaction time are 11.2 wt.%, 90 %, 47 at 403 K; 20.9 wt.%, 90 %, 88 at 413 K; 84.6 wt.%, 94 %, 355 at 423 K and 98.9 wt.%, 90%, 416 at 433 K, respectively. The apparent activation energy calculated for initial rates of reaction of four different temperatures was 112.7 kJ/mol.

6.3.11.3. Effect of Pd mol %

The concentration of Pd in Pd-OMS was varied from 1.5 x 10^{-6} to 4.8 x 10^{-6} mol while bromobenzene (2 mmol), styrene (3 mmol), potassium carbonate (2.4 mmol) and temperature (433 K) were kept constant. The time dependent conversions of bromobenzene over different concentration of Pd were given in Figure 6.19. The initial conversions show a direct dependence with respect to the catalyst concentration. At 1.5 x 10^{-6} mol Pd concentration (0.075 mol % Pd with respect to substrate) the conversion of bromobenzene at 0.5 h reaction time was low (4.2 wt.%) and it was found to increase to 14.6 wt.% when the Pd concentration was further increased from 1.5 x 10^{-6} to 2.5 x 10^{-6} mol. The initial reaction rate increases proportionally with the Pd content but at the same time increase is not linear.

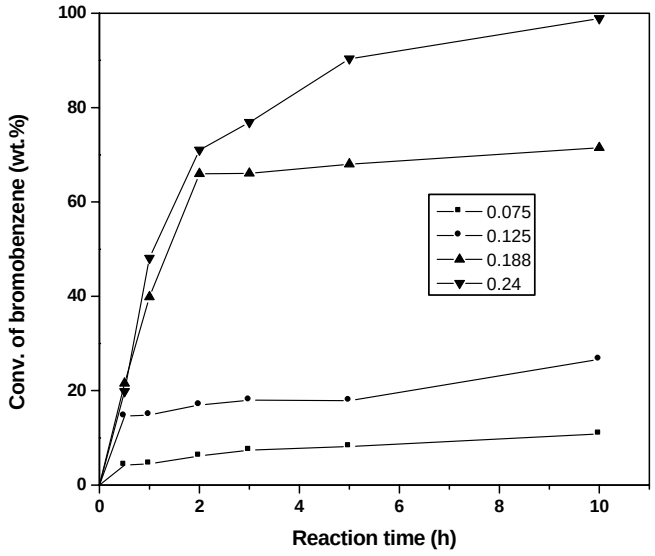

Figure 6. 19 Effect of Pd mol % and reaction time on conversion of bromobenzene

When the Pd concentration increased from 2.5 x 10^{-6} to 3.2 x 10^{-6} mol the activity increased almost four times. The sharp increase in initial conversions while the concentration of Pd was varying is evidently signifies the catalytic nature of Pd. These results show that Pd plays an

important role in activating the Heck alkenylation reaction and activity varies with the Pd concentration.

6.3.11.4 Heterogeneity study

To analyze the heterogeneity of the catalyst, a reaction was performed with PdOMS5 catalyst and depicted in Fig 6.20. After attaining 20% conversion of bromobenzene, 5 mL reaction mixture was filtered and performed reaction in a separate reaction set up. After filtering the sample the reaction was continued further up to 24 h. A higher conversion of 36 % of bromobenzene could be achieved with tributylamine as a base. The conversion of bromobenzene was lower when tributylamine was used as a base. Even though K_2CO_3 gave >90% conversion, tributylamine was chosen to study the leaching of Pd at slower conversion rate and also organic amine will be equally mixed with the reactant mixture rather than K_2CO_3. The Pd content present in the solution was measured by ICP-OES analysis and found that a negligible amount of Pd in ppm

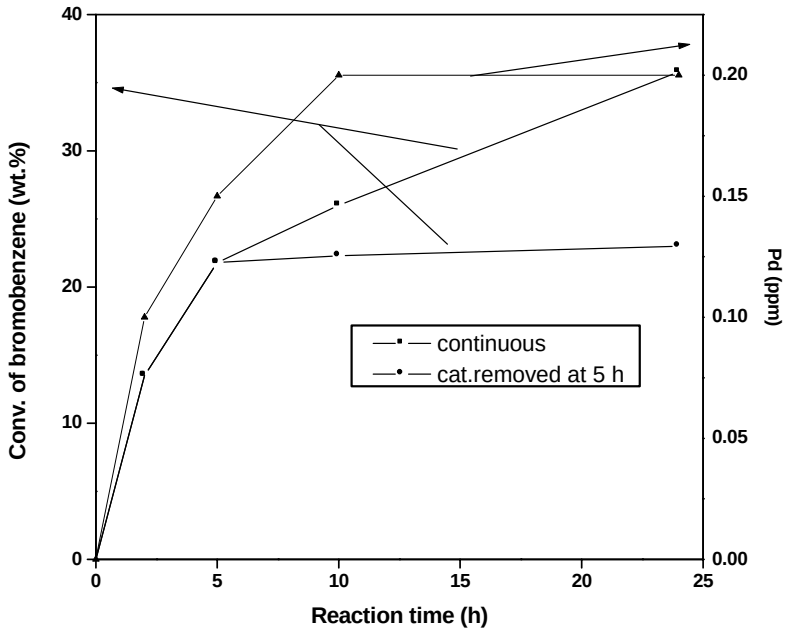

Fig. 6. 20. Heck alkenylation of bromobenzene; Reaction conditions: BB= 1 x 10^{-2} mol; styrene =1.5 x 10^{-2} mol; tributylamine= 1.2 x 10^{-2} mol; NMP=25 ml; temperature=423 K; catalyst=0.1 g.

level present in the solution. However, this Pd can be accounted that bulk Pd present in the catalyst surface may get leached out during the reaction and not the cyclised Pd. This fact can also be confirmed by the reaction performed with the reaction mixture, which was separated after 5 h reaction time shows no increase in conversion.

6.3.14. Homo aryl coupling

Table 6.6 shows results on homoaryl coupling reactions of halobenznenes. 4-4'-dinitrobiphenyl and 4,4'-dihydroxybiphenyl have been formed selectively in case of 4-chloronitrobenznene and 4-bromophenol, respectively when Pd-OMS5 (1.4) is used a catalyst. The conversion of chlorobenzene to biphenyl, 4-chlronitrobenzene to 4,4'-dinitrobiphenyl, 4-bromophenol to 4,4'-dihydroxybiphenyl were found to be 14.3, 98.0, and 100 wt.%. The corresponding selectivities for biphenyl, 4,4-dinitrobiphenyl and 4,4'-dihydroxybiphenyl were 54,70 and 60 %, respectively.

Table 6.6 Homoaryl coupling reactions of haloaromatics over Pd-OMS5 (1.4) catalyst

Substrate	Time (h)	Conv. (mol.%)[a]	Selectivity to 4,4'-biphenyl (%)
Chlorobenzene	24	14.3	54
4-Chloronitrobenzene	5	98	70
4-Bromophenol	10	100	60

[a] Halobenzene=10.0 mmol; K_2CO_3=11.0 mmol; DMF=5.0 mL; catalyst= 0.25 mol% Pd; temperature=423 K.

6.4. Conclusions

Heterogeneous carbometallated palladacycle has been successfully synthesized by treatment of palladation reagents with 3-hydroxypropyltriethoxysilane incorporated MCM-41

(OH-M) under mild reaction conditions. Palladation is found to be more effective in case of organo functionalized MCM-41 than organo-functionalized silica. The spatial confinement induced by the pore walls drives the palladation process more. It was observed through the optimization studies that the uptake and stabilization of Pd in palladacycle depend on both the concentration of ligands tethered on silica walls and concentration of Pd in the reaction medium. Palladium content increases with the concentration of ligands up to certain extent then levels off. Loading of Pd as palladacycle depends on reaction conditions. Polar solvent, methanol, favors formation of palladacycle with sodium acetate as base and at mild reaction conditions. Higher reaction temperature enhances the deposition of bulk Pd along with the formation of palladacycle. Non-polar solvent, acetone, favors only addition complex under similar reaction conditions. A number of characterization techniques supported the formation of palladacycle complex inside the pores of mesoporous materials. Heck alkenylation of bromobenzene, was set as model reaction to evaluate the catalytic activity of all the catalysts investigated in this study and found that Pd-OMS5 (1.4) having 1.4 % Pd exhibited higher activity in the conversion of bromobenzene to trans-stilbene. Heterogeneity study reveals that leaching of Pd from the complex into the solution is much lower (in ppm level) and could be used as a heterogeneous coupling catalyst.

6.5. References

1. R.F. Heck, Palladium Reagents in Organic Syntheses; Academic Press: London, 1985; J. Tsuji, Palladium Reagents and Catalysts; Wiley: Chichester, 1995; I.P. Beletskaya, A.V. Cheprakov, Chem. Rev. 100 (2000) 3009.
2. W.A. Hermann, C. Brossmer, K. Ofele, C.-P. Reisinger, T. Priermeir, M. Beller, H. Fischer, Angew. Chem. Int. Ed. Engl. 34 (1995) 1844.
3. M. Beller, H. Fischer, W.A. Hermann, K. Ofele, C. Brossmer, Angew. Chem. Int. Ed. Engl. 34 (1995) 1848.
4. W. A. Hermann, M. Elison, J. Fischer, C. Kocher, G. R. J. Artus, Angew. Chem. Int. Ed. Engl. 34 (1995) 1844
5. W. Cabri, I. Candiani, Acc. Chem. Res. 28 (1995) 2.
6. B.L. Shaw, S. D. Perara, E.A. Staley, Chem. Commun. (1998) 1361.
7. F. Miyazaki, K. Yamaguchi, M. Shibasaki, Tetrahedron Lett. 40 (1999) 7379.
8. M. T. Reetz, E. Westermann, R. Lohmer, G. Lohmer, Tetrahedron Lett. 39 (1998) 8449.
9. W.A. Hermann, V.P. W. Bohm, C.P. Reisenger, J. Organomet. Chem. 576 (1999) 23.
10. A. Biffis, M. Zecca, M. Basato, J. Mol. Catal. A: Chem. 173 (2001) 249.
11. J. Zhou, R. Zhou, L. Mo, S. Zhao, X. Zheng, J. Mol. Catal. A: Chem. 178 (2002) 289.
12. B.M. Bhanage, M. Arai, Cat. Rev. 43 (2001) 315.
13. A. Biffis, M. Zecca, M. Basato, Eur. J. Inorg. Chem. 5 (2001) 1131.
14. C.M. Andersson, K. Karabelas, A. Hallberg, J. Org. Chem. 50 (1985) 3891.
15. P. W. Wang, M.A. Fox, J. Org. Chem. 59 (1994) 5358.
16. R. L. Augustine, S.T. O'Leary, J. Mol. Catal. A: Chem. 95 (1995) 277.
17. B.M. Choudary, S. Madhi, N.S. Choudari, M. L. Kantam, B. Sreedhar, J.Am. Chem. Soc. 124 (2002) 14127.
18. T. H. Bennur, A. Ramani, R. Bal, B.M. Chanda, S. Sivasanker, Catal. Commun. 3 (2002) 493.
19. M. Dams, L. Drijkoningen, B. Pauwels, G. Van Tendeloo, D.E. De Vos, P. A. Jacobs, J. Catal. 209 (2002) 225.
20. L. Djakovitch, K. Koehler, J. Am. Chem. Soc. 123 (2001) 5990.
21. C.T. Kresge, M.E. Leonowicz, W.J. Roth, J.C. Vartuli and J.S. Beck, Nature 359 (1992) 710.
22. C.P. Mehnert, D.W. Weaver, J.Y. Ying, J. Am. Chem. Soc. 120 (1998) 12289.

23. H. Kosslick, I. Mönnich, E. Paetzold, H. Fuhrmann, R. Fricke, D. Müller, G. Oehme, Micropor. Mesopor.Mater. 44-45 (2001) 537.
24. R.B. Bedford, C.S. J. Cazin, M. B. Hursthouse, M. E. Light, K.J. Pike, S. Wimperis, J. Organometal. Chem. 633 (2001) 173.
25. A. J. Sandee, D. Dimitrijevic, R. J. van Haaren, J. N.H. Reek, P.C.J. Kamer, P.W.N.M. van Leeuwen, J. Mol. Catal. A: Chem. 182-183 (2002) 309.
26. C.Baleizao, A. Corma, H. Garcia, A. Leyva, Chem. Commun. (2003) 606.
27. H.H. Wagner, H. Hausmann, W.F. Hölderich, J. Catal. 203 (2001) 150.
28. V.V. Dunia, L.G. Kuz'mina, M.Y. Kazakova, O.N. Gorunova, Y.K. Grishin, E.I. Kazakova, Eur. J. Inorg. Chem. (1999) 1029.
29. C.Venkatesan, A.P. Singh, Catal. Lett. 88 (2003) 193.
30. C.Venkatesan, A.P. Singh, J.Catal. (2004)
31. R. Anwander, I. Nagl, M. Widenmeyer, G. Engelhardt, O. Groeger, C. Palm, T. Roser, J. Phys. Chem. B 104 (2000) 3532.
32. J.H. Clark, D. J. Macquarrie, Chem. Commun. (1998) 853.
33. X.S. Zhao, G.Q. Lu, J. Phys. Chem. B 102 (1998) 1556.
34. J. Vicente, I. Saura-Liamas, M.G. Palin, P.G. Jones, J. Chem. Soc., Dalton Trans. (1995) 2535.
35. H.M. Hultman, M.de Lang, M. Nowotny, I.W.C.E. Arends, U. Hanefeld, R.A. Sheldon, T. Maschmeyer, J. Catal. 217 (2003) 264.
36. V.V. Dunia, O.A. Zalevskaya, V.M. Potapov, Ruus. Chem. Rev. (*Engl. Transl*) **57** (1988) 434.
37. A.L. Seligson, W.C. Trogler, J. Am. Chem. Soc. 113 (1991) 2520.
38. N.P.G. Roeges, "A Guide to the Complete Interpretation of Infrared Spectra of Organic Structures". Wiley, Chichester, 1994.
39. C. Battistoni, V. Cantelli, M. Debenedetti, S. Kaciulis, G. Mattogno, A. Napoli, Appl. Surf. Sci. 144–145 (1999) 390.
40. D.S. Martin, R.M. Rush, G.A. Robin, Inorg. Chem. 19 (1980) 1705.

7. CONCLUSIONS

The present work reports the synthesis, modification and characterization of synthesized or commercially available zeolite catalysts, sulphated metal oxides, mesoporous materials such as Si-MCM-41, Na-Al-MCM-41, organo functionalized materials such as 3-aminopropyltriethoxysilyl functionalized MCM-41 (NH_2-MCM-41), 3-chloropropyltiethoxysilyl functionalized MCM-41 (Cl-MCM-41) and palladacycle-MCM-41. The catalytic activity of these catalysts in the selective benzoylation (biphenyl, and chlorobenzene), alkylation (isopropylation of isobutyl benzene and side chain monomethylation of phenylacetonitrile), condensation of acetophenone as well as C-C coupling reactions of haloaromatics is investigated for producing industrially important products in high selectivity.

The work is presented in seven chapters.

A review on the published and patented literature on the synthesis, characterization and utility of zeolites, sulphated metal oxides and mesoporous materials in the synthesis of fine chemicals, particularly in the acylation, alkylation, condensation and C-C coupling reactions of aromatics with shape selective characteristics is reported in **Chapter 1**.

Chapter 2 describes the synthesis, modification and characterization of different zeolites, sulphated zirconia, sulphated titania, Si-MCM-41, Na-Al-MCM-41 and organo functionalized MCM-41. It contains the hydrothermal synthesis of zeolite K-L, beta and ZSM-5 and reflux method synthesis of mesoporous materials. Organo-functionalized mesoporous materials have been synthesized by in-situ co-condensation of coupling agent with organosilane with

required proportions. The modification of various synthesized as well as commercial zeolites into protonic, K^+, Cs^+, and RE^{+3} forms is also included here. Characterization of these zeolites, sulphated zirconia and mesoporous materials with various physico-chemical methods such as chemical analysis, XRD, FT-IR, elemental analysis, thermal studies, SEM, TEM, NMR, surface area measurement as well as acidity measurement using TPD of ammonia is also discussed. In addition the chapter includes procedure for the experimental set up for the evaluation of catalytic activity, product identification and product analysis.

Chapter 3 focuses on liquid phase selective acylation reactions i.e. benzoylation of biphenyl, and chlorobenzene using zeolite catalysts.

Zeolite H-beta catalyzes the benzoylation of biphenyl efficiently and is superior to other zeolite catalysts. Higher selectivity to 4-PBP in the range of 97.4% is achieved at 41.0% conversion of BP over H-beta, whereas $AlCl_3$ gave lower selectivity to 4-PBP (80%) under similar reaction conditions. A higher strength of acid sites and medium pore size of H-beta are the responsible for the conversion of BP. The conversion of BP using zeolite H-beta increased significantly with an increase in reaction time, catalyst concentration, reaction temperature and BOC to BP molar ratio. The acetylation and propionylation of BP are also investigated over zeolite H-beta catalyst with different acylating agents (BOC, benzoic anhydride, propionyl chloride, propionic anhydride, acetyl chloride, acetic anhydride) and found that the conversion of BP decreases in the following order: benzoylation > propionylation > acetylation. The yield of 4-PBP over zeolite H-beta in the acylation of biphenyl with acid chlorides and acid anhydrides decreases in the following order: acid chlorides > acid anhydrides. H-beta was recycled two times (fresh plus two cycles) and a decrease in BP conversion is observed after each cycle, which is related to a minor dealumination of zeolite

catalyst and consequently a decrease in the crystallinity of H-beta due to the formation of HCl during the reaction. The formation of acylated products of BP is explained by an electrophilic attack of acyl cation ($R\text{-}CO^{+;}$ where R = C_6H_5- or CH_3CH_2- or CH_3-) on the BP ring, whose formation is facilitated by acid sites of the zeolite catalysts.

It is demonstrated for the first time that zeolite H-beta catalyzes the benzoylation of chlorobenzene with 4-ClBC efficiently, which leads to the formation of 4,4'-DCBP in high selectivity. At identical reaction conditions the activity (conversion of 4-ClBC) trend after 4 h reaction time is AlCl3> H-beta > Del. H-Y > H.mordenite ≈ RE-Y. H-mordenite and RE-Y are less active due to their weaker acid sites. It is concluded that that the presence of strong Bronsted acid sites in the zeolite catalysts appears to be very important for the polarization of ClC_6H_5COCl (4-ClBC) into an electrophile ($ClC_6H_5CO^+$), which then attacks the chlorobenzene ring resulting in the formation of dichlorobenzophenones. The higher yield of the products can be achieved by increasing the values of the catalyst concentration, reaction temperature and CB/ 4-ClBC molar ratio. Recycling of the catalyst progressively decreases the 4-ClBC conversions to a little extent.

Chapter 4 deals with the isopropylation of isobutylbenzene (IBB) and side chain monomethylation of phenylacetonitrile to 2-phneylpropionitrile.

Isopropylation of IBB to 3-isobutylcumene (3-IBC) and 4-isobutylcumene (4-IBC) is carried out at 453 K under autogeneous pressure over various zeolite catalysts viz. H-beta, H-mordenite and H-RE(70.6)Y and H-ZSM-5. Zeolite H-beta catalyzes the isopropylation of IBB efficiently with 2-propanol as the alkylating agent and is found to be superior to other zeolite catalysts. The conventional homogeneous catalyst, $AlCl_3$, does not possess shape-selectivity and favors the formation of large amount of high molecular weight products.

Among the isomers, meta-isomer was found to form in a significant amount followed by para isomer as the ortho isomer has relatively high strain energy compared to the other two isomers. Selectivity of the order of 52 % for 4-IBC and 44 % 3-IBC is achieved at 17.0 wt.% conversion level of IBB over H-beta, whereas $AlCl_3$ gave 19 % 4-IBC and 42 % 3-IBC under similar reaction conditions. A higher strength of acid sites of H-beta is responsible for the conversion of IBB. The conversion of IBB increased significantly with increase in catalyst concentration (H-beta), reaction temperature and IBB/ i-PrOH molar ratio. At higher IBB/i-PrOH molar ratio, i.e. 5, the consumption of 2-propanol is comparatively higher (95 %) compared to the equimolar ratio, (2-propanol consumption is 17.0 %). Recycling of the catalyst has not affected the activity of the catalyst significantly.

NH_2-Na-Al-MCM-41 catalysts prepared by co-condensation of APTES, TEOS and sodium aluminate, are showing higher conversion of PAN and selectivity to 2-PPN compared to the microporous zeolites, alkali ion exchanged Na-Al-MCM-41, and conventional K_2CO_3 catalysts. Catalyst optimization study reveals that 30 wt % loading of APTES group over mesoporous aliminosilica exhibits maximum conversion of PAN and selectivity to 2-PPN. Reaction parameter study reveals that higher efficiency of active sites can be exploited only at the optimum catalyst concentration corresponds to reactant concentration, optimum molar ratio of DMC/PAN and higher reaction temperature. The optimum loading of catalyst was found to be 11.4 %. Higher concentration of DMC at DMC/PAN molar ratio (>10) facilitates the formation of 2-PPN by effective solvation and maximum random distribution of the intermediates, to access the catalytic sites effectively. Increase in reaction temperature enhances the activity of PAN conversion selectively towards 2-PPN. Recycling studies show that formation of quaternary ammonium salt in case of recycling catalysts is responsible for less activity of the catalyst for the conversion of PAN to 2-PPN.

Chapter 5 deals with the self-condensation of acetophenone to dypnone over sulphated zirconia (SZ), sulphated titania (ST) and H-beta zeolite as catalysts in the temperature range of 403 K to 433 K. It is found that SZ and H-beta exhibit similar activity (rate of ACP conversion), which is higher than that of sulphated titania. From the TPD of NH_3 it is seen that both sulfated zirconia and H-beta are highly acidic and possess strong acid sites, as seen from NH_3 desorption in the temperature range of 513 K to 873 K, which are responsible for the reaction. The conversion of ACP increases with reaction time, the catalyst concentration and reaction temperature. The SZ is recycled two times to show that there is only a marginal decrease in activity on recycled catalyst with no loss in the selectivity for dypnone.

Chapter 6 deals with the synthesis, characterization of palladacycle-MCM-41 catalysts and their applications in C-C coupling reactions.

Heterogeneous carbometallated palladacycle has been successfully synthesized by treatment of palladation reagents with 3-hydroxypropyltriethoxysilane incorporated MCM-41 (OH-M) under mild reaction conditions. The spatial confinement induced by the pore walls drives the palladation process more. It was observed through the optimization studies that the uptake and stabilization of Pd in palladacycle depend both the concentration of ligands tethered on silica walls and concentration of Pd in the reaction medium. Palladium content increases with the concentration of ligands up to certain extend then levels off. A number of characterization techniques supported the formation of palladacycle complex inside the pores of mesoporous materials. Heck alkenylation of bromobenzene, was set as model reaction to evaluate the catalytic activity of all the catalysts investigated in this study and found that Pd-OMS5 (1.4) having 1.4 % Pd exhibited higher activity in the conversion of bromobenzene to trans-stilbene.

LIST OF PUBLICATION AND PATENTS

Papers

1. **C. Venkatesan**, T. Jaimol, P. Moreau, A. Finiels, A.V. Ramaswamy and A.P.Singh*
   Liquid phase selective benzoylation of chlorobenzene to 4,4'-dichlorobenzophenone over zeolite H-beta
   Catal. Lett. 75,1-2 (2001) 119.

2. M. Chidambaram, **C. Venkatesan**, P. Moreau, A. Finiels, A.V. Ramaswamy and A.P.Singh*
   Selective benzoylation of biphenyl to 4-phenylbenzophenone over zeolite H-Beta.
   Appl. Catal. A: General 224 (2002) 129.

3. **C.Venkatesan** and A.P. Singh*
   Condensation of acetophenone to α, β-unsaturated ketone (dypnone) over solid acid catalysts.
   J. Mol. Catal. A. 181 (2002) 179.

4. **C.Venkatesan** and A.P.Singh*
   Selective mono-methylation of phenylacetonitrile to 2-phenylpropionitrile over 3-aminopropylsilyl functionalized MCM-41.
   Catal. Lett. 80, 1-2 (2002) 7.

5. M. Chidambaram, **C.Venkatesan**, P.R. Rajamohanan, and A.P. Singh*
   Synthesis of acidic functionalized mesoporous Zr-O-SO_2-CF_3 catalyst: Heterogenization of CF_3SO_3H over mesoporous $Zr(OH)_4$.
   Appl. Catal. A: General 244 (2003) 27.

6. **C.Venkatesan**, M. Chidambaram, K.R. Kamble and A.P. Singh*
   Preparation of isobutylcumenes by liquid phase isopropylation of isobutylbenzene with 2-propanol using zeolite H-beta.
   Catal. Lett. 85, 3-4 (2003) 171.

7. **C.Venkatesan** and A.P.Singh*
   New aliphatic C-metallated palladacycle in the pores of 3-hydroxypropyl triethoxysilane functionalized MCM-41.
   Catal. Lett. 88, 3-4 (2003) 193.

8. A.P.Singh and **C.Venkatesan**
   Selective acylation of aromatics using solid acid catalysts.
   Bulletin of the catalysis Society of India, 2 (2003) 43.

9. **C.Venkatesan** and A.P. Singh*

   Selective preparation of 2-phenylpropionitrile from phenylacetonitrile using solid base catalysts.
   J. Catal. (Revised manuscript submitted).

10. **C.Venkatesan** and A.P. Singh*

Aliphatic C-metallated palladacycle in MCM-41 for Heck reaction

Accepted in 14th IZC.

11. **C.Venkatesan** and A.P. Singh*

    Synthesis and characterization of carbometallated palladacycles over 3-hydroxypropyltriethoxysilyl functionalized MCM-41.
    J. Catal. (Communicated).

Patents

1. M.Chidambaram, **C.Venkatesan**, A.V. Ramaswamy and A.P.Singh
   An improved process for the production of phenyl ketones
   US. Patent 6,593,499, July 15,2003.

2. **C.Venkatesan**, A.V. Ramaswamy and A.P.Singh
   An improved process for the production of4, 4'-dihalobenzophenone
   US. Patent (filed on 1.8.2003, NCL34/2001).

Conference/Workshops Attended

1. CATSYMP-15/IPCAT-2 held at National Chemical Laboratory, Pune, India on Jan. 2001 – oral presentation of thesis work "*Aldol condensation of acetophenone using solid acids* .

2. Orientation programme on catalysis for research scholars sponsored by Department of Science and Technology (DST) held at IIT, Mumbai on Feb 2001.

3. 4th National Symposium in Chemistry held at National Chemical Laboratory, Pune. India on Feb. 2002. Presented a Poster Presentation on "*Selective mono-methylation of phenylacetonitrile to 2-phenyl propionitrile using solid base catalysts*".

4. "Catalysis: Concepts to practice" held from 26 and 27 June 2002 at National Chemical Laboratory, Pune, India conference in honor of Dr. Paul Ratnasamy on his 60th birth anniversary. Presented a poster entitled "*Selective acetylation of 2-methoxynaphthalene over solid acid catalysts*".

5. 1st Indo-German and CATSYMP-16 held at Indian Institute Chemical Technology, Hyderabad, India on Feb. 2003- poster presentation on "*Aliphatic C-metallated palladacycle in the pores of 3-hydroxypropyl triethoxysilane functionalized MCM-41 for Heck reaction*".

6. "Catalysis Research in India-Some highlights" held on 30th May 2003 at National Chemical Laboratory, Pune, India. A symposium in honour of Dr. A.V. Ramaswamy on his 60th birth anniversary. Presented two posters of following titles,

   1. Heterogenization of CF_3SO_3H over Zr-TMS and its catalytic activity

   2. Selective acylation of aromatics using solid acid catalysts.